

SNOW HYDROLOGY: THE PARAMETERIZATION OF SUBGRID  
PROCESSES WITHIN A PHYSICALLY BASED SNOW ENERGY  
AND MASS BALANCE MODEL

by

Jinsheng You

A dissertation submitted in partial fulfillment  
of the requirements for the degree

of

DOCTOR OF PHILOSOPHY

in

Civil and Environmental Engineering

Approved:



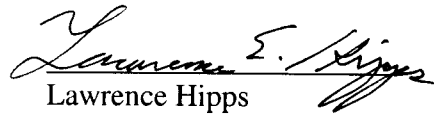
David G. Tarboton  
Major Professor



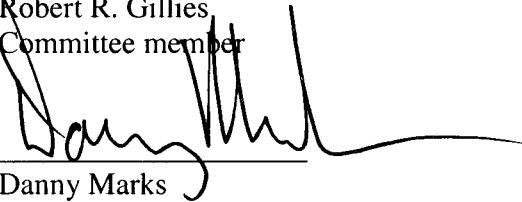
Mariush W. Kemblowski  
Committee Member



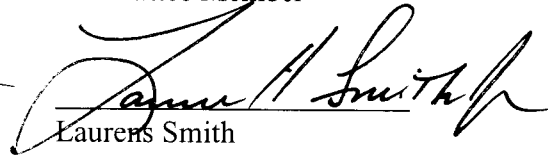
Robert R. Gillies  
Committee member



Lawrence Hipps  
Committee Member



Danny Marks  
Committee Member



Laurens Smith  
Interim Dean of Graduate Studies

UTAH STATE UNIVERSITY  
Logan, Utah

2004

## ABSTRACT

Snow Hydrology: The Parameterization of Subgrid Processes within  
a Physically Based Snow Energy and Mass Balance Model

by

Jinsheng You, Doctor of Philosophy

Utah State University, 2004

Major Professor: Dr. David G. Tarboton  
Department: Civil and Environmental Engineering

The objective of this research was to develop techniques for the representation and parameterization of subgrid and distributed snow processes within snowmelt models. Snowmelt is driven by energy exchanges at the snow surface that have horizontal variability down to scales of 1 to 10 m. When areas with large extent are modeled, it is impractical to apply models distributed on a 1 to 10 m grid. Large model elements, either grid squares or topographically delineated, need to be used. Therefore, it is necessary to develop modeling approaches that can parameterize the variability within these elements, referred to as subgrid variability. The role of subgrid variability increases as the model element size is increased, so as scale increases the representation of subgrid variability becomes more important. Computational tools are needed to explore the scale dependence of the subelement representation. Since subgrid variability is closely related

to the topography, the parameterization of subgrid variability from the topography or topographical features was investigated.

This dissertation is a collection of four papers that address some of these challenges. The goal is to combine physically based modeling emphasizing physical understanding of the reasons for and processes involved in spatial variability of snow and snowmelt with the analysis of extensive existing remotely sensed and field-based data from a Colorado Front Range watershed – Green Lakes Valley (GLV) watershed. A small-scale distributed model was used to quantify and refine the representation of the spatial snow accumulation and melt processes. This then formed the basis for parameterization of subgrid variability through the use of depletion curves and the derivation of these depletion curves from digital elevation data. As a final step the scale dependence of depletion curves was explored and to some extent quantified.

(188 pages)

DEDICATION

*This work is dedicated to my loving family.*

## ACKNOWLEDGMENTS

I appreciate David Tarboton for providing me a wealth of inspiration, guidance, and support during my studies. Special thanks to the other members of my committee, Mariush W. Kemblowski, Robert R. Gillies, Lawrence Hipps, and Danny Marks, for their thoughts, encouragement, and valuable suggestions.

Further thanks go to the research group of the NASA snow project, Charlie Luce, Don Cline, and Kelly Elder, for making their data available for analysis. In particular, I thank Charlie Luce for sharing the lumped snowmelt model. I thank Don Cline for the high resolution snow cover photographs. I thank Kelly Elder for the snow course data.

I am also grateful to all my fellow graduate students in engineering and natural resources at Utah State University and anybody else I could talk to and learn from – there is so much to explore, to learn, to experience.

Last but certainly not least, I will be forever indebted to the love and caring of my family, especially to my wife, Lianlin Zhao. Through the years, their love reminds me of what is truly important and helped me maintain perspective on life while completing this work.

This work was supported by NASA Land Surface Hydrology Program, grant number NAG 5-7597. The views and conclusions expressed are those of the authors and should not be interpreted as necessarily representing official policies, either expressed or implied, of the U.S. Government.

Jinsheng You

## CONTENTS

	Page
ABSTRACT .....	ii
DEDICATION .....	iv
ACKNOWLEDGMENTS .....	v
LIST OF TABLES .....	ix
LIST OF FIGURES .....	x
CHAPTER	
1. INTRODUCTION .....	1
REFERENCES .....	7
2. MODELING THE SNOW SURFACE TEMPERATURE IN AN ENERGY BALANCE SNOWMELT MODEL .....	10
Abstract .....	10
INTRODUCTION .....	11
MODEL DESCRIPTION .....	14
ALTERNATIVE MODELS OF SURFACE HEAT CONDUCTION .....	24
Equilibrium gradient approach .....	27
Force-restore approach .....	28
Modified force-restore approach .....	28
Theory of meltwater refreezing .....	29
Adjustment of thermal conductivity, $\lambda$ , for shallow snowpack .....	34
STUDY SITES AND DATA .....	37
RESULTS .....	40
DISCUSSION .....	49
CONCLUSIONS .....	54
REFERENCES .....	55
3 SNOW COVERED AREA IMAGE BASED REPRESENTATION OF THE SPATIAL DISTRIBUTION PATTERN OF SNOW IN A MOUNTAINOUS WATERSHED .....	59

Abstract .....	59
INTRODUCTION.....	60
STUDY SITES AND DATA .....	63
MODELING APPROACH.....	65
Disappearance date-based accumulation factor calculation.....	67
Accumulation factor interpolation .....	67
RESULTS.....	71
Accumulation factor interpolation .....	71
Validation against calculated accumulation factor bounds.....	77
Distributed modeling comparison .....	78
DISCUSSION AND CONCLUSIONS.....	81
REFERENCES .....	82
<b>4. TERRAIN BASED PARAMETERIZATION OF THE SUBGRID</b>	
<b>VARIABILITY OF SNOW .....</b>	<b>85</b>
Abstract .....	85
INTRODUCTION.....	86
METHODS.....	92
Large scale lumped model with depletion curve parameterization.....	93
Relationship between depletion curve and spatial distribution of snow ...	97
Derivation of depletion curve from terrain attributes.....	102
STUDY SITES AND DATA .....	112
RESULTS.....	113
Estimation of depletion curves .....	113
Evaluation of lumped model results using different depletion curves ...	120
DISCUSSION AND CONCLUSIONS.....	122
REFERENCES .....	126
<b>5. TESTING THE SCALING PROPERTIES OF A LUMPED MASS AND</b>	
<b>ENERGY BALANCE SNOWMELT MODEL .....</b>	<b>130</b>
Abstract .....	130
INTRODUCTION.....	131

THEORY.....	134
PHYSICAL ENERGY BALANCE MODEL.....	136
STUDY SITES.....	138
RESULTS AND ANALYSIS.....	141
Distributed model variability.....	141
Relationship between CV of snow and CV of causative processes.....	144
Performance of depletion curve approach and size of modeling element.....	146
DISCUSSION AND CONCLUSIONS.....	158
REFERENCES.....	160
6. SUMMARY, CONCLUSIONS, AND RECOMMENDATIONS.....	163
SUMMARY AND CONCLUSIONS.....	163
RECOMMENDATIONS.....	165
REFERENCES.....	167
APPENDIX.....	168
CURRICULUM VITAE.....	173



## LIST OF TABLES

Table	Page
2-1 Model parameter values .....	43
3-1 Information about 5 bands.....	74
3-2 Number and fraction of specific interpolated accumulation factor values falling within bounds of calculated values .....	77
3-3 Modeled and measured snow covered area.....	80
4-1 Comparisons of measured and modeled area fraction .....	120
5-1 Modeled snow water equivalent and mass loss in different models (m) for the period September 1, 1995 to May 2, 1996 .....	156

## LIST OF FIGURES

Figure	Page
2-1 Schematic illustration of temperature profile during the downward propagation of a refreezing front.....	31
2-2 Heat conduction scheme for combined snow/soil system.....	35
2-3 Measured snow, ground and snow surface temperatures .....	41
2-4 Comparisons of internal energy of snowpack during the first two freezing weeks at the USU Drainage Farm .....	42
2-5 Comparisons of snow water equivalent in 1993 at USU Drainage Farm .....	44
2-6 Comparisons of internal energy of snowpack in 1993 at USU Drainage Farm....	44
2-7 Comparisons between the measured and modeled internal energy of the snowpack at USU Drainage Farm in the new model and the original model .....	45
2-8 Comparisons of snow surface temperature in 1993 at USU Drainage Farm .....	45
2-9 Comparisons of snow water equivalent in 1986 at CSSL.....	46
2-10 Comparisons of accumulative melt in 1986 at CSSL .....	47
2-11 Comparisons of meltwater outflow rate in 1986 at CSSL .....	47
2-12 Comparisons of surface temperature of snow in 1986 at CSSL .....	47
2-13 Comparisons of snow water equivalent in 1996 at Subnivean Snow Laboratory at Niwot Ridge watershed, CO.....	48
2-14 Comparison of albedo at USU drainage farm .....	53
3-1 Green Lakes Valley watershed location map and its relative location in U.S.A. ....	64
3-2 Observed snow covered area images at four dates, May 22, June 9, June29, and July 21, 1996 .....	64

Figure	Page
3-3 Schematic of time series solutions for snow water equivalent for varying accumulation factor .....	68
3-4 Schematic map showing definition of edge cells where specific accumulation factor values are calculated .....	68
3-5 Illustration of some terrain attributes .....	70
3-6 Calculated versus predicted accumulation factor for single regression model .....	72
3-7 Calculated versus predicted accumulation factor for each band in the 5 bands regression model .....	75
3-8 Calculated versus predicted accumulation factor for combined 5 bands regression model .....	76
3-9 Accumulation factor map .....	76
3-10 Estimated snow accumulation factor compared to directly calculated snow accumulation factor bounds .....	78
3-11 Modeled snow water equivalent and observed snow covered area .....	79
3-12 a) Snow covered area fraction comparison; b) Snow covered area fraction time series .....	80
4-1 Schematic of lumped snowmelt model .....	94
4-2 Depletion curve parameterization of subgrid variability in a lumped snowmelt model .....	96
4-3 Schematic of generic snow water equivalent probability distribution .....	99
4-4 Illustration of the time evolution of snow accumulation and melt distributions and the combined snow water equivalent distribution that results .....	108
4-5 Green Lakes Valley watershed location map .....	113
4-6 Relationships involved in the derivation of depletion curves .....	114
4-7 Depletion curves derived with the different approaches evaluated .....	115

Figure	Page
4-8 Depletion curves derived from gamma distributions with different Coefficients of Variation.....	119
4-9 Comparisons of measured, modeled snow covered area fraction by large scale snowmelt model and distributed snowmelt model.....	121
4-10 Comparisons of measured, modeled snow covered area fraction at four dates by large scale snowmelt model and distributed snowmelt model.....	122
4-11 Comparisons of modeled time series of basin average snow water equivalent by large scale snowmelt model and distributed snowmelt model.....	123
5-1 Model elements (subwatersheds) within Green Lakes Valley watershed.....	140
5-2 Coefficient of variation of variables for model elements with different sizes....	142
5-3 CV of peak Snow Water Equivalent calculated from equation 5-5 under various assumptions versus the CV obtained from the spatially explicit distributed model.....	143
5-4 Derived depletion curves for 4 modeling elements from the distributed modeled snow water equivalent at peak accumulation on May 2, 1996.....	147
5-5 Modeled time series of snow covered area fraction using three snowmelt models for four modeling elements.....	149
5-6 Modeled time series of snow water equivalent using three snowmelt models for four modeling elements.....	150
5-7 Modeled snow water equivalent and snow covered area fraction for some example subwatersheds with specific topographical settings .....	151
5-8 Comparison of mass changes in model element 11 for each time step during the accumulation season (Sept. 1, 1995 ~ May 2, 1996) between the lumped snowmelt model and reference distributed snowmelt model.....	153
5-9 Distribution of mass loss (E+M) from 18:00 to 20:00 January 11, 1996 and its relationship with topography and topographical variables.....	154
5-10 Distribution function of snow water equivalent change in distributed snowmelt model during the period Sept. 1, 1995 to May 2, 1996 .....	156

Figure	Page
5-11 Distribution of cumulative radiation during the period Sept. 1, 1995 to May 2, 1996.....	157

## CHAPTER 1

### INTRODUCTION

Snowmelt runoff is an important water resource in much of the world including the semiarid regions of the western U.S. Understanding the processes involved with the accumulation and ablation of snow and capability for the modeling of snowmelt runoff is therefore important for water resources planning and management, as well as flood control or mitigation.

Snow accumulation and melt involve spatially variable processes leading to spatial heterogeneity over a range of scales. At the largest scale snow varies with latitude and elevation. At smaller scales snow varies due to wind drifting and avalanching, sliding or sloughing that results in the redistribution of snow as well as differential melt due to variability in exposure to melt energy inputs. The heterogeneity in the snowpack that results from these processes poses challenges to the modeling of snow accumulation and melt.

This dissertation explores the broad problems associated with the spatial heterogeneity of snow and approaches to quantify heterogeneity and accommodate heterogeneity into snow models. The focus is on understanding the sources of variability and using parameterizations such as an accumulation factor field in distributed modeling and depletion curve to parameterize subgrid variability within large model elements. The accumulation factor is a quantity that describes the variability of snow accumulation at each point relative a reference precipitation input (Tarboton *et al.*, 1995; Luce *et al.*, 1998). A depletion curve quantifies the reduction in snow-covered area during the

progress of snowmelt and is related to the spatial distribution of snow (Luce *et al.*, 1999). Specific questions that are addressed are: What are the sources of snow variability leading to the spatially distributed snow patterns observed? How can we understand the linkage between these sources of variability and the resultant heterogeneity in the distribution of snow? Can efficient numerical approximations be developed to quantify and model the heterogeneity of snow over watersheds?

Spatial variability of snow is a result of variations in topography (Gray and Male, 1981), prevailing winds (Gray and Male, 1981; Schmidt, 1982; Tabler *et al.*, 1990; Elder *et al.*, 1991; Blöschl and Kirnbauer, 1992; Luce *et al.*, 1998; Prasad *et al.*, 2000), radiation exposure (Marks and Dozier, 1979; Dozier, 1980; Dozier and Frew, 1990), and vegetation (e.g. Verstraete *et al.*, 1990; Ni *et al.*, 1997). Spatially distributed models subdivide the modeling domain into model elements. Snow processes are explicitly represented in each model element. However, spatial variability consists of two components, the inter-element variability and subgrid variability. Subgrid variability is variability with length scales smaller than the modeling element size which cannot be explicitly interpreted, and an effective approach is required to parameterize or represent it (Beven, 1995; Blöschl, 1999). The role of subgrid variability becomes more important and the proportion of variability that is subgrid variability increases with increasing size of the modeling element. Nonlinearity of the snow hydrologic processes, e.g. wind redistribution and surface-atmosphere energy exchanges poses an additional challenge to modeling subgrid variability because calculations based on average properties do not give the same result as calculations over a distribution of properties. Model parameterizations that address the subgrid variability should be physically based and founded on a good

understanding of the sources of the variability and the relative roles that these sources play in the total variability.

Snowmelt is primarily driven by energy exchanges at the snow surface. Snow accumulation and melt have horizontal variability down to scales of 1 to 10 m (hereafter referred to as the point scale). The physical processes responsible for snowmelt at these point scales are relatively well understood and modeled by a variety of point models (Anderson, 1976; Morris, 1990; Jordan, 1991; Tarboton *et al.*, 1995; Tarboton and Luce, 1996). However when larger scales are considered, it is frequently computationally prohibitive or there is insufficient data to apply such models in a distributed fashion at each grid point at a 1 to 10 m resolution; this being the requirement for a physical representation of the process. Therefore it is necessary to develop modeling approaches that can parameterize the subgrid variability.

The objective of this work was to develop techniques for the representation and parameterization of subgrid and distributed snow processes within snowmelt models. The goal was to combine physically based modeling emphasizing physical understanding of the reasons for, and processes involved in, spatial variability of snow and snowmelt with analysis of remotely sensed and field based data sets. The specific objectives were to:

- (1) Enhance the UEB point snowmelt model incorporating results from recent research to provide a parameterization of our current understanding of point snowmelt processes appropriate for application at the study site.
- (2) Apply the enhanced UEB model at each grid point over the study area to provide an explicitly spatially distributed parameterization. Calibrate input accumulation



factors against observations to provide an encoding of our fine scale understanding of snow processes within the study area.

- (3) Use results from the explicitly distributed model to develop depletion curves for areas typical of broad scale model elements. Explore the relationship between depletion curves and digital elevation data, recognizing that topography is the primary physical determinant of spatial variability in the high alpine basin studied.
- (4) Quantify the scale dependence of depletion curves. Since the variability with model elements depends upon scale (size) a hypothesis is that depletion curves are scale dependent. The objective here was to develop general scaling rules for working with depletion curves in the context of the physically based snowmelt model being used.

This dissertation is organized into six chapters, including this introduction and the summary. Chapters two through five address each of the objectives enumerated above.

Chapter 2 incorporates recent findings to enhance the physically based point scale implementation of the Utah Energy Balance (UEB) snowmelt model. The modified force-restore approach was incorporated into the original UEB to better approximate the surface temperature of snow following the suggestions of Luce (2000) and Luce and Tarboton (2001). A new refreezing scheme to represent the penetration of a refreezing front following melt was added. The thermal conductivity of the snow for the shallow snowpack was adjusted since the heat conduction in the shallow snow penetrates into the underlying soil layer. The enhanced model (hereinafter referred to as the new model) was then calibrated and tested against the snow water equivalent, surface temperature of snow, meltwater output, and the internal energy of snowpack measurements. The new

model was validated for the Green Lakes Valley watershed study site that was the focus of the remaining chapters.

Chapter 3 applied the point scale UEB model to the spatially explicit simulation of snow accumulation and melt on a 10 m grid over the Green Lakes Valley Watershed. Four snow covered images were used to calibrate an “accumulation factor” (Tarboton *et al.*, 1995; Luce *et al.*, 1998) to represent the wind blowing and sliding/sloughing redistribution of snow. The snow covered area images were used to establish the date at which snowcover was last observed and the later date at which a snow free surface was first observed at each grid cell. The accumulation factor in the mass balance equation of the UEB model was adjusted to have the model predicting snow disappearance on each of these dates and thus provide upper and lower bound estimates for the accumulation factor at each grid cell. An assumption was made that edge grid cells in the snow covered area images, if snow covered are about to be snow free, or if snow free have just become snow free. Based upon this the accumulation factor was assumed at the appropriate specific bound value, providing accumulation factor for the subset of the domain consisting of edge cells. This subset was used to calibrate a regression model related to topographic attributes to estimate accumulation factor over the entire domain. The spatially explicit point UEB model with these accumulation factors was evaluated by comparison against snow covered area images over the entire watershed and deemed to provide an adequate representation of spatially distributed snow accumulation and ablation processes in this watershed. The results from this model were then used as the fine scale reference representation of spatially distributed snow accumulation and ablation for use in the evaluation of subgrid parameterizations.

Chapter 4 examined whether the depletion curve could be derived from various surrogate variables such as: elevation; accumulation factor, in this case estimated from the snow covered area images; and peak accumulation estimated based on regression with accumulation factor and elevation as predictor variables. The regression parameters were calibrated against peak accumulation from the spatially explicit model used as a reference. Chapter 4 also evaluated the derivation of a depletion curve from spatial distributions of accumulation and ablation (melt and sublimation combined) combined using the convolution integral either assuming independence or explicitly recognizing the spatial dependence between accumulation and ablation. This chapter found that it was possible to get depletion curves that approach the reference depletion curve based on surrogate variables, but that the better estimates still require some reliance on spatially explicit modeling.

Chapter 5 examined the scaling properties of the depletion curve subgrid parameterization through an analysis of sub-watersheds of different sizes. The coefficient of variation of the snow accumulation and melt related variables was examined for sub-watersheds covering a range of scales and physical attributes. The depletion curve parameterization in the lumped model was shown to produce acceptable results in comparison to both the reference explicitly distributed model and observed snow covered area fraction when applied treating the entire study area as a single model element. This would suggest that there is not a scale limitation on this theory up to the scale of  $8.1 \text{ km}^2$  in this setting. However when the depletion curve parameterization was applied to selected subwatersheds within this domain, discrepancies were noted in certain topographic settings. The fact that these discrepancies do not impact the overall results

when applied to a large watershed suggests that there are perhaps offsetting errors, or that these discrepancies occur in a relatively small fraction of the area. Nevertheless the physical cause and limitations implied by these issues need to be the subject of further investigation.

Chapter 6 summarizes the overall conclusions and discusses opportunities for future research. Overall this work has significantly improved the performance of the UEB point model through the enhancements described in chapter 2. The approach described in chapter 3 provides a practical way for the estimation of accumulation factors making use of this methodology practical for domains too large for field surveys. Chapters 4 and 5 further advance the practical use of depletion curves by evaluating methods for their derivation based on surrogate data and examining scale dependencies.

## REFERENCES

- Anderson EA. 1976. A Point Energy and Mass Balance Model of a Snow Cover. NOAA Technical Report NWS 19, U.S. Department of Commerce. 150 pp.
- Beven K. 1995. Linking parameters across scales: subgrid parameterizations and scale dependent hydrological models. *Hydrological Processes* **9**: 507-525.
- Blöschl G. 1999. Scaling issues in snow hydrology. *Hydrological Processes* **13**: 2149-2175.
- Blöschl G, Kirnbauer R. 1992. An analysis of snow cover patterns in a small alpine catchment. *Hydrological Processes* **6**: 99-109.
- Dozier J. 1980. A clear-sky spectral solar radiation model for snow-covered mountainous terrain. *Water Resources Research* **16**: 709-718.
- Dozier J, Frew J. 1990. Rapid Calculation of Terrain Parameters for Radiation Modeling From Digital Elevation Data. *IEEE Transactions on Geoscience and Remote Sensing* **28**(5): 963-969.

- Elder K, Dozier J, Michaelsen J. 1991. Snow accumulation and distribution in an alpine watershed. *Water Resources Research* **27**(7): 1541-1552.
- Gray DM, Male DH. 1981. Handbook of Snow, Principles, Processes, Management & Use. Pergamon Press: New York.
- Jordan R. 1991. A one-dimensional temperature model for a snow cover. Technical documentation for SNTHERM.89, special technical report 91-16, US Army CRREL. 49 pp.
- Luce CH. 2000. Scale influences on the representation of snowpack processes. Ph. D Dissertation, Civil and Environmental Engineering: Utah State University, Logan, Utah.
- Luce CH, Tarboton DG. 2001. A modified force-restore approach to modeling snow-surface heat fluxes. In *Proceedings of The 69th Annual Meeting of the Western Snow Conference*, Sun Valley, Idaho., <http://www.westernsnowconference.org/2001/2001papers.htm> (Accessed Jul. 31, 2004).
- Luce CH, Tarboton DG, Cooley KR. 1998. The influence of the spatial distribution of snow on basin-averaged snowmelt. *Hydrological Processes* **12**(10-11): 1671-1683.
- Luce CH, Tarboton DG, Cooley KR. 1999. Subgrid parameterization of snow distribution for an energy and mass balance snow cover model. *Hydrological Processes* **13**: 1921-1933.
- Marks D, Dozier J. 1979. A clear-sky longwave radiation model for remote alpine areas. *Archev fur Meteorologie Geophysik und Bioklimatologie Ser B*, **27**: 159-187.
- Morris EM. 1990. Physics-based models of snow. In *Recent Advances in the Modeling of Hydrologic Systems*, Bowles DS, O'Connell PE (eds). Kluwer Academic Publishers: Dordrecht, The Netherlands; 85-112.
- Ni W, Li X, Woodcock CE, Roujean JL, Davis RE. 1997. Transmission of solar radiation in boreal conifer forests: measurements and models. *Journal of Geophysical Research* **102**(D24): 29397-29406.
- Prasad R, Tarboton DG, Liston GE, Luce CH, Seyfried MS. 2000. Testing a blowing snow model against distributed snow measurements at Upper Sheep Creek. *Water Resources Research* **37**(5): 1341-1350.
- Schmidt RA. 1982. Vertical profiles of wind speed, snow concentration, and humidity in blowing snow. *Boundary Layer Meteorology* **34**: 213-241.

- Tabler RD, Pomeroy JW, Santana BW. 1990. Drifting snow. In *Technical Council on Cold Regions Monograph*, Ryan WL, Crissman RD (eds). American Society of Civil Engineering: New York; 95-145.
- Tarboton DG, Chowdhury TG, Jackson TH. 1995. A spatially distributed energy balance snowmelt model. In *Proceedings of a Boulder Symposium*, Tonnessen KA, Williams MW, Tranter M (eds). Boulder, CO., July 3-14, IAHS Publ. no. 228.
- Tarboton DG, Luce CH. 1996. Utah Energy Balance Snow Accumulation and Melt Model (UEB). Computer model technical description and users guide, Utah Water Research Laboratory and USDA Forest Service Intermountain Research Station (<http://www.engineering.usu.edu/dtarb/>). (Accessed Jul. 31, 2004).
- Verstraete MM, Pinty B, Dickinson RE. 1990. A physical model of the bidirectional reflectance of vegetation canopies, 1. Theory. *Journal of Geophysical Research* **95**(D8): 11755-11765.

CHAPTER 2  
MODELING THE SNOW SURFACE TEMPERATURE IN AN ENERGY  
BALANCE SNOWMELT MODEL

Abstract:

Snow surface temperature is a key control on energy exchanges at the snow surface, particularly net longwave radiation and turbulent energy fluxes. The snow surface temperature is in turn controlled by the balance between various external fluxes and the conductive heat flux, internal to the snowpack. Because of the strong insulating properties of snow, thermal gradients in snow packs are large and nonlinear a fact that has led many to advocate multiple layer snowmelt models over single layer models. In an effort to keep snowmelt modeling simple and parsimonious, the Utah Energy Balance (UEB) snowmelt model used only one layer, but allowed the snow surface temperature to be different from the snow average temperature by using an equilibrium gradient parameterization based on the surface energy balance. Although this procedure was considered an improvement over the ordinary single layer snowmelt models, it still resulted in discrepancies between modeled and measured snowpack energy contents. In this paper we examine the parameterization of snow surface temperature in single layer snowmelt models from the perspective of heat conduction into a semi-infinite medium. We evaluate the equilibrium gradient approach, the force-restore approach, and a modified force-restore approach. In addition, we evaluate a scheme for representing the penetration of a refreezing front in cold periods following melt. We also introduce a

method to adjust effective conductivity to account for the presence of ground near to a shallow snow surface. These parameterizations were tested against data from the Central Sierra Snow Laboratory, CA, Utah State University experimental farm, UT, and Subnivean snow laboratory at Niwot Ridge, CO. These tests compare modeled and measured snow surface temperature, snow energy content, snow water equivalent, and snowmelt outflow. We found that with these refinements the model is able to better represent the snowpack energy balance and internal energy content while still retaining a parsimonious one layer format.

## INTRODUCTION

Snowmelt is an important source of water in the western United States and much of the world. Modeling snowmelt is important for water resources management and the assessment of spring snowmelt flood risk. The processes involved in snowmelt have been widely described (U.S. Army Corps of Engineers, 1956; Linsley *et al.*, 1975; Gray and Male, 1981; Bras, 1990; Dingman, 1994; Viessman *et al.*, 2002). In snowmelt modeling, the heat flux between the snowpack and the atmosphere is partially governed by the atmospheric conditions and the snow surface temperature (Gray and Male, 1981; Dozier, 1989; Dingman, 1994) which depends on the conductive heat flux into the snow. Modeling conductive heat flux through the snowpack is a complex problem due to the changing nature of the snowpack through the influences of heating and cooling history. One of the primary reasons for the poor performance of single layer models in comparative validations is the poor representation of internal snowpack heat transfer process (Blöschl and Kirnbauer, 1991; Koivasulo and Heikenkeimo, 1999). Some



snowmelt models use finite difference solutions of the heat equation (Yen, 1967; Anderson, 1976; Flerchinger and Saxton, 1989; Jordan, 1991; Dickinson *et al.*, 1993). Possible inaccuracies in modeling the internal snowpack properties could lead to errors in estimating the snowpack and snow surface temperature (Colbeck and Anderson, 1982). Thus, it is desirable to have a simple model to avoid introducing errors due to attempts to represent complex internal snow processes.

The UEB snowmelt model (Tarboton *et al.*, 1995; Tarboton and Luce, 1996) is a physically-based point energy and mass balance model for snow accumulation and melt. The snowpack is characterized using two primary state variables, namely, snow water equivalent,  $W$ , (m) and the internal energy of the snowpack and top layer of soil,  $U$  (kJ m<sup>-2</sup>). The physical basis of the model is the conservation of mass and energy. Snow surface temperature, a key variable in calculating latent and sensible heat fluxes and outgoing longwave radiation, is modeled using a thin surface skin or equilibrium gradient approach. The surface skin is assumed to have zero heat capacity. Snow surface temperature is calculated from the energy balance at the surface of the snowpack by equating incoming and outgoing fluxes between the snow mass and the air above; this allows the snow surface skin temperature to be different from the average temperature of the snowpack as reflected by the energy content. This also reflects the insulating effect of snow and facilitates modeling of the surface energy balance without the need to introduce multiple layers and without difficult to model details of within-snow energy transfers. The approximation of the snow surface temperature used by UEB is not perfect given what we know about the penetration of radiation into the snowpack (Warren, 1982) and the movement of air into the snowpack (Colbeck, 1989).

The UEB model was initially tested against snow accumulation and melt measurements and was found to perform well. Later tests included comparisons against internal energy through measurement of the temperature profile in a snowpack (Tarboton, 1994). These tests indicated a discrepancy between the modeled and the measured internal energy (Tarboton, 1994; Tarboton and Luce, 1996). Luce (2000) analyzed the snowpack energy fluxes from a season of measurements collected at the USU drainage farm in Cache Valley, Utah to evaluate the reasons for the discrepancies in the internal energy. They found that one cause was the estimation of longwave radiation inputs based on air temperatures in an environment subject to frequent temperature inversions. Another cause of the discrepancies was the parameterization of snow surface temperature. These problems had been offsetting each other in a way that when the longwave radiation inputs were corrected, the modeled surface temperatures no longer matched measurements. To address this problem, Luce (2000) and Luce and Tarboton (2001; submitted 2004) evaluated various alternative parameterizations against the currently used equilibrium gradient approach. These included the force-restore approach (e.g. Deardorff, 1978; Dickinson *et al.*, 1993; Hu and Islam, 1995) and a modified force-restore approach that was suggested (Luce 2000; Luce and Tarboton 2001; submitted 2004) to improve the representation of snow surface temperature and help improve the representation of energy content in the snowpack. In this paper these suggestions are implemented and tested within the UEB snowmelt model.

Snowmelt generated at the snow surface is initially held in the snowpack as liquid water up to the liquid holding capacity. When the surface forcing changes to cooling, this water refreezes and a refreezing front penetrates into the snow. The rate of

penetration of the refreezing front is governed by the rate of heat loss, the latent heat of fusion, and the temperature gradient in the layer above the refreezing front. The UEB model currently uses the equilibrium gradient approach to estimate snow surface temperature that does not account for the presence of liquid water during refreezing periods with the result that the snow surface temperature is modeled as too low with too little heat loss during these periods. Multiple-layer snow models (e.g. Flerchinger and Saxton, 1989; Jordan, 1991) account for this effect because the liquid content and temperature of each layer is explicitly represented. Here we present and test a formulation for representing this refreezing effect in the single layer UEB model. In addition to the two changes mentioned above we also introduce a method to adjust the effective thermal conductivity of shallow snowpacks to account for the combined effect of snow and the ground below the snow.

## MODEL DESCRIPTION

The original UEB model is described by Tarboton *et al.* (1995) and Tarboton and Luce (1996). A comprehensive review is given here so that the reader can understand the context for the modifications that were made. We refer to the Tarboton *et al.* (1995) model as the *original* UEB model. Methods introduced in this work are referred to as the new UEB model. Where we do not use a qualifier the methods are the same in both models. In the UEB model (Tarboton *et al.*, 1995; Tarboton and Luce, 1996), the time evolution of the snowpack is driven by the energy exchange between the snowpack, the air above and the soil below according to mass and energy balance equations,

$$\frac{dU}{dt} = Q_{sn} + Q_{li} - Q_{le} + Q_p + Q_g + Q_h + Q_e - Q_m, \quad (\text{kJ m}^{-2} \text{ h}^{-1}) \quad (2-1)$$

$$\frac{dW}{dt} = P_r + P_s - M_r - E, \quad (\text{m h}^{-1}) \quad (2-2)$$

where  $Q_{sn}$  is the net shortwave energy received by the snowpack,  $Q_{li}$  is the incoming longwave radiation,  $Q_{le}$  is outgoing longwave radiation,  $Q_p$  is the energy advected by precipitation into the snow,  $Q_g$  is the ground heat flux to the snow,  $Q_h$  is the sensible heat flux to/from the snow with sign convention that flux to the snow is positive,  $Q_e$  is the latent heat flux to/from the snow with sign convention that flux to the snow is positive, and  $Q_m$  is the advected heat removed by meltwater.  $P_r$  is the rate of precipitation as rain;  $P_s$  is the rate of precipitation as snow;  $M_r$  is the melt rate; and  $E$  is the sublimation rate;  $t$  is time (h). Internal energy  $U$  is not defined relative to absolute 0, but rather relative to the melting point.  $U$  is taken as  $0 \text{ kJ m}^{-2}$  when the snowpack is frozen at  $0^\circ\text{C}$  and contains no liquid water. With this definition negative internal energies correspond to the cold content (e.g., Dingman, 1994, p. 182) and positive internal energies reflect change in phase of some fraction of snow from frozen to liquid. The model requires inputs of air temperature, wind speed and incident radiation that are used to drive the energy balance, and precipitation that is used to drive the mass balance. Precipitation is partitioned into snowfall or rainfall based upon air temperature (U.S. Army Corps of Engineers, 1956) interpolated from measurements at weather stations and adjusted with elevation based upon a lapse rate. The fraction of precipitation falling as snow,  $f_{snow}$ , is given by:

$$\begin{aligned}
f_{snow} &= 1.0 && \text{when } T_a < T_s \\
&= \frac{T_r - T_a}{T_r - T_{sn}} && \text{when } T_{sn} \leq T_a \leq T_r \\
&= 0.0 && \text{when } T_a > T_r
\end{aligned} \tag{2-3}$$

Here  $T_a$  is the air temperature,  $T_r$  ( $=3$  °C) is the air temperature above which all precipitation is assumed to fall as rain, and  $T_{sn}$  ( $=-1$  °C) is the air temperature below which all precipitation is assumed to fall as snow.

In locations where snow is subject to redistribution due to wind blown drifting or sliding, an accumulation factor (Tarboton *et al.*, 1995; Tarboton and Luce, 1996) relates a measured or reference snowfall input to the snow accumulation at each point in the watershed. Snow deposition at each location is modified by applying a spatially variable accumulation factor,  $\phi$ , to account for redistribution and differential accumulation effects.

$$P_s = f_{snow} \cdot \phi \cdot P \tag{2-4}$$

where  $P$  is the measured point or reference precipitation (m) and  $P_s$  is snowfall to location. The total precipitation to each grid cell is the sum of  $P_s$  and precipitation as rainfall,  $P_r = (1 - f_{snow})P$ . The accumulation factor is an empirical factor that includes the combined effect of all processes involved in variability in snow accumulation, including wind blown drifting, sliding and precipitation variability.

The use of energy content as a state variable means that the model does not explicitly prognose snowpack temperature. Since snowpack temperature is important for

energy fluxes into the snow, it needs to be obtained diagnostically from internal energy and snow water equivalent as follows:

$$\text{If } U < 0 \quad T_{ave} = U / (\rho_w W C_i + \rho_g D_e C_g) \quad \text{All solid phase} \quad (2-5 \text{ a})$$

$$\text{If } 0 < U < \rho_w W h_f \quad T_{ave} = 0^\circ\text{C} \quad \text{with } L_f = U / (\rho_w h_f W) \quad \text{Solid and liquid mixture} \quad (2-5 \text{ b})$$

$$\text{If } U > \rho_w W h_f \quad T_{ave} = \frac{U - \rho_w W h_f}{\rho_g D_e C_g + \rho_w W C_w} \quad \text{All liquid} \quad (2-5 \text{ c})$$

In the equations above,  $T_{ave}$  denotes snowpack average temperature ( $^\circ\text{C}$ ),  $h_f$  denotes the heat of fusion ( $333.5 \text{ kJ kg}^{-1}$ ),  $\rho_w$  the density of water ( $1000 \text{ kg m}^{-3}$ ),  $C_i$  the specific heat of ice ( $2.09 \text{ kJ kg}^{-1} \text{ }^\circ\text{C}^{-1}$ ),  $\rho_g$  the soil density,  $C_g$  the specific heat of soil,  $C_w$  the specific heat of water ( $4.18 \text{ kJ kg}^{-1} \text{ }^\circ\text{C}^{-1}$ ),  $D_e$  the depth of soil that interacts thermally with the snowpack and  $L_f$  the liquid fraction by mass. The basis for equations 2-5 a to 2-5 c is that the heat required to melt the entire snow water equivalent at  $0 \text{ }^\circ\text{C}$  is  $\rho_w W h_f$  ( $\text{kJ m}^{-2}$ ). Where  $U$  is between 0 and this quantity the liquid fraction is determined by proportioning, i.e.  $L_f = U / (\rho_w h_f W)$ . The heat capacity of the snow combined with thermally interacting soil layer is  $\rho_w W C_i + \rho_g D_e C_g$  ( $\text{kJ }^\circ\text{C}^{-1} \text{m}^{-2}$ ), so in the case that  $U < 0$ , dividing  $U$  by this combined heat capacity gives  $T_{ave}$ . Where  $U > \rho_w W h_f$  the snow contains sufficient energy to melt completely and the temperature of the remaining liquid phase is given by equation 2-5 c. Practically, the condition in equation 2-5 c only occurs when  $W$  is zero since a completely liquid snowpack cannot exist; it becomes melt runoff. Nevertheless, this equation is included for completeness to keep track of the energy content during periods of intermittent snow cover, with  $T_{ave}$  representing the temperature

of the ground, with the possibility of snowfall melting immediately due to coming in contact with warm ground.

The net shortwave radiation is calculated as:

$$Q_{sn} = Q_{si}(1 - Alb), \quad (2-6)$$

where  $Alb$  is the albedo of snow calculated as a function of snow age and solar illumination angle following Dickinson *et al.* (1993).  $Q_{si}$  is the incident shortwave radiation which is either measured or estimated from the diurnal temperature range (Bristow and Campbell, 1984). On sloping surfaces, incident radiation is adjusted for slope, and aspect (e.g. Dingman, 1994).

In the albedo model which follows Dickinson *et al.* (1993) and is described in detail in Tarboton and Luce (1996) the dimensionless age of the snow surface,  $\tau$ , is retained as a state variable, and is updated with each time step, dependent on snow surface temperature and snowfall. Reflectance is computed for two bands; visible ( $< 0.7 \mu\text{m}$ ) and near infrared ( $> 0.7 \mu\text{m}$ ) with adjustments for illumination angle and snow age. Then albedo is taken as the average of the two reflectances. A parameter  $d_{NewS}$  (m) represents the depth of snowfall that is assumed to restore the snow surface to new conditions ( $\tau = 0$ ). With snowfall,  $P_s$ , less than  $d_{NewS}$  in a time step the dimensionless age is reduced by a factor  $(1 - P_s/d_{NewS})$

When the snowpack is shallow (depth  $D < h = 0.1$  m) the albedo is taken as  $r_\alpha \alpha_{bg} + (1 - r_\alpha) Alb$  where  $r_\alpha = (1 - D/h)e^{-z/2h}$ . This interpolates between the snow albedo and

bare ground albedo ( $\alpha_{bg}$ ) with the exponential term approximating the exponential extinction of radiation penetration of snow.

The incident longwave radiation is estimated based on air temperature,  $T_a$  (K) using the Stefan-Boltzmann equation:

$$Q_{li} = \varepsilon_a \sigma T_a^4, \quad (2-7)$$

where  $\varepsilon_a$  is emissivity of air, and  $\sigma$  the Stefan Boltzmann constant ( $2.07 \times 10^{-7} \text{ kJ m}^{-2} \text{ h}^{-1} \text{ K}^{-4}$ ). The emissivity of air is estimated using Satterlund's (1979) equation for clear conditions. The presence of clouds increases downward longwave radiation. This is modeled by estimating the cloud cover fraction based on the Bristow and Campbell (1984) atmospheric transmission factor. The outgoing longwave radiation is calculated using the snow surface temperature:

$$Q_{le} = \varepsilon_s \sigma T_s^4, \quad (2-8)$$

where  $\varepsilon_s$  is emissivity of snow (0.99), and  $T_s$  is the temperature (K) of snow surface.

The latent heat flux,  $Q_e$  and sensible heat flux,  $Q_h$  are modeled using bulk aerodynamic formulae (Anderson, 1976):

$$Q_h = \rho_a C_p (T_a - T_s) K_h \quad (2-9)$$



and

$$Q_e = \rho_a h_v (q_s - q_a) K_e, \quad (2-10)$$

where  $\rho_a$  is the density of air,  $C_p$  is the specific heat of air at constant pressure (1.005 kJ kg<sup>-1</sup> °C<sup>-1</sup>),  $h_v$  is the latent heat of vaporization (sublimation) of ice (2834 kJ kg<sup>-1</sup>),  $q_a$  is the air specific humidity,  $q_s$  is the specific humidity at the snow surface which is assumed to be saturated relative to the vapor pressure over ice (e.g., Lowe, 1977), and  $K_h$  and  $K_e$  are turbulent transfer conductances for sensible and latent heat, respectively. Under neutral atmospheric conditions  $K_e$  and  $K_h$  are given by

$$K_n = \frac{k_v^2 u}{[\ln(z_m / z_0)]^2} \quad (2-11)$$

where  $z_m$  is the measurement height for wind speed, air temperature, and humidity,  $u$  is the wind speed,  $k_v$  is von Kármán's constant (0.4), and  $z_0$  is the aerodynamic roughness. When there is a temperature gradient near the surface, buoyancy effects may enhance or dampen the turbulent transfers, necessitating adjustments to  $K_n$ . We use

$$K_h = K_n \frac{1}{\Phi_M \Phi_H} \quad (2-12)$$

and

$$K_e = K_n \frac{1}{\Phi_M \Phi_E} \quad (2-13)$$

where  $\Phi_M$ ,  $\Phi_H$ ,  $\Phi_E$  are the stability functions for momentum, sensible heat, and water vapor, respectively. The stability functions are estimated using the bulk Richardson number:

$$R_i = \frac{gz_m(T_a - T_s)}{\frac{1}{2}(T_a + T_s)u^2}, \quad (2-14)$$

where  $g$  is gravity acceleration ( $9.8 \text{ m s}^{-2}$ ). For stable conditions ( $R_i > 0$ ), we use the approximation of Price and Dunne (1976),

$$\frac{1}{\Phi_M \Phi_H} = \frac{1}{\Phi_M \Phi_E} = \frac{1}{1 + 10R_i}. \quad (2-15)$$

For unstable conditions ( $R_i < 0$ ) we use (Dyer and Hicks, 1970; Anderson, 1976; Jordan, 1991),

$$\frac{1}{\Phi_M \Phi_H} = \frac{1}{\Phi_M \Phi_E} = (1 - 16R_i)^{0.75}. \quad (2-16)$$

Because information for estimating turbulence under extremely unstable conditions is poor, we capped the value of  $1/\Phi_M\Phi_H$  at 3, which occurs near  $R_i = -0.2$ . Anderson (1976) shows that iterative solutions of Deardorff's (1968) empirical equations begin to level off for more strongly unstable situations as the value of 3 is approached. These approximations assume that  $K_h=K_e$ .

In early applications of the UEB model that did not include capping of  $1/\Phi_M\Phi_H$  at 3 we found that large temperature differences and low wind speeds resulted in unreasonable correction factors, beyond the range for which they had been developed, so we included in the code a factor  $F_{stab}$  that controls the extent to which the stability corrections are applied:

$$K_{adj} = K_n + F_{stab}(K - K_n) \quad (2-17)$$

where  $K$  represents either  $K_h$  or  $K_e$ , and  $K_{adj}$  is used in equations 2-9 and 2-10 when calculating the energy balance.

Putting  $F_{stab} = 0$  uses neutral conductances. Putting  $F_{stab} = 1$  gives the full stability corrections and  $F_{stab}$  between 0 and 1 interpolates between these. Currently we recommend using  $F_{stab} = 1$ .

A unique characteristic of the UEB model is its separate representation of surface temperature and average snowpack temperature. This facilitates good modeling of surface energy exchanges that depend on snow surface temperature, while retaining a parsimonious single layer model. In this paper we introduce new parameterizations for

the snow surface temperature. The sum of energy fluxes in equation 2-1 from above the snowpack are referred to as the surface energy forcing.

$$Q_{forcing}(T_s) = Q_{sn} + Q_{li} + Q_h(T_s) + Q_e(T_s) + Q_p - Q_{le}(T_s) \quad (2-18)$$

The sensible heat, latent heat, and outgoing longwave radiation are functionally dependent on the surface temperature,  $T_s$ . In the original model, the heat conducted into the snow,  $Q_{cs}$ , is calculated as a function of the snow surface temperature,  $T_s$ , and average snowpack temperature,  $T_{ave}$ .

$$Q_{cs}(T_s, T_{ave}) = k \rho_s C_i \frac{(T_s - T_{ave})}{Z_e} = K_s \rho_s C_i (T_s - T_{ave}) \quad (2-19)$$

where  $\rho_s$  is the snow density ( $\text{kg m}^{-3}$ ),  $k$  the snow thermal diffusivity ( $\text{m}^2 \text{h}^{-1}$ ),  $Z_e$  the effective depth over which the temperature gradient acts (m), and  $K_s = k/Z_e$  is termed snow surface conductance. In the original model, because there is uncertainty in values for  $Z_e$  and  $k$ ,  $K_s$  was used as a calibration parameter.

The energy balance at the surface is given by

$$Q_{cs}(T_s, T_{ave}) = Q_{forcing}(T_s). \quad (2-20)$$

Equation 2-20, representing a balance between surface forcing and gradient driven conduction into the snow, is solved numerically for  $T_s$  using the Newton-Raphson

method. This is what we mean when we refer to an equilibrium gradient solution for surface temperature. Physically,  $T_s$  is constrained to be no greater than  $0^\circ\text{C}$  when there is snow present. When the equilibrium solution produces a solution of  $T_s > 0^\circ\text{C}$ , this means that conduction into the snow cannot accommodate all the energy input through surface forcing. The extra energy will produce meltwater at the surface, which then infiltrates into the lower parts of the snowpack and if  $U < 0$  refreezes, representing the meltwater advection process for transport of energy into the snow. In these cases the surface energy flux terms in equation 2-1 are calculated using  $T_s = 0^\circ\text{C}$  to model the snow energy content change.

This section described the mass and energy balance equations, the quantification of energy components, and the parameterization of the snow surface temperature used in the original UEB snowmelt model (Tarboton *et al.*, 1995; Tarboton and Luce, 1996). The next section describes the theory for heat conduction into an infinite domain with sinusoidal surface forcing. The approximations of surface heat conduction into snow are presented in the context of this theory and include the gradient approach used in the original UEB snowmelt model and the force restore and modified force restore approaches suggested by Luce (2000), Luce and Tarboton (2001). These have been implemented in the new UEB snowmelt model.

## ALTERNATIVE MODELS OF SURFACE HEAT CONDUCTION

Heat flow in a snowpack can be described using the diffusive heat transfer equation and assuming homogeneity of snow properties (Yen, 1967)

$$\frac{\partial T}{\partial t} = k \frac{\partial^2 T}{\partial z^2}, \quad (2-21)$$

where  $T$  is the temperature ( $^{\circ}\text{C}$ ),  $z$  is depth relative to snow surface (m), and  $k$  is the thermal diffusivity of snow ( $\text{m}^2 \text{h}^{-1}$ ). Thermal diffusivity is related to thermal conductivity and specific heat by

$$k = \frac{\lambda}{C_i \rho_s}, \quad (2-22)$$

where  $\lambda$  is the thermal conductivity of snow ( $\text{kJ m}^{-1} \text{K}^{-1} \text{h}^{-1}$ ). For semi-infinite boundary conditions ( $0 < z < \infty$ ) with sinusoidal temperature fluctuation at the upper boundary ( $z=0$ ):

$$T(0, t) = \langle T \rangle + A \sin(\omega t), \quad (2-23)$$

the differential equation 2-21 has solution (Berg and McGregor, 1966):

$$T(z, t) = \langle T \rangle + A \exp\left(-z \sqrt{\frac{\omega}{2k}}\right) \sin\left(\omega t - z \sqrt{\frac{\omega}{2k}}\right) \quad (2-24)$$

In this solution,  $A$  is the amplitude of the imposed temperature fluctuation at the surface,  $\omega$  is the frequency, and  $\langle T \rangle$ , the average about which surface temperature fluctuations are centered. At the snow surface, the primary forcing is diurnal, suggesting  $\omega = \omega_I = 2\pi/24 \text{ h}^{-1}$ .

By defining  $d_1 = \sqrt{\frac{2k}{\omega_1}}$  as the damping depth corresponding to frequency  $\omega_1$ , we can

rewrite equation 2-24 as:

$$T(z,t) = \langle T \rangle + Ae^{-\frac{z}{d_1}} \sin\left(\omega_1 t - \frac{z}{d_1}\right). \quad (2-25)$$

Equation 2-25 indicates that temperature oscillations are damped by a factor  $1/e$  for each increment of depth  $d_1$ , and the time-averaged temperature at each depth is  $\langle T \rangle$ , so at great depth, the average temperature is  $\langle T \rangle$ . Equation 2-25 can be differentiated on the depth ( $z$ ) to evaluate the temperature gradient, and the surface temperature flux (at  $z=0$ ) can be written as:

$$Q_{cs} = -\lambda \frac{\partial T}{\partial z}(0,t) = \frac{\lambda A}{d_1} [\sin(\omega_1 t) + \cos(\omega_1 t)]. \quad (2-26)$$

The time derivative of temperature in equation 2-25 can be written as:

$$\frac{\partial T}{\partial t} = Ae^{-\frac{z}{d_1}} \omega_1 \cos\left(\omega_1 t - \frac{z}{d_1}\right). \quad (2-27)$$

Recognizing that  $\omega_1 \cos(\omega_1 t)$  is the derivative of  $\sin(\omega_1 t)$  and substituting into equation 2-26 yields:

$$Q_{cs} = \frac{\lambda}{d_1 \omega_1} \frac{\partial T}{\partial z}(0, t) + \frac{\lambda}{d_1} (T(0, t) - \langle T \rangle). \quad (2-28)$$

This expresses the surface heat flux as a function of both the time derivative of surface temperature and the difference between the surface temperature and average temperature at great depth. This analytic solution for the simplified setting of a semi-infinite domain with sinusoidal surface temperature forcing serves as the basis for the numerical approximations of surface temperature,  $T_s$ , that are evaluated.

#### *Equilibrium gradient approach*

The original equilibrium gradient method of surface temperature parameterization used in equation 2-21 can be seen to be an approximation to equation 2-28 that ignores the time derivative of the surface temperature term and approximates the average temperature at great depth  $\langle T \rangle$  by the snowpack average temperature,  $T_{ave}$ , while using actual surface temperature,  $T_s$ , in place of the sinusoidal forcing  $T(0, t)$ . This method approximates the energy flux as a gradient between the surface temperature and average temperature of snow over an effective distance  $Z_e$ , equivalent to  $d_1$ . In the original UEB model  $Z_e$  was absorbed into the parameter  $K_s$  that was calibrated, however here  $d_1$  is related to the diurnal frequency, so to retain this calibration capability we use  $Z_e = r d_1$  (i.e., the damping depth  $d_1$  scaled by a dimensionless adjustable parameter  $r$ ) and write equation 2-21 in the form showing the similarity to equation 2-28:



$$Q_{cs} = \frac{\lambda}{rd_1} (T_s - T_{ave}). \quad (2-29)$$

### *Force-restore approach*

The force-restore parameterization (e.g. Deardorff, 1978; Dickinson *et al.*, 1993; Hu and Islam, 1995) is:

$$Q_{cs} = \frac{\lambda}{d_1} \frac{1}{\omega_1 \Delta t} (T_s - T_{slag1}) + \frac{\lambda}{rd_1} (T_s - T_{ave}). \quad (2-30)$$

Here  $\Delta t$  is the time step and  $T_{slag1}$  is the surface temperature of snow in the previous time step. A finite difference approximation has been used for the time derivative and  $\langle T \rangle$  has been replaced by the depth average snowpack temperature  $T_{ave}$ . Again, we have scaled the damping depth by a parameter  $r$ .

### *Modified force-restore approach*

Luce (2000) and Luce and Tarboton (2001; submitted 2004) found that the diurnal cycle may be superimposed on a temperature gradient that varied at a longer weekly to seasonal time scales, causing variations in the temperature gradient and heat fluxes with depth. They found occasions where there was greater spectral power in the lower frequency variability. Luce (2000) and Luce and Tarboton (2001; submitted 2004) suggested that the heat flux and the surface temperature could be estimated using the following modification to the force-restore equation:

$$Q_{cs} = \frac{\lambda}{d_1} \frac{1}{\omega_1 \Delta t} (T_s - T_{s_{lag1}}) + \frac{\lambda}{rd_1} (T_s - \bar{T}_s) + \frac{\lambda}{d_{lf}} (\bar{T}_s - \bar{T}_{ave}), \quad (2-31)$$

where  $\bar{T}_s$  is the average surface temperature estimated for the previous 24 hours, and  $\bar{T}_{ave}$  is the 24 hour time average of the depth average snowpack temperature. The 3<sup>rd</sup> term represents the superimposed gradient, a lower frequency effect, approximated using an equilibrium gradient approach similar to in equation 2-28. In this parameterization  $d_{lf}$  is the dampening depth associated with the longer time scale forcing having lower

frequency  $\omega_{lf}$ , i.e.  $d_{lf} = \sqrt{\frac{2k}{\omega_{lf}}}$ . The introduction of the third term to account for the

lower frequency effect is to improve the representation of surface temperature in the presence of a large gradient that overwhelms temperature gradient cycling on a daily scale. In equation 2-31 since the appropriate low frequency parameter ( $\omega_{lf}$ ) is not known *a priori*, Luce (2000) and Luce and Tarboton (2001; submitted 2004) suggested that  $d_{lf}$  be calibrated.

#### *Theory of meltwater refreezing*

The approaches described above solve for surface temperature based upon a balance between surface forcing and the capacity of the snow near the surface to conduct heat into or out of the snowpack. However, during a cooling period following melting where there is liquid water present in the snow, the depression of snow surface temperature is inhibited by the energy required to refreeze liquid water near the surface before a temperature gradient can be established and conduction can occur. The net

effect of this is that when there is liquid water present the snow surface stays warmer longer and heat loss at night and in cooling periods is more rapid. To accommodate this effect we have developed a parameterization for the penetration of a refreezing front and conduction of heat between the surface and refreezing front while there is liquid water present in the snow.

When snow energy content  $U$  is greater than 0, liquid water exists in the snowpack. The snowpack is assumed to be isothermal at 0 °C. Using the relationship between energy content and liquid fraction (Equation 2-5 b), the equivalent depth of liquid water in the snowpack  $w_m$  (m) is calculated as:

$$w_m = L_f W = \frac{U}{\rho_w h_f}. \quad (2-32)$$

The capillary holding capacity of the snow is defined as mass fraction liquid holding capacity  $L_c$  times snow water equivalent  $L_c W$ , which implies that the maximum density of capillary water ( $\rho_m$ ) is  $\rho_m = \frac{L_c W}{D} = L_c \rho_s$ , where  $D$  is the depth of snowpack.

We assume that prior to melt outflow, when the liquid water content is less than the capillary holding capacity, the meltwater is held at the maximum density of capillary water in the upper portion of the snowpack. With this assumption the depth to which meltwater has penetrated is:

$$d_w = \frac{w_m \rho_w}{\rho_m} = \frac{U}{\rho_w h_f} \frac{\rho_w}{\rho_m} = \frac{U}{\rho_m h_f}. \quad (2-33)$$

This describes the state of the snowpack prior to the onset of a refreezing episode during which  $Q_{forcing}$  is negative. The negative forcing will result in refreezing that penetrates down from the surface as illustrated in Figure 2-1. The rate of increase of the depth to the refreezing front,  $d_r$ , is given by

$$\frac{dd_r}{dt} = -\frac{Q(T_s)}{\rho_m h_f}, \quad (2-34)$$

where  $Q(T_s)$  is the heat flux just above the refreezing front, here indicated to be a function of surface temperature  $T_s$ . The sign convention is that heat flux is positive into the snow which is why there is a negative sign in equation 2-34.

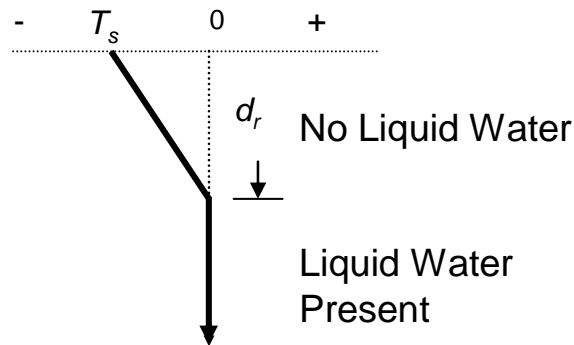


Figure 2-1 Schematic illustration of temperature profile during the downward propagation of a refreezing front

We assume a linear temperature gradient above the refreezing front with  $Q(T_s)$  given by

$$Q(T_s) = \lambda \frac{T_s}{d_r}. \quad (2-35)$$

We use an equilibrium approach for surface temperature that balances the surface forcing with the conduction into the snow above the refreezing front, neglecting any heat stored in the snow between the refreezing front and the surface (as this will be small because the heat capacity of snow is less than the latent heat of fusion). This is written

$$Q(T_s) = Q_{forcing}(T_s). \quad (2-36)$$

To solve for  $d_r(t)$  the dependence of  $Q_{forcing}(T_s)$  on  $T_s$  is linearized,

$$Q_{forcing}(T_s) = a - bT_s. \quad (2-37)$$

Here  $a$  is the forcing surface energy flux when the surface temperature of snow is  $0^\circ\text{C}$ .  $b$  is the slope of surface forcing flux to surface temperature function. This is a positive value since  $Q(T_s)$  decreases with  $T_s$ .  $a$  is obtained by putting  $T_s=0$  into  $Q_{forcing}(T_s)$ .  $b$  is obtained by putting a small negative (below freezing)  $T_s$  into  $Q_{forcing}(T_s)$  and solving equation 2-37. If  $a$  is greater than 0, then the surface forcing is positive and meltwater is

being generated at the surface so  $d_r$  is set to 0. When  $a$  becomes less than 0, the snowpack starts refreezing. Combining equations 2-35 and 2-37 gives:

$$\frac{\lambda}{d_r} T_s = a - bT_s, \quad (2-38)$$

$T_s$  can then be expressed as:

$$T_s = \frac{a}{\frac{\lambda}{d_r} + b}. \quad (2-39)$$

Substituting this  $T_s$  into equation 2-34 we have:

$$\frac{dd_r}{dt} = -\frac{Q(T_s)}{\rho_m h_f} = -\frac{a - \frac{abd_r}{\lambda + bd_r}}{\rho_m h_f} = -\frac{\lambda a}{\rho_m h_f (\lambda + bd_r)}, \quad (2-40)$$

Integrating equation 2-40 starting from the initial refreezing depth  $d_{r1}$  during a time step, we get:

$$\lambda d_r + \frac{b}{2} d_r^2 - (\lambda d_{r1} + \frac{b}{2} d_{r1}^2) = -\frac{a\lambda}{\rho_m h_f} \Delta t. \quad (2-41)$$

This has the following solution:

$$d_r = \frac{-\lambda + \sqrt{\lambda^2 + 2b(\lambda d_{r1} + \frac{b}{2} d_{r1}^2 - \frac{a\lambda\Delta t}{\rho_m h_f})}}{b}. \quad (2-42)$$

Only the positive root has been retained since only positive values of  $d_r$  are physically interpretable and  $b$  is a value greater than 0. When  $d_r$  is greater than  $r d_1$ , the effective depth associated with diurnal temperature fluctuations, or all meltwater is refrozen, the model reverts back to the surface temperature parameterization without refreezing of meltwater as described above.

*Adjustment of thermal conductivity,  $\lambda$ ,  
for shallow snowpack*

In equations 2-19, 2-29, 2-30, and 2-31 the temperature gradient is calculated over an effective depth ( $Z_e = r d_1$ ) estimated from the depth of penetration of surface temperature forcing at a diurnal frequency. When the snow is shallow this depth may extend into the ground below the snow cover. In such cases the thermal conductivity used in the surface temperature parameterizations above needs to reflect the combined conductivity of snow and soil below. We therefore take the effective thermal conductivity of the snowpack,  $\lambda_e$ , as the harmonic mean to the effective depth,  $Z_e$ , where the amplitude is damped by the same factor as it would be for deep snow (see Figure 2-2). In deep snow the amplitude of diurnal temperature fluctuations at depth  $Z_e$  is damped by (Equation 2-21)  $e^{-Z_e/d_1} = e^{-r}$ . In the combined snow/soil system, given  $r$ , we first solve for the depth into the soil  $z_2$  at which the amplitude of diurnal temperature

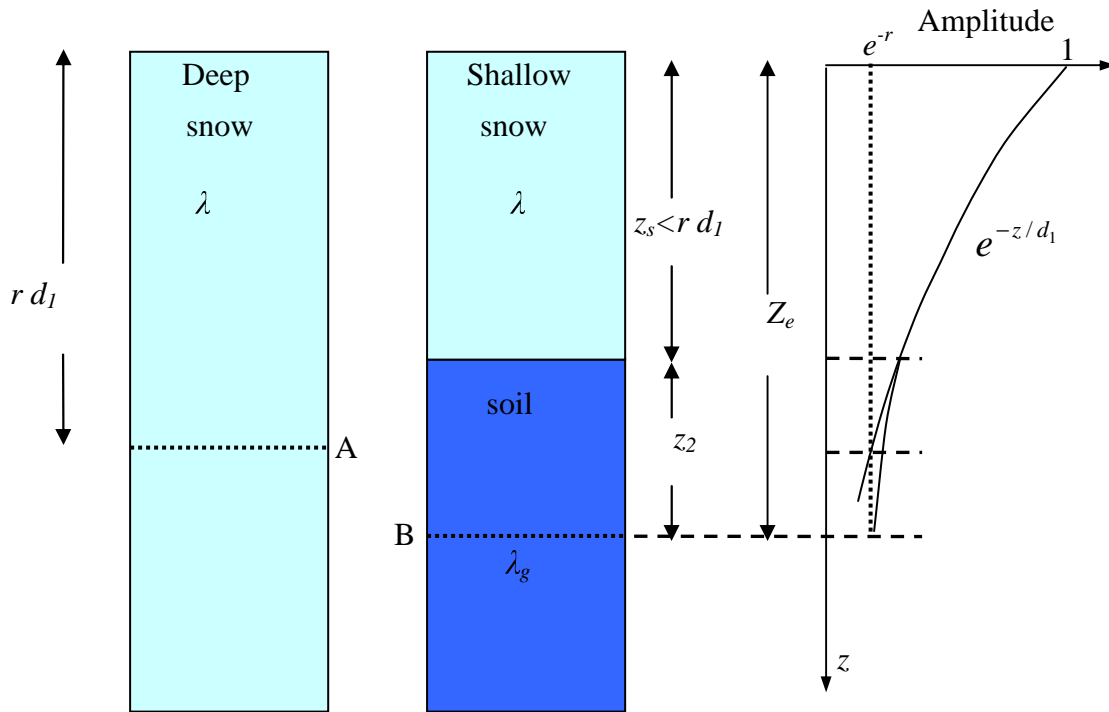


Figure 2-2 Heat conduction scheme for combined snow/soil system. The dashed lines at depths A and B indicate the depths at which temperature fluctuation amplitude is damped by  $e^{-r}$  in the deep snow and combined snow/soil system respectively

fluctuations is damped by this same factor  $e^{-r}$ . Then  $\lambda_e$  is obtained by taking the harmonic mean to this depth. The thermal diffusivity of the ground below the snow,  $k_g$ , is related to the thermal conductivity,  $\lambda_g$ , heat capacity,  $C_g$  and density,  $\rho_g$  of the ground through:

$$k_g = \frac{\lambda_g}{C_g \rho_g} \tag{2-43}$$

The diurnal damping depth,  $d_g$ , associated with this ground thermal diffusivity is:



$$d_g = \sqrt{\frac{2k_g}{\omega_1}}. \quad (2-44)$$

The amplitude of diurnal temperature fluctuation at depth  $z_2$  into the ground, relative to the surface temperature fluctuation is therefore damped by  $e^{-z_s/d_1} e^{-z_2/d_g}$ . Equating this to  $e^{-r}$  we obtain:

$$\frac{z_s}{d_1} + \frac{z_2}{d_g} = r. \quad (2-45)$$

Thus  $z_2$  is:

$$z_2 = d_g \left( r - \frac{z_s}{d_1} \right). \quad (2-46)$$

The effective thermal conductivity,  $\lambda_e$ , and the effective depth,  $Z_e$ , for the shallow snowpack are then estimated through:

$$Z_e = z_s + z_2 = z_s + d_g \left( r - \frac{z_s}{d_1} \right), \quad (2-47)$$

$$\frac{1}{\lambda_e} = \frac{\frac{z_s}{\lambda} + \frac{z_2}{\lambda_g}}{Z_e}, \quad (2-48)$$

equation 2-48 is used to obtain the effective thermal conductivity near the surface when the snow is shallow. This is used in the parameterizations for surface temperature that calculate the surface heat flux between the snowpack and the atmosphere as well as conduction into the snow.

Summarizing our model improvements, the force restore and modified force restore approach have been included in the new UEB snowmelt model to better parameterize the surface temperature of snow. A new refreezing scheme was developed to model heat loss following partial melt through modeling the penetration of a refreezing front into the snowpack. The model was changed to adjust effective thermal conductivity used in the surface temperature parameterization for a shallow snowpack where the penetration depth for diurnal temperature fluctuations extends into the ground.

## STUDY SITES AND DATA

The new UEB model was calibrated and tested using data from three locations in the Western U.S.

### *1. Utah State University Drainage and Evapotranspiration Experimental Farm.*

The USU drainage and evapotranspiration experimental farm is located in Cache Valley near Logan, Utah, USA (41.6° N, 111.6° W, 1350 m elevation). The weather station and instrumentation are in a small fenced enclosure at the center of an open field

with no obstructions to wind in any direction for at least 500 m. Cache Valley is a flat-bottomed valley surrounded by mountains that reach elevations of 3000 m. During the period of this experiment the ground was snow covered from November 20, 1992 to March 22, 1993. Air temperatures ranged from  $-23^{\circ}\text{C}$  to  $16^{\circ}\text{C}$  and there was 190 mm of precipitation (mostly snow, but some rain). The snow accumulated to a maximum depth of 0.5 m with maximum water equivalent of 0.14 m. Data collected included measurements of snow water equivalent, snow surface temperature, temperatures within the snowpack and the upper soil layer, and the meteorological variables necessary to drive UEB.

Shallow soil temperatures were measured using two thermocouples placed below the ground surface at depths of 25 mm and 75 mm. Another thermocouple was placed at the ground surface. The snowpack temperature was measured using thermocouples suspended at 50, 125, 200, 275 and 350 mm above the ground surface on fishing line strung between two upright posts. These temperature measurements were corrected for high frequency fluctuations in the panel reference temperature by Luce (2000). Snowpack surface temperature was measured with two Everest Interscience model 4000 infrared thermometers. Internal energy content of the snowpack was calculated from the temperature profile of the snowpack and upper soil layer accounting for the near surface nonlinearity through an analytic integral of equation 2-18 as described by Luce (2000), Luce and Tarboton (submitted 2004). Snow water equivalent was measured using a snow tube. Snow pits provided measurements of density and depth. On each measurement occasion snow water equivalent was measured at eight locations (fewer when snow had

disappeared from some) and averaged. The experiment is described more fully in Tarboton (1994) and Luce (2000).

A complete dataset including the air temperature, wind speed, relative humidity, incident shortwave radiation, outgoing shortwave radiation, temperature profile through the snow and surface temperature of snowpack was available from January 26, 1993 to March 22, 1993 when the snow completely melted away.

### *2. Central Sierra Snow Laboratory*

The Central Sierra Snow Laboratory located 1 km east of Soda Springs, California, measures and archives comprehensive data relevant to snow. It is located at 39°19' N, 120°22' W, at an elevation of 2100 m. The meteorological data is reported each hour and consists of temperature, radiation, humidity, precipitation, and wind measurements at two levels in a 40 m by 50 m clearing and in mixed conifer fir forest with 95% forest cover. Snow depths and water equivalent are measured daily (except on weekends) and eight lysimeters record melt outflow each hour. The data at the open site used in this study was from November 14, 1985 to July 1, 1986 when the snowpack disappeared at the open site. A total of 124 snow water equivalent measurements in addition to hourly lysimeter data were available for this time period.

### *3. Niwot Ridge, Colorado*

Another dataset used to test the new model comes from Subnivean snow laboratory at Niwot Ridge on the eastern slope of the Front Range of Colorado (3517 m MSL, 40°03' N, 105°35' W) collected during the 1995~1996 winter seasons. The instrument site is located in a relatively flat area above the treeline within a broad saddle of the ridge. The high elevation and exposure of Niwot Ridge, and typically dry

atmospheric conditions result in large clear-sky atmospheric transmissivity, increased solar insolation, and low magnitudes of incident longwave radiation, low air temperatures, and high wind velocities. The dataset includes measurements of air temperature, wind speed, relative humidity, and incident shortwave radiation from April 28, 1996 to September 30, 1996 with a time step of 2 hours. Measured lysimeter data is also available although there are concerns as to how representative it is due to preferential flow paths (finger-flow) in the snow resulting in under-catch of meltwater (Cline, 1997b).

## RESULTS

The UEB model was designed to be physically-based and require minimal calibration for different locations. The original model was calibrated and tested against the data from Central Sierra Snow Laboratory (CSSL), USU drainage farm (USU DF), and Reynolds Creek Experimental Watershed (Tarboton *et al.*, 1995; Tarboton and Luce, 1996; Luce *et al.*, 1998; Prasad *et al.*, 2000). The new model with the new method of surface temperature parameterization was calibrated against the data from the USU DF and CSSL to adjust some parameters and reflect the model changes. The model was validated using the data from the Niwot ridge site.

Figure 2-3 shows the time series of measured snow, ground and snow surface temperatures at the USU Drainage Farm that were used to calculate the internal energy content of the snowpack. Because this measured internal energy of snow is only based on temperatures and does not account for any liquid water present, measured internal energy content is only comparable to modeled internal energy during cold periods when liquid water is not present. During warm periods, the modeled energy content is expected

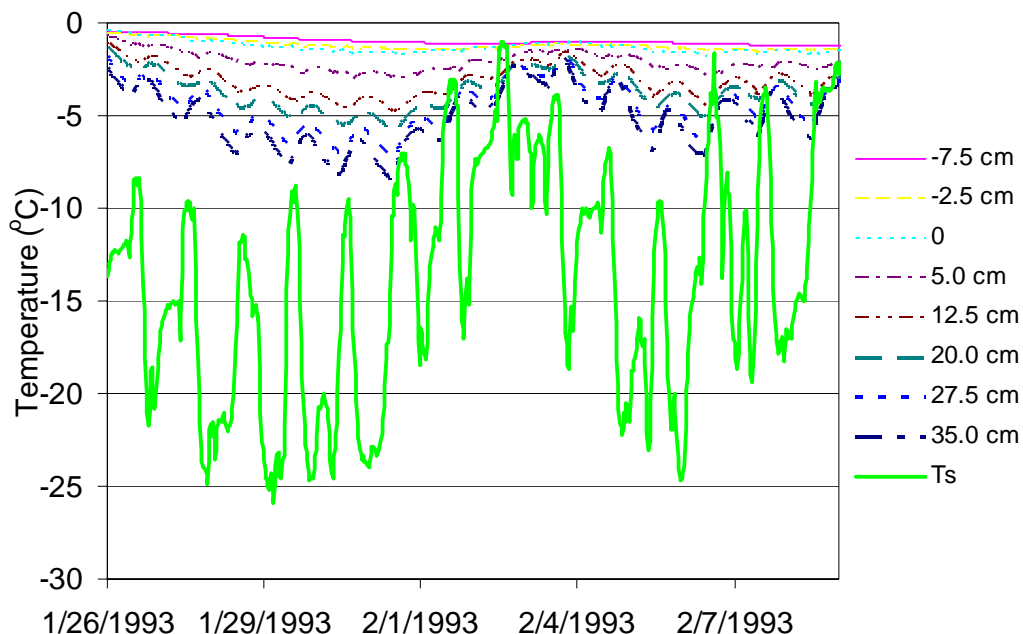


Figure 2-3 Measured snow, ground and snow surface temperatures.  $T_s$  is the measured surface temperature of snow from an infrared sensor. Other temperatures are from thermocouples labeled according to their height relative to the ground surface. Negative heights are below the ground surface and positive heights above the ground surface. 0 refers to the measured temperature at the ground surface

to go above zero while measured energy content remains close to (just below) zero. The three approaches for surface temperature approximation described above were included as options in the new UEB. (The original UEB model only had the gradient approach). The comparisons between the modeled and measured internal energy values (Figure 2-4) focus on periods when the snow is cold and liquid water is not present. These comparisons appear similar to the initial work of Luce (2000, Figure 2-5) and Luce and Tarboton (2001; submitted 2004) that indicates that the modified force restore snow surface temperature approximation compares best to the internal energy content of snowpack. However these results differ from the earlier work of Luce (2000) and Luce and Tarboton (2001; submitted 2004) in that the new results are complete model

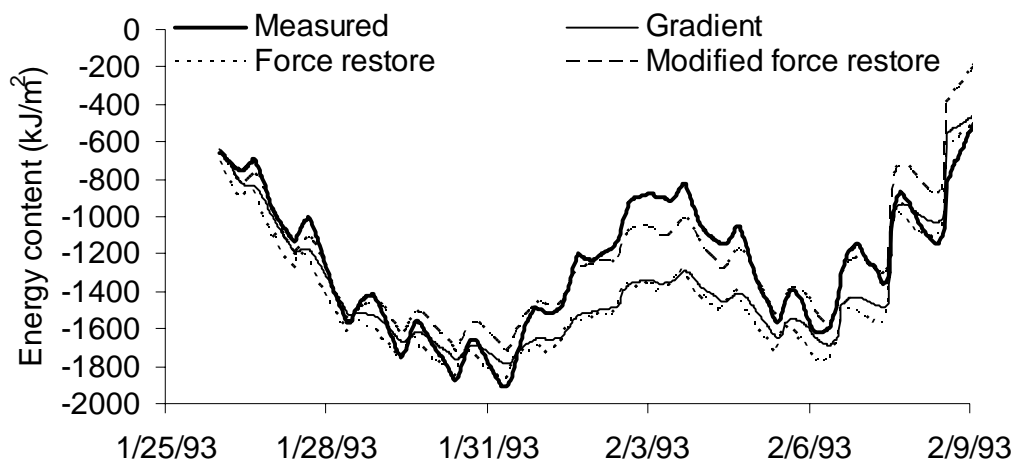


Figure 2-4 Comparisons of internal energy of snowpack during the first two freezing weeks at the USU Drainage Farm. Observed is the internal energy of snowpack calculated from the temperature profile (Figure 2-3). Gradient, Force restore, and Modified force restore represent the modeled internal energy of snowpack using the equilibrium approach, the force-restore approach, and the modified force restore approach, respectively

simulations driven by inputs of air temperature, humidity, radiation and wind with surface temperature calculated by the model. The earlier Luce work used the actual measured surface temperature to drive calculations of internal energy focusing only on the conduction into the snow. The parameters estimated by the earlier work of Luce were used in the model. Following this success of the modified force-restore surface temperature approach it was used in all subsequent work.

The new model was then calibrated using the data collected from USU drainage farm. Luce (2000) found evidence that the estimates of the incoming longwave radiation used in the original model (Tarboton *et al.*, 1995; Tarboton and Luce, 1996) were too low due to frequent inversions during much of the time. Luce (2000) then calculated the downward longwave radiation given all other energy components such as ground heat flux, net shortwave radiation, turbulent fluxes and outgoing longwave radiation. In the

calibration processes we used the measured shortwave radiation, the downward longwave radiation estimated by Luce (2000), and the measured ground heat flux to drive the new model. Table 2-1 lists the model parameters. We used as initial values, the calibrated parameters in the original UEB model. New parameters or parameters whose values were changed are indicated. Comparisons between modeled and measured variables at USU Drainage Farm are shown in Figures 2-5, 2-6, 2-7, and 2-8. Figure 2-5 includes measured snow water equivalent and the results from five model runs. Four

Table 2-1 Model parameter values

Parameters	Value
Thermal conductivity of snow $\lambda_s$	**0.33 kJ m <sup>-1</sup> K <sup>-1</sup> h <sup>-1</sup>
Thermal conductivity of soil $\lambda_g$	**6.5 kJ m <sup>-1</sup> K <sup>-1</sup> h <sup>-1</sup>
Low frequency forcing frequency $\omega_{lf}$	**0.0654 radians h <sup>-1</sup> ( $\omega_1/4$ )
Dimensionless damping depth factor $r$	**1
Threshold depth for fresh snow $d_{NewS}$	**0.002 m
Saturated hydraulic conductivity $K_{sat}$	*200 m h <sup>-1</sup>
Turbulent heat flux coefficient $F_{stab}$	*1
Surface aerodynamic roughness $z_o$	*0.01 m
Capillary retention fraction $L_c$	*0.02
Soil effective depth $D_e$	*0.1 m
Snow density $\rho_s$	*200 kg m <sup>-3</sup>
Ground heat capacity $C_g$	2.09 kJ kg <sup>-1</sup> K <sup>-1</sup>
Density of soil layer $\rho_g$	1700 kg m <sup>-3</sup>
Emissivity of snow $\varepsilon_s$	0.99
Temperature above which precipitation is rain $T_r$	3°C
Temperature below which precipitation is snow $T_{sn}$	-1 °C
Wind/air temperature measurement height $z_m$	2 m
Bare ground albedo $\alpha_{bg}$	0.25
New snow near infrared band reflectance $\alpha_{iro}$	65%
New snow visible band reflectance $\alpha_{vo}$	85%

\*\* These parameters are new, i.e., they were not present in the Original UEB.

\* These parameters were calibrated to have new values.



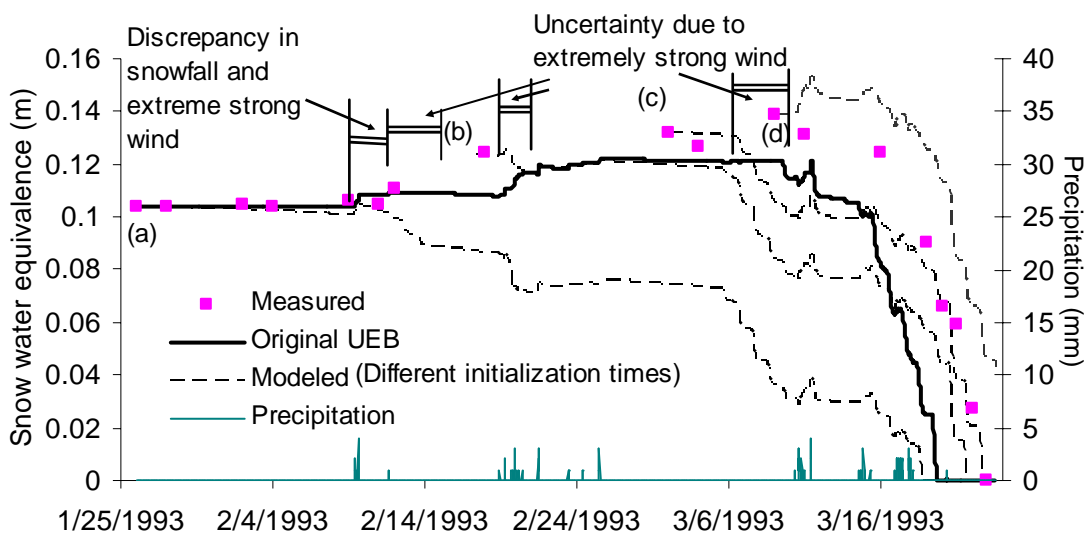


Figure 2-5 Comparisons of snow water equivalent in 1993 at USU Drainage Farm. The dashed lines are the modeled values with new model starts at different times. Precipitation input is shown (spiky line at the bottom) relative to the axis at the right. Letters (a) through (d) indicate points where the model was re-initialized following periods of likely erroneous inputs due to severe weather

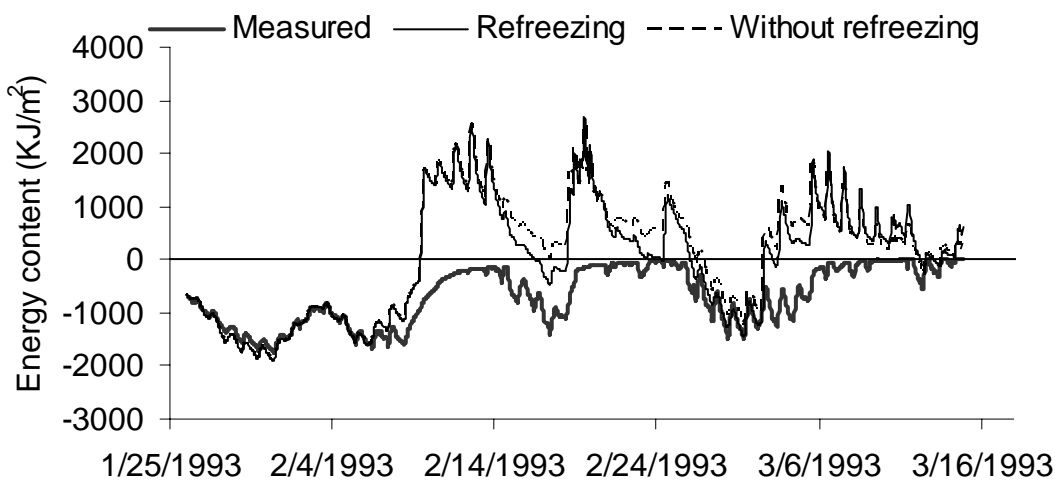


Figure 2-6 Comparisons of internal energy of snowpack in 1993 at USU Drainage Farm. The wide solid line is the measured values. Refreezing represents the modeled internal energy of snowpack with new UEB model. Without refreezing represents the model without the refreezing scheme

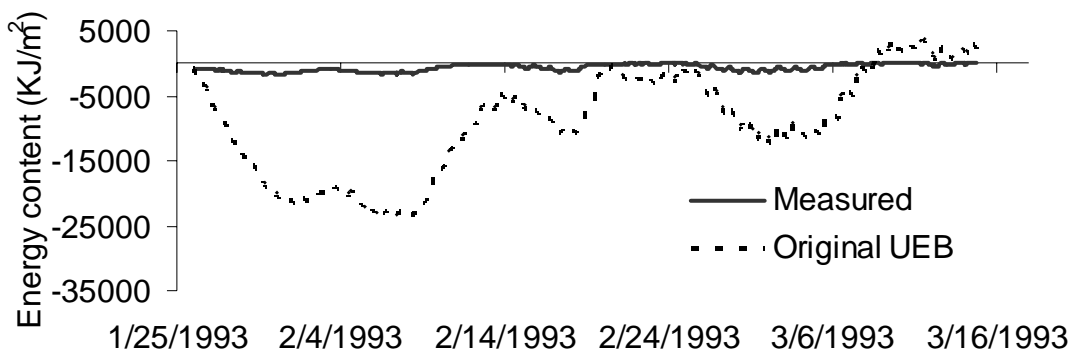


Figure 2-7 Comparisons between the measured and modeled internal energy of the snowpack at USU Drainage Farm in the new model and the original model

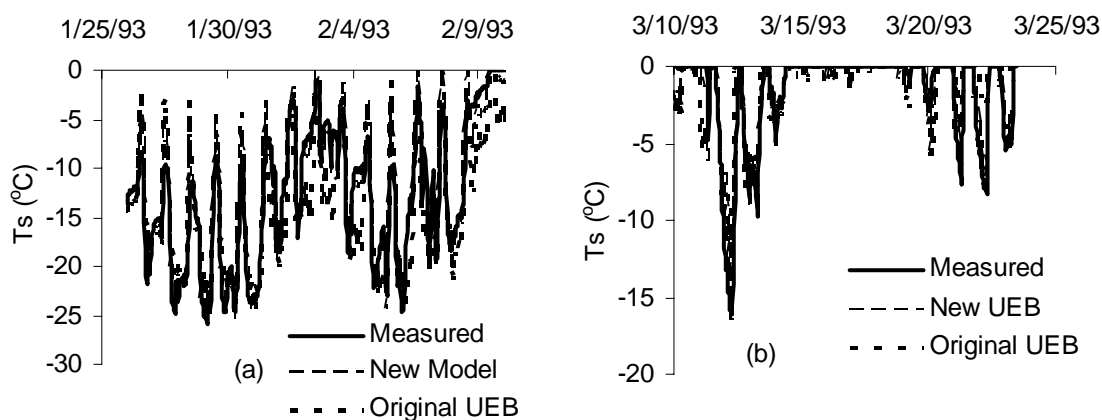


Figure 2-8 Comparisons of snow surface temperature in 1993 at USU Drainage Farm. (a) the first two subfreezing weeks, and (b) end of the modeling period when the snowpack is occasionally in an isothermal state

model runs are from the new UEB model using the parameters listed in Table 2-1, each initialized on a different date indicated by the letters (a) through (d) following periods of severe weather and likely erroneous inputs. The fifth model run is from the original UEB model with its original parameters reported by Tarboton (1994). Figure 2-6 shows the measured and modeled energy content from the new UEB model run initialized on

1/26/1993 together with a model run using the code prior to the addition of the refreezing parameterization. Figure 2-7 shows measured and modeled energy content from the original UEB model, indicating the rather large discrepancy in energy content. Figure 2-8 shows surface temperature comparisons for two time intervals chosen to be illustrative of periods prior to the onset of melt and during the period when snow is melting. The model runs shown in Figure 2-8 (a) were initialized on Jan. 26, 1993. The original UEB model run shown in Figure 2-8 (b) is the same as in Figure 2-8 (a) while the new UEB model run shown was initialized on Mar. 9, 1993.

The new model and the calibrated model parameters were then tested using the 1985 -1986 data from the CSSL, CA. Comparisons of the modeled and the measured variables are shown in Figures 2-9, 2-10, 2-11, and 2-12.

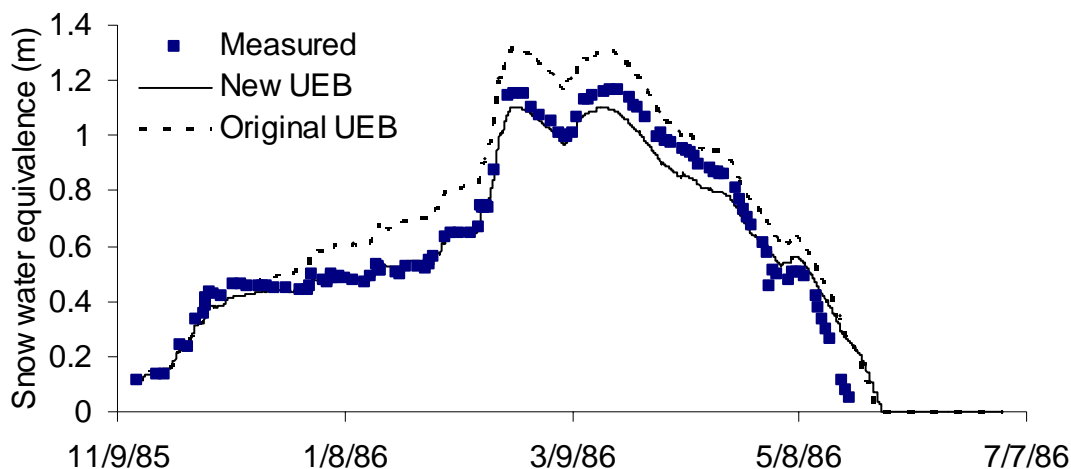


Figure 2-9 Comparisons of snow water equivalent in 1986 at CSSL

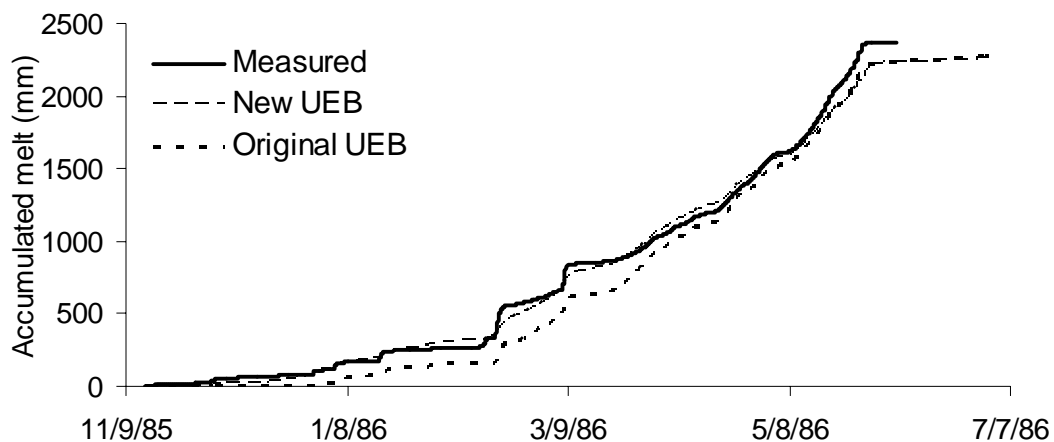


Figure 2-10 Comparisons of accumulative melt in 1986 at CSSL

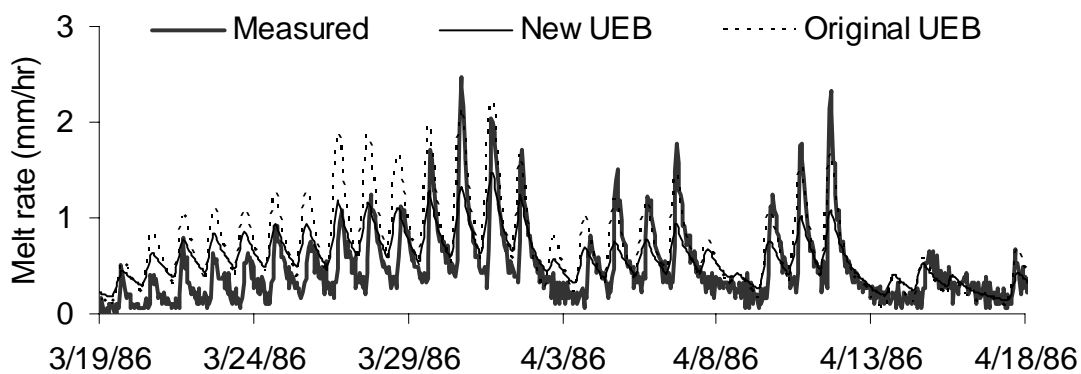


Figure 2-11 Comparisons of meltwater outflow rate in 1986 at CSSL

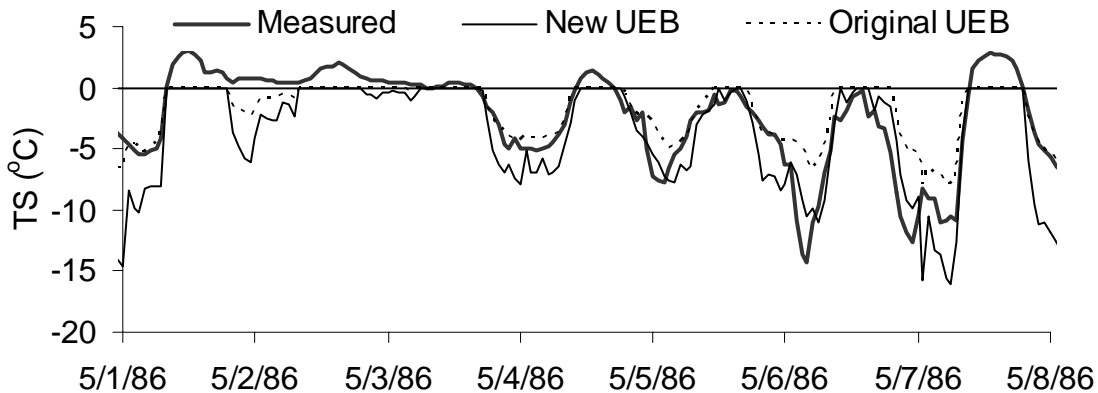


Figure 2-12 Comparisons of surface temperature of snow in 1986 at CSSL

The model was also tested using 1995 -1996 data from Subnivean Snow Laboratory at Niwot Ridge, CO where modeled and observed snow water equivalent are compared in Figure 2-13. The model was initialized with the beginning observed snow water equivalent value of 1.4 m. Melt outflows that totaled to 0.23 m were recorded. These were used to infer the snow water equivalent back through time. However, as shown in Figure 2-13, there is a big discrepancy between the measured total melt (0.23 m) and observed initial snow water equivalent (1.4 m). This is presumed to be due to preferential meltwater drainage flow paths in the snow as reported previously at this location (Cline, 1997a). An adjustment factor was calculated as  $\frac{W_{ini} + \sum p}{\sum m}$ , where  $W_{ini}$  is the initial measured snow water equivalent,  $\sum p$  is the total precipitation during the modeling time, and  $\sum m$  is the total measured meltwater outflow. This was used to adjust the measured melt outflows and infer snow water equivalent back through time.

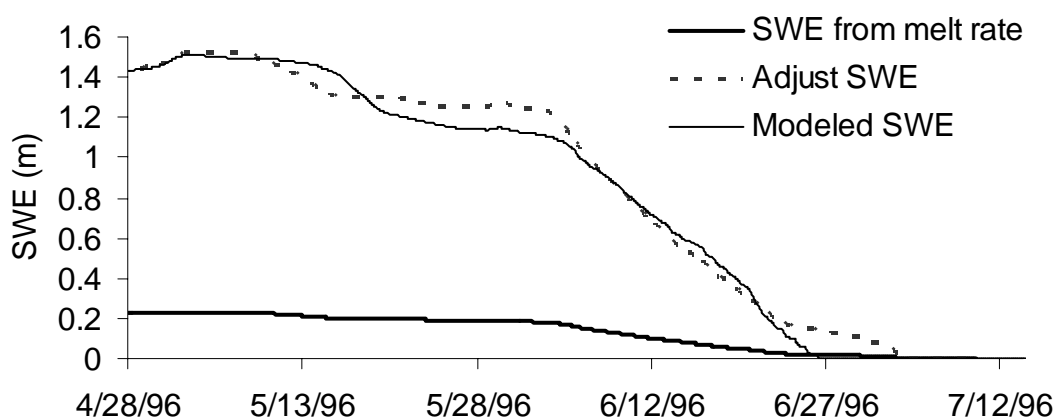


Figure 2-13 Comparisons of snow water equivalent in 1996 at Subnivean Snow Laboratory at Niwot Ridge watershed, CO

## DISCUSSION

The most significant change introduced into the model was the change to the surface temperature parameterization. Figure 2-9 shows the snow water equivalent data originally used to validate the UEB model, together with surface temperature comparisons, such as Figure 2-8 and melt outflow comparisons such as Figure 2-10. These results looked satisfactory at the time, but once measurements of internal energy (Figure 2-7) were obtained it was realized that the original UEB had problems representing internal energy and this deficiency was traced to the surface temperature parameterization by Luce (2000). Here with the inclusion of the Modified Force Restore approach suggested by Luce (2000) and Luce and Tarboton (2001; submitted 2004) modeled internal energy better represents measured internal energy as exemplified in Figure 2-4.

Density and thermal conductivity are the primary parameters introduced in the upgraded parameterization of surface temperature (Equations 2-31, 2-30, 2-29, and 2-22). In the literature there is variability in the values reported for thermal conductivity (Anderson, 1976; Lee, 1980; Gray and Male, 1981). Anderson (1976, p30 Figure 3.1) shows that the thermal conductivity of the snowpack may change over a wide range from  $0.15 \text{ kJ m}^{-1} \text{ h}^{-1} \text{ K}^{-1}$  to  $7.5 \text{ kJ m}^{-1} \text{ h}^{-1} \text{ K}^{-1}$  at a density of  $200 \text{ kg m}^{-3}$ . Lee (1980) also reported a range from  $0.25 \text{ kJ m}^{-1} \text{ h}^{-1} \text{ K}^{-1}$  at a density of  $100 \text{ kg m}^{-3}$  to  $5.3 \text{ kJ m}^{-1} \text{ h}^{-1} \text{ K}^{-1}$  at a density of  $700 \text{ kg m}^{-3}$ . Gray and Male (1981) indicated that thermal conductivity changes are nonlinear from  $0.18 \text{ kJ m}^{-1} \text{ h}^{-1} \text{ K}^{-1}$  at a density of about  $175 \text{ kg m}^{-3}$  to  $5.76 \text{ kJ m}^{-1} \text{ h}^{-1} \text{ K}^{-1}$  at a density of  $800 \text{ kg m}^{-3}$ .

The UEB model retains a degree of simplicity by not modeling surface density and thermal conductivity as time varying quantities. The values of  $\lambda_s = 0.33 \text{ kJ m}^{-1} \text{ h}^{-1} \text{ K}^{-1}$  and  $\rho_s = 200 \text{ kg m}^{-3}$  were calibrated to fit the internal energy measurements of Figure 2-4 considering the snow thermal properties inferred from frequency analysis by Luce and Tarboton (submitted 2004). Snow density is reflective of the density of the snow surface, involved in surface energy exchanges, rather than the snowpack as a whole.

A value of  $r=1$  was used for the dimensionless dampening depth factor. This nominal value corresponds to a gradient over the depth to which diurnal temperature fluctuations are attenuated by a factor of  $1/e$ . The soil thermal conductivity parameter also plays a role in the model when the snowpack is shallow (Equation 2-48) and was set to a value of  $6.5 \text{ kJ m}^{-1} \text{ h}^{-1} \text{ K}^{-1}$ , within the range of soil heat conductivity reported for the Logan Area (Hanks and Ashcroft, 1980; Luce, 2000). The low frequency forcing frequency value,  $w_{lf}$ , was set to  $0.0654 \text{ rad/h}$  based on Luce and Tarboton (submitted 2004).

It is interesting to note that with a new surface temperature parameterization calibrated to USU DF data, the model better represents the CSSL snow water equivalent data (Figure 2-9) and cumulative melt data (Figure 2-10) early in the season. The model now holds energy content closer to zero and is able to represent early season melt, a small discrepancy at CSSL that has been ignored until now. Small discrepancies still exist in the modeled snow water equivalent and the measurement snow water equivalent at the high accumulation period. This may be due to remaining model errors and some uncertainty (undercatch) in the snowfall measurements that are inputs. The disappearance date of the snow at CSSL was still modeled about one week later than the

observed, which may be due to errors in modeling the decrease of albedo perhaps due to contamination of the snow or due to the increase of longwave radiation from the nearby forest canopy.

Representation of observed snow water equivalent at USU DF in a single model run proved to be difficult. We attributed this to uncertainty and likely erroneous input quantities during windy and stormy severe weather periods. Snowfall was recorded in a heated unshielded precipitation gauge so is uncertain and likely to suffer from undercatch. There was also snow drifting resulting in accumulation and scour associated with strong winds, and griming of the instruments recording radiation.

One of the problems discovered with the original UEB model was that it offsets the bias due to the surface temperature parameterization by a bias in heat loss following surface melting; this is exemplified in Figure 2-6. Following a period of snowmelt, the observed energy content is observed to fall below 0 but the modeled energy content remained above 0. Without the refreezing parameterization surface temperature immediately drops in a cooling period, limiting the heat loss by reducing the outgoing longwave radiation. The parameterization of the refreezing front corrected this to some extent (Figure 2-6) keeping the surface temperature warmer and sustaining greater outgoing longwave radiation energy losses, the extra energy loss going to refreeze liquid water present and allow the model energy content to drop more in line with the observations.

Melt outflow rates were not measured at USU DF. The changes in surface temperature and refreezing parameterization changed the modeled amount of liquid water, which changed melt outflow. We used measured melt outflow at CSSL (Figure 2-



11) to adjust the snow hydraulic conductivity to  $200 \text{ m h}^{-1}$ , a value still within the range from  $20 \text{ m h}^{-1}$  to  $300 \text{ m h}^{-1}$  reported in the literature (Gray and Male, 1981). Liquid holding capacity was adjusted to 0.2 to better fit melt outflow.

$D_e$  and  $z_0$  were adjusted based on the research of Luce (2000) and Luce and Tartboton (submitted 2004) where a value of 0.1 m was suggested for the soil effective depth and a value 0.01 m suggested for the surface aerodynamic roughness of snow  $z_0$  in the calculation of turbulent heat flux.  $F_{stab}$  was taken as 1 to fully incorporate stability corrections in the turbulence parameterizations consistent with other work (Blöschl and Kirnbauer, 1991; Jordan, 1991; Dickinson *et al.*, 1993; Marks *et al.*, 1998; Jin *et al.*, 1999; Sun *et al.*, 1999).

The USU DF instrumentation included a net radiometer and downward and upward pointing pyranometers. Examination of albedo estimated from these measurements indicated that albedo was not being refreshed to new snow values following snowfall. This was corrected by changing the threshold of new snow water equivalent that restores albedo to the new snow cover,  $d_{NewS}$ , to 0.002 m; this was previously 0.01 m. This resulted in a more responsive modeling of albedo, consistent with observations (Figure 2-14). The offset between modeled and observed albedo in this figure is, we believe, due to downward pointing limited band pyranometers not being appropriate for measuring snow reflectance. However they do still provide us with relative measurements useful in quantifying the timing and responsiveness of albedo changes.

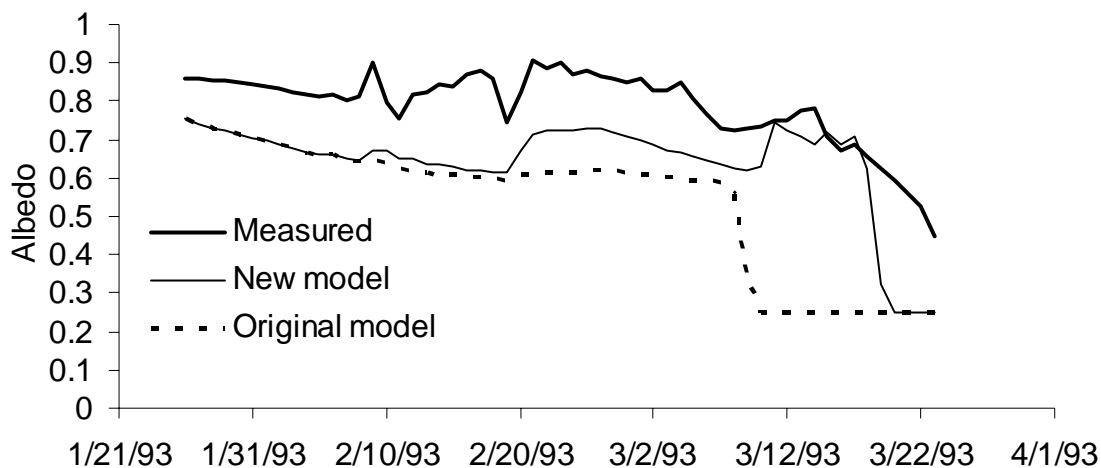


Figure 2-14 Comparison of albedo at USU drainage farm

As was observed at the USU drainage farm, the new model also gave a good approximation of the surface temperature of snow (Figure 2-12) at the CSSL snow laboratory. Both the new model and the original model perform well in approximating the surface temperature of snow at CSSL site. However, the new model corrects the offsets between the modeling of snow surface temperature and the modeling of the internal energy of the snowpack in the original model. Here we note that uncertainties exist in the measurements, e.g. the measurement of surface temperature of snow has positive value during some daytime periods. Better field measurements of the surface temperature would contribute to more precise snowmelt models.

Much of this modeling was motivated by a need to apply the model at Niwot ridge in Colorado, where driving weather inputs as well as measured melt rate was available. The comparison between modeled and measured snow water equivalent inferred from observed initial snow water equivalent and melt outflow is given in Figure 2-13. This shows that after the adjustment to correct the discrepancy between initial

snow water equivalent and measured melt that the back-calculated snow water equivalent compares well with modeled snow water equivalent. Due to the adjustment involved this is really only a check on the timing of the ablation due to snowmelt.

## CONCLUSIONS

Refinements to the parameterization of snow surface temperature were introduced into the single layer Utah Energy Balance snowmelt model. A modified force restore approach that had been previously suggested, but not implemented was incorporated, together with a parameterization for the penetration of a refreezing front during cold periods following melt. These modifications required adjusting some of the other calibrated model parameters. With these refinements, the model was better able to represent internal energy content and early and late season snowmelt. Previously reported problems the model had in representing internal energy were resolved. Through this modeling work the understanding of snow surface energy exchanges and how they can be more effectively modeled has improved.

The new UEB snowmelt model has been calibrated and tested against datasets from the USU Drainage Farm and CSSL snow laboratory and performed well at these two sites. However some discrepancies still exist between the modeled variables and the observations. Also some variables cannot be strictly compared or compared against a complete dataset. A more complete dataset of the liquid water content, together with continuous observation of snow water equivalent, snow surface temperature, melt, and depth, is necessary for a comprehensive test of the model improvements given here.

## REFERENCES

- Anderson EA. 1976. A Point Energy and Mass Balance Model of a Snow Cover. NOAA Technical Report NWS 19, U.S. Department of Commerce. 150 pp.
- Berg PW, McGregor JL. 1966. *Elementary Partial Differential Equations*. Holden-Day: Oakland.
- Blöschl G, Kirnbauer R. 1991. Point snowmelt models with different degrees of complexity - internal processes. *Journal of Hydrology* **129**: 127-147.
- Bras RL. 1990. *Hydrology, an Introduction to Hydrologic Science*. Addison-Wesley: Reading, MA.
- Bristow KL, Campbell GS. 1984. On the relationship between incoming solar radiation and the daily maximum and minimum temperature. *Agricultural and Forest Meteorology* **31**: 159-166.
- Cline DW. 1997a. Snow surface energy exchanges and snowmelt at a continental, midlatitude alpine site. *Water Resources Research* **33**(4): 689-701.
- Cline DW. 1997b. Effect of seasonality of snow accumulation and melt on snow surface energy exchanges at a continental alpine site. *Journal of Applied Meteorology* **36**: 22-41.
- Colbeck SC. 1989. Air movement in snow due to windpumping. *Journal of Glaciology* **35**(120): 209-213.
- Colbeck SC, Anderson EA. 1982. The Permeability of a Melting Snow Cover. *Water Resources Research* **18**(4): 904-908.
- Deardorff JW. 1968. Dependence of Air-Sea Transfer Coefficients on Bulk Stability. *Journal of Geophysical Research* **73**(8): 2549-2557.
- Deardorff JW. 1978. Efficient prediction of ground surface temperature and moisture with inclusion of a layer of vegetation. *Journal of Geophysical Research* **83**: 1889-1903.
- Dickinson RE, Henderson-Sellers A, Kennedy PJ. 1993. Biosphere-Atmosphere Transfer Scheme (BATS) Version 1e as Coupled to the NCAR Community Climate Model. NCAR/TN-387+STR, National Center for Atmospheric Research. Boulder, CO; 71 pp.
- Dingman SL. 1994. *Physical Hydrology*. Macmillan: New York.

- Dozier J. 1989. Spectral Signature of Alpine Snow Cover from the Landsat Thematic Mapper. *Remote Sensing of Environment* **28**: 9-22.
- Dyer AJ, Hicks BB. 1970. Flux-gradient Relationships in the Constant Flux Layer. *Quart. J. R. Met. Soc.* **96**: 715-721.
- Flerchinger GN, Saxton KE. 1989. Simultaneous Heat and Water Model of a Freezing Snow-Residual- Soil System I. Theory and Development. *Transactions of the ASAE* **32**(2): 565-571.
- Gray DM, Male DH. (eds) 1981. Handbook of Snow, Principles, Processes, Management & Use. Pergamon Press: New York.
- Hanks RJ, Ashcroft GL. 1980. *Applied Soil Physics*. Vol 8, Advanced Series in Agricultural Sciences, Springer-Verlag: Berlin Heidelberg.
- Hu Z, Islam S. 1995. Prediction of ground surface temperature and soil moisture content by the force-restore method. *Water Resources Research* **31**(10): 2531-2539.
- Jin J, Gao X, Sorooshian S, Yang Z-L, Bales R, Dickinson RE, Sun S-F, Wu G-X. 1999. One-dimensional snow water and energy balance model for vegetated surfaces. *Hydrological Processes* **13**: 2467-2482.
- Jordan R. 1991. A One-dimensional Temperature Model for a Snow Cover. Technical documentation for SNTHERM.89, special technical report 91-16, US Army CRREL. 49 pp.
- Koivasulo H, Heikenkeimo M. 1999. Surface energy exchange over a boreal snowpack. *Hydrological processes* **13**(14/15): 2395-2408.
- Lee R. 1980. *Forest Hydrology*. Columbia University Press: New York.
- Linsley RK, Kohler MA, Paulhus JLH. 1975. *Hydrology for Engineers*. 2nd Edition, McGraw-Hill: Kogakusha, Ltd.
- Lowe PR. 1977. An approximating polynomial for the computation of saturation vapour pressure. *Journal of Applied Meteorology* **16**: 100-103.
- Luce CH. 2000. Scale influences on the representation of snowpack processes. Ph. D Dissertation, Civil and Environmental Engineering: Utah State University, Logan, Utah.

- Luce CH, Tarboton DG. 2001. A modified force-restore approach to modeling snow-surface heat fluxes. In *Proceedings of the 69th Annual Meeting of the Western Snow Conference*, Sun Valley, Idaho.  
<http://www.westernsnowconference.org/2001/2001papers.htm>. (Accessed Jul. 31, 2004).
- Luce CH, Tarboton DG, Cooley KR. 1998. The influence of the spatial distribution of snow on basin-averaged snowmelt. *Hydrological Processes* **12**(10-11): 1671-1683.
- Luce CH, Tarboton DG. submitted 2004. A frequency domain analysis of conductive heat fluxes in snowpacks. *Hydrological Processes*.
- Marks D, Kimball J, Tingey D, Link T. 1998. The sensitivity of snowmelt processes to climate conditions and forest cover during rain-on-snow: a case study of the 1996 Pacific Northwest flood. *Hydrological Processes* **12**(10-11): 1569-1598.
- Prasad R, Tarboton DG, Liston GE, Luce CH, Seyfried MS. 2000. Testing a blowing snow model against distributed snow measurements at Upper Sheep Creek. *Water Resources Research* **37**(5): 1341-1350.
- Price AG, Dunne T. 1976. Energy balance computations of snowmelt in a subarctic area. *Water Resources Research* **12**(4): 686-694.
- Satterlund DR. 1979. An improved equation for estimating long-wave radiation from the atmosphere. *Water Resources Research* **15**: 1643-1650.
- Sun S, Jin J, Xue Y. 1999. A simple snow-atmosphere-soil transfer model. *Journal of Geophysical Research* **104**(D16): 19587-19597.
- Tarboton DG. 1994. Measurement and modeling of snow energy balance and sublimation from snow. In *Proceedings of International Snow Science Workshop*, Snowbird, Utah, October 31 to November 2; 260-279.
- Tarboton DG, Chowdhury TG, Jackson TH. 1995. A spatially distributed energy balance snowmelt model. In *Proceedings of a Boulder Symposium*, Tonnessen KA, Williams MW, Tranter M (eds). Boulder, CO., July 3-14, IAHS Publ. no. 228.
- Tarboton DG, Luce CH. 1996. Utah Energy Balance Snow Accumulation and Melt Model (UEB). Computer model technical description and users guide, Utah Water Research Laboratory and USDA Forest Service Intermountain Research Station (<http://www.engineering.usu.edu/dtarb/>). (Accessed Jul. 31, 2004).
- U.S. Army Corps of Engineers. 1956. Snow Hydrology, Summary Report of the Snow Investigations. U.S. Army Corps of Engineers, North Pacific Division, Portland, Oregon. 142 pp.

Viessman W, Lewis GL, Knapp JW. 2002. *Introduction to Hydrology*. 5th Edition, Prentice Hall: New York.

Warren SG. 1982. Optical properties of snow. *Review of Geophysics* **20**: 67-89.

Yen YC. 1967. The rate of temperature propagation in moist porous mediums with particular reference to snow. *Journal of Geophysical Research* **72** (4): 1283-1288.

CHAPTER 3  
SNOW COVERED AREA IMAGE BASED REPRESENTATION  
OF THE SPATIAL DISTRIBUTION PATTERN OF SNOW IN A  
MOUNTAINOUS WATERSHED

Abstract:

Spatially distributed models are needed in snow hydrology to represent and understand the spatial pattern of snow accumulation and melt and how these patterns are related to topography. Snow accumulation is highly variable due to drifting and precipitation variability, yet the inputs available for snowmelt models are typically point precipitation measurements that do not capture this variability. An accumulation factor approach has been developed to relate the spatial pattern of snow accumulation over an area to measured precipitation at a point. Each point is assumed to have a propensity to accumulate snow represented by a factor that multiplies the measured precipitation to obtain spatially distributed precipitation inputs. This paper presents an approach to estimating the accumulation factor over a watershed using remotely sensed images of the snow covered area. Bounds on the accumulation factor are calibrated in accordance with the last day snow cover was observed, and first day snow was not observed at each point. Grid cells at the edges of the snow covered area were assumed to have accumulation factor fixed at the bound value corresponding to whether they are snow covered or snow free. The accumulation factor values from these grid cells were used to develop regression models based on terrain variables that interpolate the accumulation factor over



the entire domain. These interpolations are tested using the bound values based upon snow disappearance date. We were unable to find a good single regression covering the entire domain, which may have given some generality to this approach, but were able to obtain successful regressions for the bands of the domain that became snow free between each pair of observations. This approach is therefore still useful for the estimation of accumulation factor, but relies on direct observations of snow cover. This approach presents a new way to calibrate accumulation factors for use in distributed snowmelt modeling relying on snow covered area images that are more readily available than distributed measurements of snow water equivalent.

## INTRODUCTION

The spatial distribution of snow water equivalent is an important control on the timing and rate of snowmelt runoff. Spatially distributed snowmelt models that attempt to explicitly represent the spatial distribution and patterns of snow require spatially distributed inputs of snow that account for variations in accumulation due to variability in precipitation and wind blown drifting. Energy exchanges, topographical characteristics, surface roughness, and wind redistribution all contribute to the spatial heterogeneity of snow (Elder *et al.*, 1991; Cline *et al.*, 1998; Luce *et al.*, 1998; Prasad *et al.*, 2000). Much work has been conducted to represent the spatial characteristics of the snowmelt processes (Blöschl *et al.*, 1991a, 1991b; Wigmosta *et al.*, 1994; Luce *et al.*, 1998; Marks *et al.*, 1999), while the representation process is still not completed.

Wind blowing processes contribute to the variability of snow ( Gray, 1979; Gray and Male, 1981; Elder *et al.*, 1991; Blöschl and Kirnbauer, 1992; Hardy *et al.*, 1997;

Elder *et al.*, 1998; Liston and Sturm, 1998; Luce *et al.*, 1998; Prasad *et al.*, 2000; Marks and Winstral, 2001; Winstral *et al.*, 2002). Efforts have focused on the effects of wind on snow distribution for some time (Schmidt, 1982; Tabler *et al.*, 1990), but the development of a means to include such effects within a model of alpine snow distribution has not yet been accomplished. Two physically based continuous models directly calculate the redistribution of snow due to wind. The Prairie Blowing Snow (Pomeroy *et al.*, 1993) and SnowTran-3D (Liston and Sturm, 1998) models have been calibrated and validated for the flat areas to gentle sloping terrain in the Canadian Prairie and subarctic Alaska. However, both models have limitations in the rugged terrain of an alpine watershed.

The accumulation factor approach (Tarboton *et al.*, 1995; Tarboton and Luce, 1996; Luce *et al.*, 1998; Prasad *et al.*, 2000) has been developed to empirically relate the spatial pattern of snow accumulation over an area to point precipitation measurements. Each point is assumed to have a propensity to accumulate snow that is quantified by a factor that multiplies the measured precipitation and so obtains spatially distributed precipitation inputs. Past work (Luce *et al.*, 1998) has derived the pattern of accumulation factors over a watershed using measurements of snow water equivalent or by running a blowing snow model (Prasad *et al.*, 2000). These approaches are not feasible in large watersheds in rugged terrain because spatial measurements of snow are not available and a blowing snow model has limited effectiveness.

In this chapter, an approach is developed to estimate the accumulation factor based upon snowcover from a sequence of aerial photographs. The Utah Energy Balance (UEB) snowmelt model is used (Tarboton *et al.*, 1995; Tarboton and Luce, 1996). First

the aerial photographs are used to prepare binary (snow/no snow) maps of the domain on each survey date. This gives the date snowcover was last observed and the date snow free conditions were first observed at each point. The date of disappearance of snow increases monotonically with the accumulation factor because an increased accumulation factor results in more snow that takes longer to melt. A lower bound on accumulation factor is obtained by adjusting the accumulation factor until the snowmelt model (UEB) predicts disappearance of snow on the last date snow cover was observed. An upper bound on the accumulation factor is obtained by adjusting the accumulation factor until the snowmelt model predicts the disappearance of the snow on the first observation of snow free conditions.

Second, we assume that edge cells in the snow cover images have an accumulation factor equal to the one of the bounds. If a grid cell is at the edge of the snow covered domain (i.e. adjacent to snow free area), it is assumed to be about to have the snow disappear so the accumulation factor is assumed to be at the lower bound value. If a grid cell is at the edge at the snow free domain (i.e. adjacent to snow covered area) it is assumed that the last snow has just melted and the accumulation factor is assumed to be at the upper bound value. These edge locations where fixed values are assumed comprise a subset of the domain that was used in a series of regression models to develop relationships between accumulation factor and terrain attributes. These regression models then provide the means to estimate an accumulation factor at the remainder of grid cells, which are not edge cells, in the domain, providing a complete accumulation factor map. The complete accumulation factor map is used as input to the distributed snowmelt model, and modeled snow water equivalent maps were evaluated against the

images of snow covered area. Estimated internal accumulation factors are compared to the accumulation factor bounds as an additional check on the accumulation factors.

## STUDY SITES AND DATA

The 8.1 km<sup>2</sup> Green Lakes Valley watershed (GLV) is a high Rocky mountain basin with steep cliffs, talus slopes, and limited soil cover located 40 km west of Boulder, CO (see Figure 3-1). Bare rock comprises about 1/3 of the basin area, talus slopes comprise about 1/3 of the basin area, and soil comprises the other 1/3 of the basin area. The 8-ha Arikaree cirque glacier lies at about 3800 m just below the Continental Divide within the basin. Elevation in Green Lakes Valley watershed ranges from 3204 to 4087 m, with most of the basin lying above treeline. Mean monthly minimum temperatures are below 0 °C from October through May with monthly maxima below freezing from November to April (Berg, 1986). The area is characterized by a mountain continental climate, annually receiving about 1000 mm of precipitation (Williams *et al.*, 1996), 80% of which is in the form of snow (Caine, 1995). Weather data has been collected at the four stations shown, whose locations range from valley to ridge top. The weather data comprise air temperature, relative humidity, wind speed and direction, and incident solar radiation. Precipitation is measured at the ridge location, D1. Digital elevation data at 10-m resolution was produced photogrammetrically. Metric 1:24,000 aerial photographs were taken on four dates in 1996 and have produced high-resolution orthophotos (~10 m). The snow covered area images classified from these orthophotos provides information about the snowpack depletion processes (see Figure 3-2).

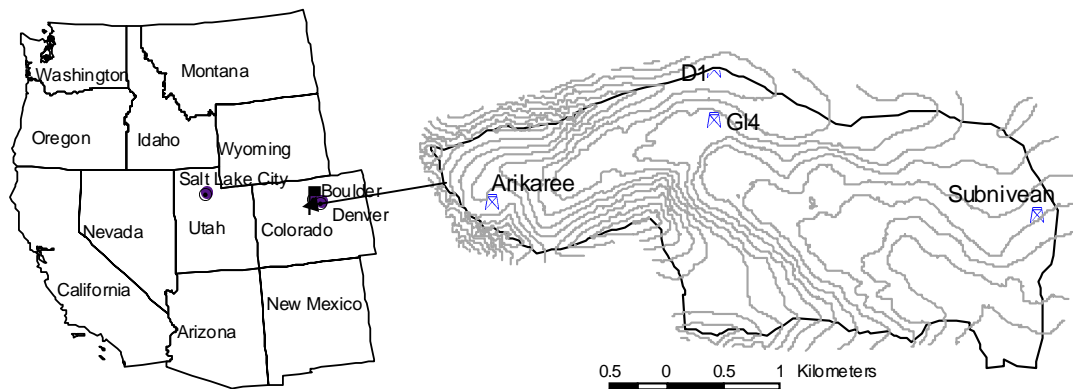
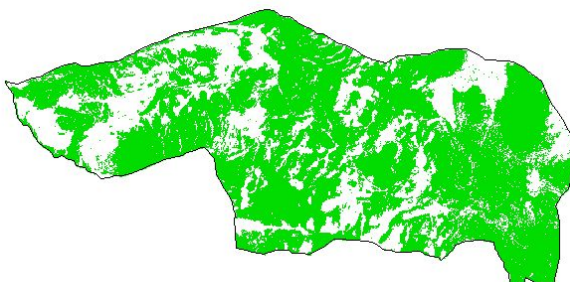
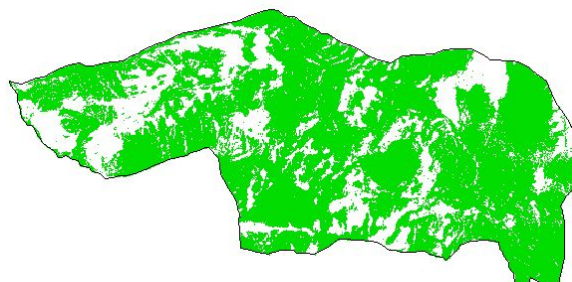


Figure 3-1 Green Lakes Valley watershed location map and its relative location in U.S.A. The contour interval is 50 m. Four weather stations are located

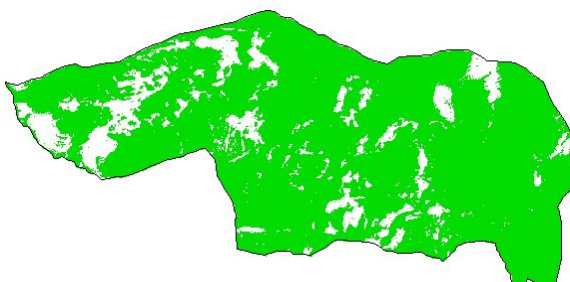
May 22



June 9



June 29



July 21

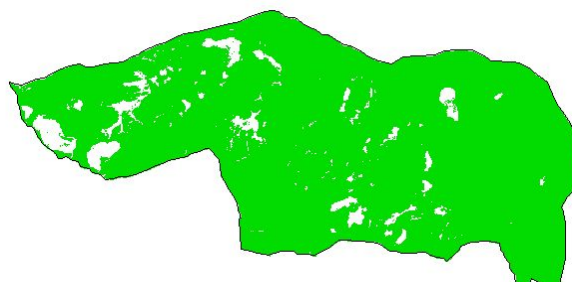


Figure 3-2 Observed snow covered area images at four dates, May 22, June 9, June 29, and July 21, 1996. White areas represent the snow covered areas and green areas are the snow free areas

## MODELING APPROACH

The new UEB model described in chapter 2 was used in this work. The time evolution of the snowpack is driven by the energy exchange between the snowpack, the air above and the soil below according to mass and energy balance equations,

$$\frac{dU}{dt} = Q_{sn} + Q_{li} - Q_{le} + Q_p + Q_g + Q_h + Q_e - Q_m, \quad (\text{kJ m}^{-2} \text{ h}^{-1}) \quad (3-1)$$

$$\frac{dW}{dt} = P_r + P_s - M_r - E, \quad (\text{m h}^{-1}) \quad (3-2)$$

where  $U$  is the energy content,  $W$  is the snow water equivalent,  $Q_{sn}$  is the net shortwave energy received by the snowpack,  $Q_{li}$  is the incoming longwave radiation,  $Q_{le}$  is outgoing longwave radiation,  $Q_p$  is the energy advected by precipitation into the snow,  $Q_g$  is the ground heat flux to the snow,  $Q_h$  is the sensible heat flux to the snow,  $Q_e$  is the latent heat flux into the snow, and  $Q_m$  is the advected heat removed by meltwater.  $P_r$  is the rate of precipitation as rain;  $P_s$  is the rate of precipitation as snow;  $M_r$  is the melt rate; and  $E$  is the sublimation rate;  $t$  is time (h). The model requires inputs of air temperature, wind speed and incident radiation that are used to drive the energy balance, and precipitation that is used to drive the mass balance. Precipitation is partitioned into snowfall or rainfall based upon air temperature (U.S. Army Corps of Engineers, 1956) interpolated from measurements at weather stations and adjusted with elevation based upon a lapse rate. The fraction of precipitation falling as snow,  $f_{snow}$ , is given by:

$$\begin{aligned}
f_{snow} &= 1.0 && \text{when } T_a < T_s \\
&= \frac{T_r - T_a}{T_r - T_{sn}} && \text{when } T_{sn} \leq T_a \leq T_r \\
&= 0.0 && \text{when } T_a > T_r
\end{aligned} \tag{3-3}$$

here  $T_r$  ( $=3$  °C) is the air temperature above which all precipitation is assumed to fall as rain, and  $T_{sn}$  ( $=-1$  °C) is the air temperature below which all precipitation is assumed to fall as snow.

The accumulation factor (Tarboton *et al.*, 1995; Tarboton and Luce, 1996) relates a point or reference precipitation measurement to the snow accumulation at each point in the watershed. Snow deposition at each location is modified by applying a spatially variable accumulation factor,  $\phi$ , to account for redistribution and differential accumulation effects.

$$P_s = f_{snow} \cdot \phi \cdot P \tag{3-4}$$

where  $P$  is the measured point or reference precipitation (m). The total precipitation at each grid cell is the sum of  $P_s$  and precipitation as rainfall ( $P_r = (1 - f_{snow})P$ ). The accumulation factor is an empirical factor that includes the combined effect of all processes involved in variability in snow accumulation, including wind blown drifting, sliding and precipitation variability.

*Disappearance date-based accumulation factor calculation*

Equation 3-4 substituted into equation 3-2 gives

$$\frac{dW}{dt} = (1 - f_{snow})P + f_{snow} \cdot \phi \cdot P - M_r - E . \quad (3-5)$$

The model was initialized on September 20, 1995, the date of first significant snowfall that season and driven by climate inputs following that date. The positive term containing accumulation factor  $\phi$  results in a positive monotonic relationship between  $\phi$  and the corresponding  $W$  on any specific date (Figure 3-3). There is also a positive relationship between  $\phi$  and the disappearance date. A lower bound on accumulation factor is calculated at each point by assuming the snow disappears on the last date snow was observed at each location. The lower bound is not defined for locations where snow was never observed. An upper bound on accumulation factor is calculated by assuming the snow disappears on the first date snow free conditions were observed. At those grid cells where the snow was observed in the latest snow image, the snow was assumed, for the purposes of calculating an upper bound to have disappeared by August 30, before the next accumulation season commences.

*Accumulation factor interpolation*

Figure 3-4 illustrates schematically the ablation of snow covered area with time as represented by snow cover images on three dates,  $T_1$ ,  $T_2$ , and  $T_3$ . Indicated are edge cells where there is snow cover adjacent to snow free areas, or snow free area adjacent to



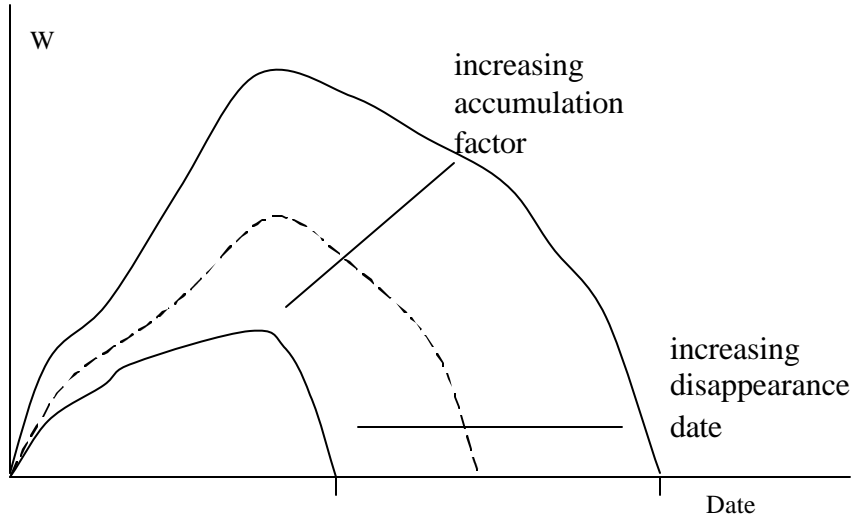
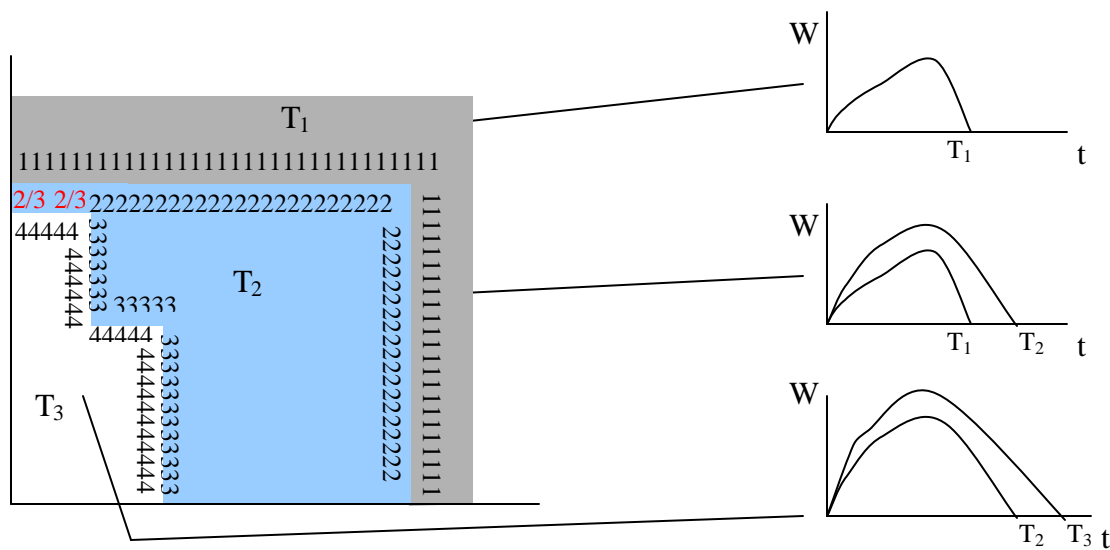


Figure 3-3 Schematic of time series solutions for snow water equivalent for varying accumulation factor



1. Use upper bound (snow disappearing at  $T_1$ )
  2. Use lower bound (snow disappearing at  $T_1$ )
  3. Use upper bound (snow disappearing at  $T_2$ )
  4. Use lower bound (snow disappearing at  $T_2$ )
- 2/3 – Mixed, not used

Figure 3-4 Schematic map showing definition of edge cells where specific accumulation factor values are calculated

snow covered area. At these locations it is assumed that the accumulation factor is equal to one of the bound values. The region labeled  $T_1$  was observed to be snow free at  $T_1$  so had snow disappear on or before  $T_1$ . The assumption is that the edge cells labeled 1 have snow disappear at  $T_1$  and therefore assume the upper bound value for their accumulation factor. The region labeled  $T_2$  was snow covered at  $T_1$  but was observed to be snow free at  $T_2$ , so had snow disappear between  $T_1$  and  $T_2$ . The outer edge cells bounding the snow free area, labeled 2 in the figure, are assumed to have snow disappearing at  $T_1$  and therefore assume the lower bound value for their accumulation factor. The inner edge cells bounding the area that remains snow covered past  $T_2$ , labeled 3 in Figure 3-4, are assumed to have snow disappearing at  $T_2$  and therefore assume the upper bound value for their accumulation factor. Similarly the outer edge cells for region  $T_3$ , labeled 4 in the figure, assume the lower bound for their accumulation factor calculated from the snow disappearing at  $T_2$ . Cells that belong to both outer and inner edges (labeled 2/3 in the figure) and non edge cells are indeterminate and are not used for the purposes of determining a relationship between accumulation factor and terrain attributes. This process results in the calculation of specific accumulation factor values for the subset of the domain comprising determinate edge cells. The remaining grid cells in the domain have upper and lower bounds for the accumulation factor based on the date snow was last observed and a date snow free conditions were first observed. The subset of grid cells with specific accumulation factor values were used to develop a series of regression models for the estimation of accumulation factor based on terrain variables. The upper and lower bounds on accumulation factor in the remaining grid cells were used

to perform test the regression models on data out of their calibration set. The regression function for the accumulation factor was written as:

$$\phi = f(X), \quad (3-6)$$

where  $X = (z, slp, asp, curv, d2r, d2v, e2r, e2v \dots)$  is a vector of terrain variables,  $z$  is the elevation,  $slp$  is the slope,  $asp$  is the aspect,  $curv$  is the plane curvature,  $d2r$  is the distance to ridge,  $d2v$  is the distance to valley,  $e2r$  is elevation difference to ridge, and  $e2v$  is elevation difference to valley. Figure 3-5 illustrates the latter four terrain attributes. Mean square error of the predicted accumulation factor can be written as:

$$mse = \sum_n (\phi_i - f(x_i))^2 / n, \quad (3-7)$$

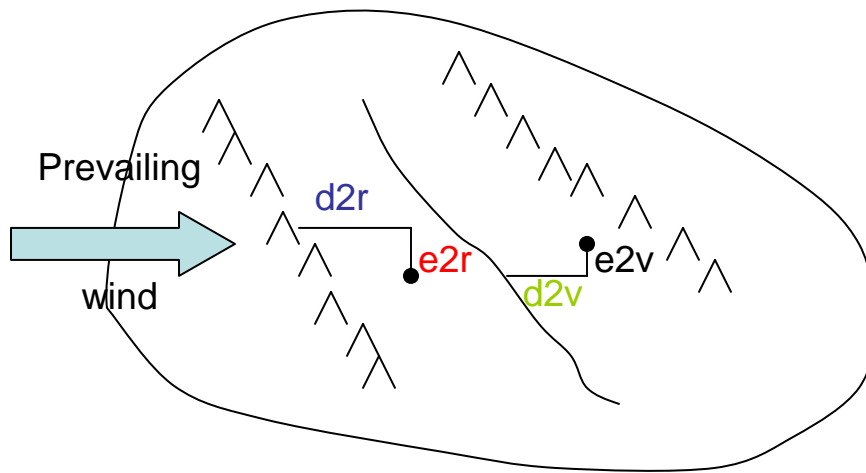


Figure 3-5 Illustration of some of the terrain attributes

here  $f(x_i)$  is the predicted accumulation factor of the boundary cells,  $n$  is the size of samples, and  $\phi_i$  is the calibrated bound value of cells.

## RESULTS

### *Accumulation factor interpolation*

The first regression model developed pooled the accumulation factor calculated for all edge grid cells. There are a total of 32046 edge cells comprising 37% of the domain. The terrain attributes evaluated as explanatory variables included elevation, slope, aspect, plane curvature, profile curvature, distance to ridge, distance to valley, elevation to ridge, and elevation to valley to the west, the direction from which the prevailing wind blows. Aspect was represented as  $\cos(asp)$  and  $\sin(asp)$  where  $asp$  is the downslope direction (represented as a bearing clockwise from east) to avoid the sharp discontinuity associated with the north direction where  $0^\circ=360^\circ$ . Distance to the valley was log transformed ( $\log(d2v+1)$ ), plus 1 is to avoid the numeric errors. Following exploratory data analysis where terrain attributes were initially plotted against the calculated accumulation factor of edge cells, several combinations of these variables were included as explanatory variables in the construction of local polynomial regression models (Loader, 1999). The regression used the Splus LOESS function (Cleveland and Devlin, 1988) default span value of 0.5. Mean square error of the difference between predicted and calculated accumulation factor at edge cells was used as the objective function to select the best model. The best model had elevation, distance to valley and  $\cos(asp)$  as explanatory variables. Figure 3-6 shows the predicted versus calculated accumulation factor from this regression. The Nash-Sutcliffe goodness of fit measure

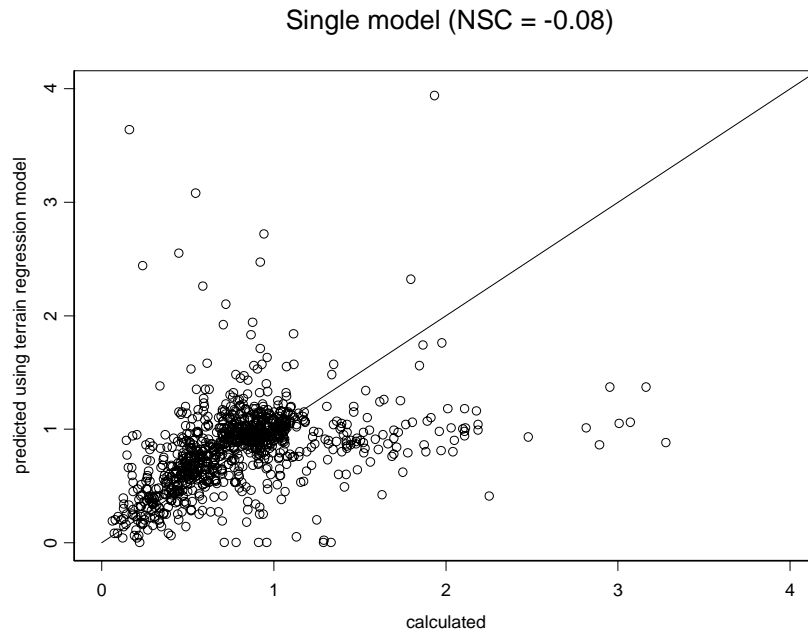


Figure 3-6 Calculated versus predicted accumulation factor for single regression model (1000 randomly selected points)

(Nash and Sutcliffe, 1970) quantifies the variability explained by the modeled on a scale  $-\infty$  to 1 where 1 is perfect and is given by:

$$NSC = \frac{\sum_{k=1}^N (y_k - \bar{y})^2 - \sum_{k=1}^N (y_k - \hat{y}_k)^2}{\sum_{k=1}^N (y_k - \bar{y})^2}, \quad (3-8)$$

where  $N$  is the number of cells in regression model,  $y_k$  and  $\hat{y}_k$  are calculated accumulation factor and predicted accumulation factor at location  $k$ ,  $\bar{y}$  is the mean value of the calculated accumulation factor in the model. This model was used to calculate accumulation factor at the remaining 53652 non edge cells in the domain. Only 34% of

the accumulation factor values obtained in this way fall between the upper and lower bound accumulation factor values calculated from the snow covered area images. We judged this model to be inadequate for the purpose of quantifying the spatial pattern of snow distribution.

Examination of the accumulation factor calculated at edge cells reveals that the mean of the accumulation factor increases from 0.68 at edge cells where the snow disappeared on May 22, to 2.1 for grid cells with snow disappearing on July 21. The single regression model was unable to determine a relationship between this range of variability and the topographic parameters used as explanatory variables. We therefore decided to develop a separate regression for bands defined based on the snow covered area images. Band 1 is defined as that region where snow was never observed, i.e. it disappeared before the first image on May 22. Band 2 is defined as that region that was snow covered on May 22 but snow free on June 9. Similarly band 3 and 4 are defined between June 9, 29 and July 21. Band 5 is the region where snow was present in all images, i.e. present after July 21. Table 3-1 summarizes information about these bands.

Local polynomial regression was used to develop an accumulation factor model for each band. Again the explanatory variables used were elevation, distance to valley and  $\cos(asp)$ . For band 1 we were only able to calculate upper bound accumulation factor value. The local polynomial regression in band 1 therefore only used these upper bound values as input. When results were compared against bound values calculated for all grid cells in band 1 we found that a large number of interpolated grid cell accumulation factor values were above the upper bound. This apparent over prediction of accumulation factor in band 1 is not surprising given that only upper bound values have

Table 3-1 Information about 5 bands

Band #	Snow cover at date	Snow free before date	Total number of cells	Number of inner edge cells	Number of outer edge cells	Mean accumulation factor of edge cells	Mean accumulation factor of inner edge cells	Mean accumulation factor of outer edge cells
Band 1	Not observed	May 22, 1996	57817	0	14675	0.67	N/A	0.68
Band 2	May 22, 1996	June 09, 1996	8447	1561	3870	0.71	0.68	0.82
Band 3	June 09, 1996	June 29, 1996	8714	1563	4235	1.01	0.90	1.3
Band 4	June 29, 1996	July 21, 1996	6096	853	2905	1.47	1.3	2.1
Band 5	July 21, 1996	Not observed	4624	5431	0	2.02	2.0	N/A

been used as input. We therefore reduced all interpolated accumulation factor value in band 1 by a factor of 0.65. This was chosen (admittedly somewhat subjectively) to reduce the number of grid cells having interpolated accumulation factor exceeding their calculated upper bound value, while at the same time holding the mean accumulation factor to what we felt was a reasonable value.

In band 5 upper bound accumulation factor bound values were available based on the assumed August 30 season end date. These are not very limiting as we know that the snow disappears well before this date in most locations. Therefore the local polynomial regression in band 5 only used the lower bound values as input. When results were compared against bound values calculated for all grid cells in band 5 we found that a large number of interpolated grid cell accumulation factor values were below the lower bound. This apparent under prediction is not surprising given that only lower bound values were used as input. We increased all interpolated accumulation factor values in

band 5 by a factor of 1.2. This was chosen as the value that minimizes the number of grid cells out of bounds calculated for band 5.

Figure 3-7 shows predicted versus calculated accumulation factor from these regressions. The adjustments for band 1 and 5 are included in the data plotted and are responsible for the bias between the 1:1 line and point clouds for these bands. Figure 3-8 shows predicted versus calculated accumulation factor for these models combined.

Although the fit of some of the individual models is poor, when considered together the models do appear to have same explanatory capability so we proceeded with the evaluation against accumulation factor bounds for internal grid cells not used in developing these regression models. Figure 3-9 shows the map of accumulation factor obtained by applying the 5 band interpolation model to each grid cell.

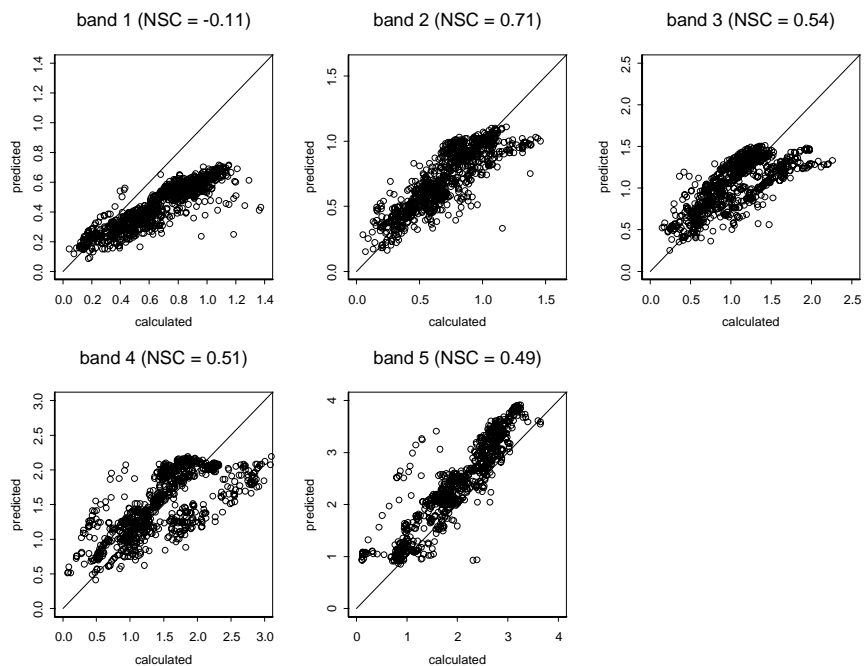


Figure 3-7 Calculated versus predicted accumulation factor for each band in the 5 bands regression model (1000 randomly selected points)



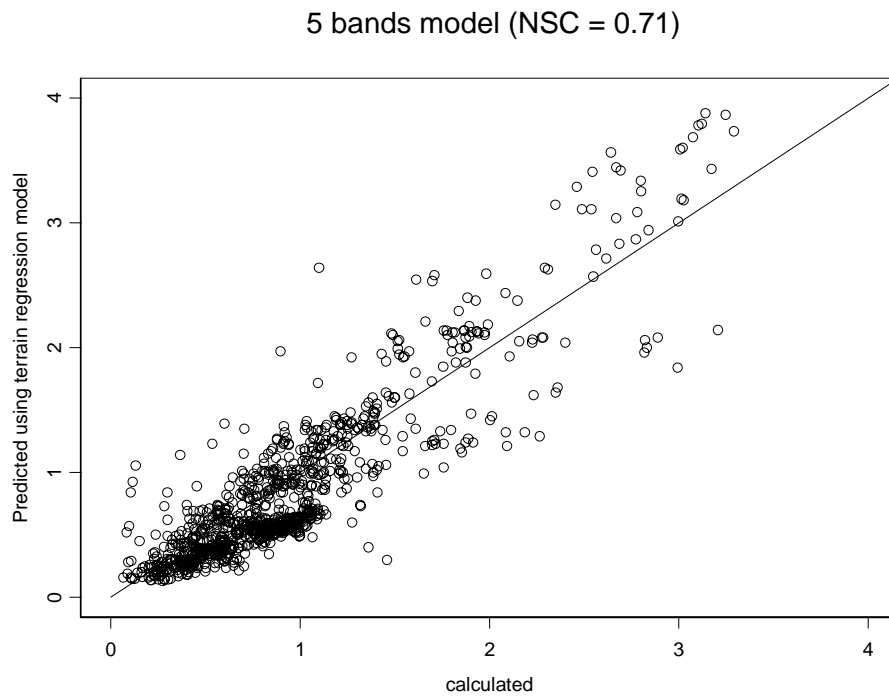


Figure 3-8 Calculated versus predicted accumulation factor for combined 5 bands regression model (1000 randomly selected points)

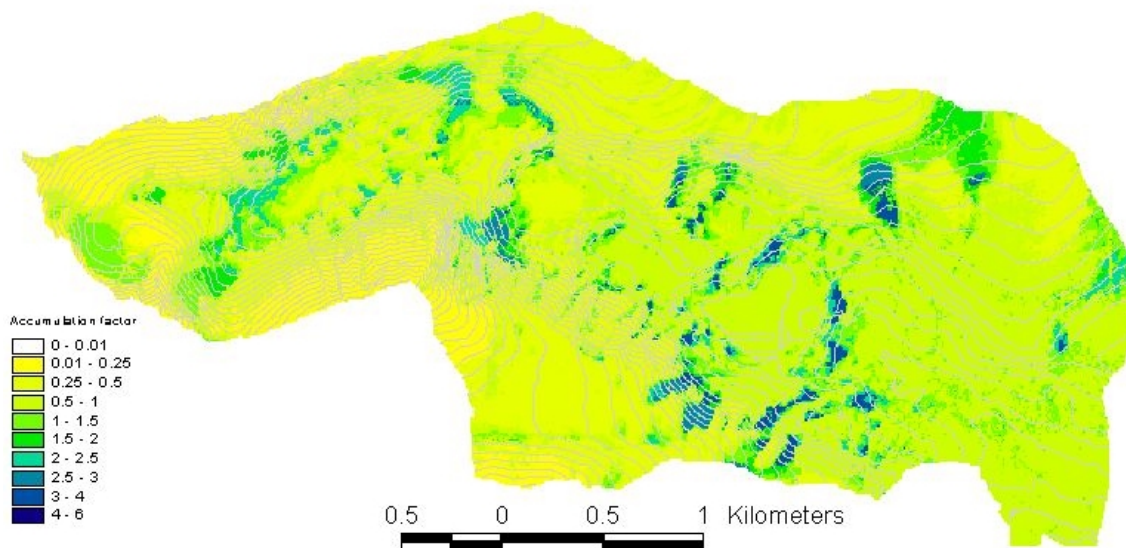


Figure 3-9 Accumulation factor map

*Validation against calculated accumulation factor bounds*

Figure 3-9 provides a specific estimated accumulation factor value at each grid cell estimated using a local polynomial regression model with terrain attributes as explanatory variables. Each grid cell also has directly calculated lower and upper bounds for the accumulation factor calculated using the UEB model, climate inputs and snow covered area images following the procedure described above. Table 3-2 summarizes the comparison of the estimated accumulation factor to directly calculated accumulation factor bounds for each band. This information is presented in map form in Figure 3-10 where the spatial locations where accumulation factor is estimated out of the bounds calculated are shown. Overall 89% of the interpolated accumulation factor values fall within the calculated bounds. This validation tested the accumulation factor interpolation against all 85698 grid cells. Only the 32046 edge cells were used in developing the model so this is an out of sample test against data not used in calibration of the regression.

Table 3-2 Number and fraction of specific interpolated accumulation factor values falling within bounds of calculated values

	Number of grid cells				Fraction of grid cells		
	Total	Incorrect below	Correct	Incorrect above	Incorrect below	Correct	Incorrect above
Overall	85698	4560	75895	5243	0.05	0.89	0.06
Band 1	57817	-	54656	3161	-	0.95	0.05
Band 2	8447	2140	5144	1163	0.25	0.61	0.14
Band 3	8714	1240	7098	376	0.14	0.81	0.04
Band 4	6096	890	4987	219	0.15	0.82	0.04
Band 5	4624	290	4010	324	0.06	0.87	0.07

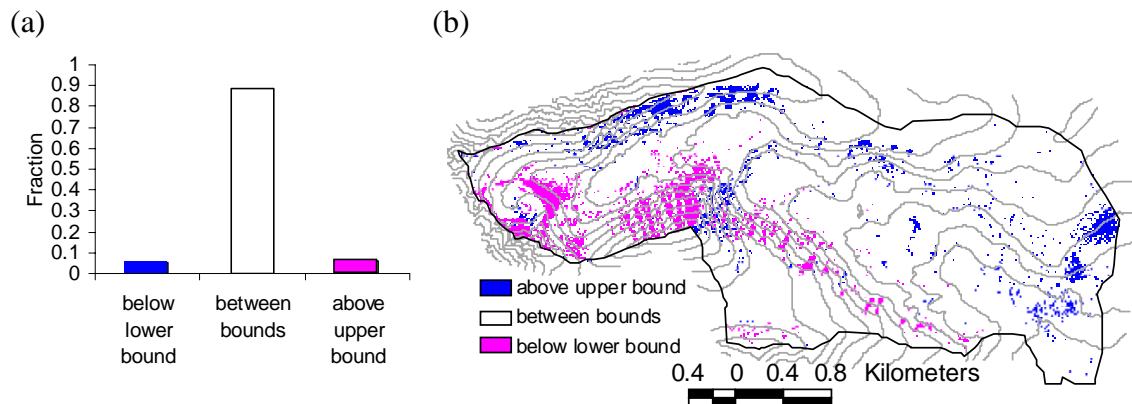


Figure 3-10 Estimated snow accumulation factor compared to directly calculated snow accumulation factor bounds

#### *Distributed modeling comparison*

The specific estimated accumulation factors mapped in Figure 3-9 were used as input to the UEB snowmelt model run for an entire year at each grid cell over Green Lakes Valley. The model was initialized on September 20, 1996, the date of the first snowfall that season, and driven by observed climate inputs from the meteorological stations. Figure 3-11 shows modeled snow water equivalent compared against observed snow covered area on the dates snow covered area images were available. A categorical comparison of these maps is given in Table 3-3 where the number and fraction of area modeled as containing snow cover consistent, or inconsistent with the observations is tabulated. Figure 3-12 shows the fraction of snow covered and snow free area that is correctly or incorrectly modeled at each observation date, together with the time series of modeled and observed snow covered area. The spikes in the time series occur due to new snowfall.

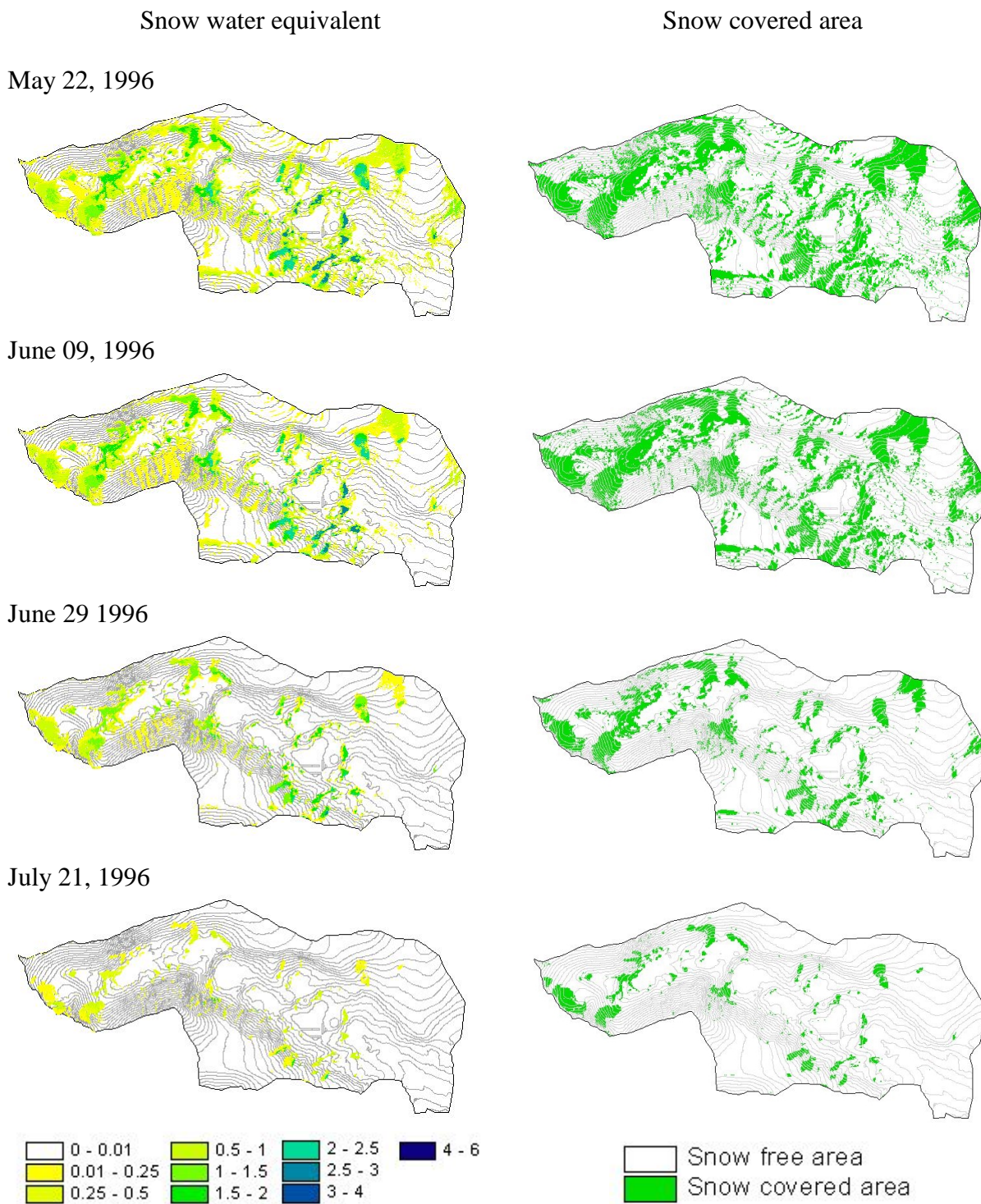


Figure 3-11 Modeled snow water equivalent and observed snow covered area

Table 3-3 Modeled and measured snow covered area

Date	Snow covered correct	No snow correct	Snow covered incorrect	No snow incorrect	SCA	Snow Free
Number of grid cells						
05/22/96	26500	54846	1381	2971	29471	56227
06/09/96	18869	57437	6283	3109	21978	63720
06/29/96	9634	71989	2421	1654	11288	74410
07/21/96	4075	79926	1068	629	4704	80994
Fraction of total area						
05/22/96	0.31	0.64	0.02	0.03	0.34	0.66
06/09/96	0.22	0.67	0.07	0.04	0.26	0.74
06/29/96	0.11	0.84	0.03	0.02	0.13	0.87
07/21/96	0.05	0.93	0.01	0.01	0.05	0.95

Note:

Snow covered correct: means both modeled and observed snow covered area;

No snow correct: means both modeled and observed snow free area;

Snow covered incorrect: means observed snow covered area that was modeled as snow free;

Now snow incorrect: mean observed snow free area that was modeled as snow covered.

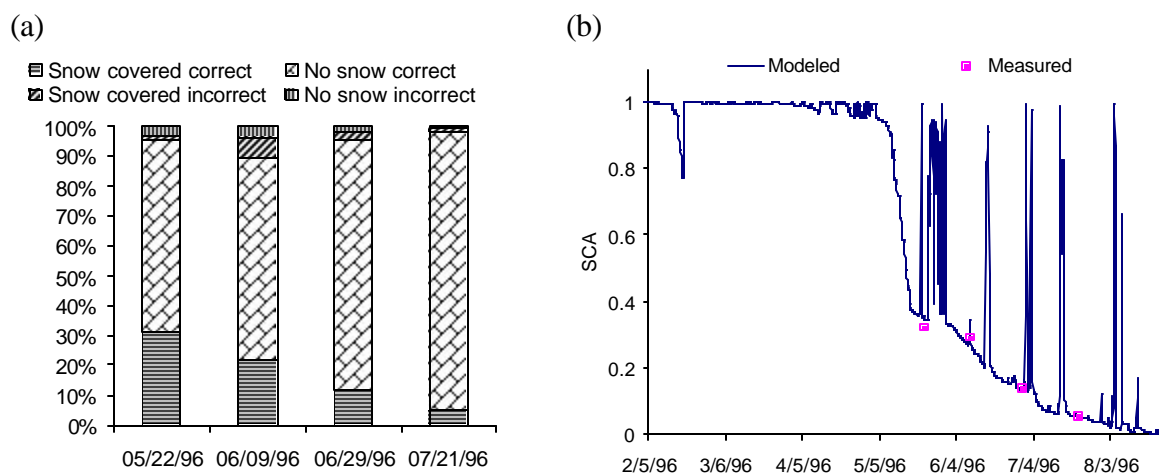


Figure 3-12 a) Snow covered area fraction comparison; b) Snow covered area fraction time Series

Snow covered correct: means both modeled and observed snow covered area;

No snow correct: means both modeled and observed snow free area;

Snow covered incorrect: means observed snow covered area that was modeled as snow free;

No snow incorrect: means observed snow free area that was modeled as snow covered.

## DISCUSSION AND CONCLUSIONS

A new approach has been presented that combines physically based snowmelt modeling with the use of a limited number of snow covered area images to estimate the snow accumulation factor necessary to explicitly represent spatially distributed snow processes. We had limited success in developing a general relationship between snow accumulation factors and terrain variables. This may have been due to the terrain variables tested not being the most appropriate explanatory variables, or due to compounding of uncertainty both in the snow modeling and local polynomial regression approach. It is plausible that other statistical modeling approaches may have been better at capturing a relationship between terrain attributes and snow accumulation factors, but the local polynomial approach was chosen for its generality and broad non-parametric strength so we feel it more likely that there is not a robust single relationship between terrain variables and accumulation factors discernable in this dataset. We were able to successfully parameterize snow accumulation factors using terrain attributes as explanatory variables for specific subsets of the domain categorized by when they were observed to become snow free. This suggests that the direct observations of snow cover are at this stage necessary to determine accumulation factor using this method.

The large majority (89%) of snow accumulation factors obtained using the five band specific regressions fall within the directly calculated snow accumulation factor bounds. This provides a basis for using these snow accumulation factors as input to a distributed snow accumulation and melt model. The results from this model compare favorably against snow cover observations.

A limitation of the results presented here are that they are derived from only four snow covered area images obtained during the melt season when less than 35% of the watershed was snow covered. Therefore the lower bound on accumulation factor for the majority of the domain is unconstrained. It would be useful to repeat this work with more snow covered area images, including images collected early in the season to establish tighter bounds on accumulation factor for more of the domain.

Overall, this work suggests that snow covered area images, combined with meteorological inputs can be used to calibrate the accumulation factor needed to represent snow distribution and redistribution effects in an alpine watershed. This method has value in large mountainous watersheds where snow covered area images are more readily available than intensive snow water equivalent measurements. This study also opens the opportunity to study fine scale spatial snow distribution patterns over larger areas than can be covered by field surveys and by doing this improve our understanding of the spatial processes and patterns of snow accumulation and melt.

## REFERENCES

- Berg N. 1986. Blowing snow at a Colorado alpine site: measurements and implications. *Arctic and Alpine Research* **18** (2): 147-161.
- Blöschl G, Gutnecht D, Kirnbauer R. 1991a. Distributed snowmelt simulations in an alpine catchment. 2. Parameter study and model predictions. *Water Resources Research* **27**(12): 3181-3188.
- Blöschl G, Kirnbauer R, Gutnecht D. 1991b. Distributed snowmelt simulations in an alpine catchment. 1. Model evaluation on the basis of snow cover patterns. *Water Resources Research* **27**(12): 3171-3179.
- Blöschl G, Kirnbauer R. 1992. An analysis of snow cover patterns in a small alpine catchment. *Hydrological Processes* **6**: 99-109.

- Caine N. 1995. Snowpack influences on geomorphic processes in Green Lakes Valley, Colorado Front Range. *Geographical Journal* **161**(1): 55-68.
- Cleveland WS, Devlin SJ. 1988. Locally weighted regression: an approach to regression by local fitting. *Journal of the American Statistical Association* **83**(403): 596-610.
- Cline DW, Bales RC, Dozier J. 1998. Estimating the spatial distribution of snow in mountain basins using remote sensing and energy balance modeling. *Water Resources Research* **34**(5): 1275-1285.
- Elder K, Dozier J, Michaelsen J. 1991. Snow accumulation and distribution in an alpine watershed. *Water Resources Research* **27**(7): 1541-1552.
- Elder K, Rosenthal W, Davis R. 1998. Estimating the spatial distribution of snow water equivalence in a montane watershed. *Hydrological Processes* **12**(10-11): 1793-1808.
- Gray DM. 1979. Snow Accumulation and Distribution. In *Proceedings of a Meeting on Modeling of Snow Cover Runoff*, Colbeck SC, Ray M (eds). U. S. Army Cold Regions Research and Engineering Laboratory, Hanover, New Hampshire, September 26-28, 1978; 3-33.
- Gray DM, Male DH. (eds) 1981. *Handbook of Snow, Principles, Processes, Management & Use*. Pergamon Press: New York.
- Hardy JP, Davis RE, Jordan R, Li X, woodcock C, Ni W, McKenzie JC. 1997. Snow ablation modeling at the standing scale in a boreal jack pin forest. *Journal of Geophysical Research* **102**(D24): 29397~29405.
- Liston GE, Sturm M. 1998. A Snow-Transport Model for Complex Terrain. *Journal of Glaciology* **44**(148): 498-516.
- Loader C. 1999. *Local Regression and Likelihood*. Springer-Verlag: New York.
- Luce CH, Tarboton DG, Cooley KR. 1998. The influence of the spatial distribution of snow on basin-averaged snowmelt. *Hydrological Processes* **12**(10-11): 1671-1683.
- Marks D, Domingo J, Susong D, Link T, Garen D. 1999. A spatially distributed energy balance snowmelt model for application in mountain basins. *Hydrological Processes* **13**: 1935-1959.
- Marks D, Winstral A. 2001. Comparison of snow deposition, the snow cover energy balance, and snowmelt at two sites in a semiarid mountain basin. *Journal of Hydrometeorology* **2**(3): 213-227.



- Nash JE, Sutcliffe JV. 1970. River flow forecasting through conceptual models, 1. A discussion of principles. *Journal of Hydrology* **10**(3): 282-290.
- Pomeroy JW, Gray DM, Landine PG. 1993. The Prairie Blowing Snow Model: characteristics, validation, operation. *Journal of Hydrology* **144**: 165-192.
- Prasad R, Tarboton DG, Liston GE, Luce CH, Seyfried MS. 2000. Testing a blowing snow model against distributed snow measurements at Upper Sheep Creek. *Water Resources Research* **37**(5): 1341-1350.
- Schmidt RA. 1982. Vertical profiles of wind speed, snow concentration, and humidity in blowing snow. *Boundary Layer Meteorology* **34**: 213-241.
- Tabler RD, Pomeroy JW, Santana BW. 1990. Drifting snow. In *Technical Council on Cold Regions Monograph*, Ryan WL, Crissman RD (eds). American Society of Civil Engineering: New York; 95-145.
- Tarboton DG, Chowdhury TG, Jackson TH. 1995. A spatially distributed energy balance snowmelt model. In *Proceedings of a Boulder Symposium*, Tonnessen KA, Williams MW, Tranter M (eds). Boulder, CO., July 3-14, IAHS Publ. no. 228.
- Tarboton DG, Luce CH. 1996. Utah Energy Balance Snow Accumulation and Melt Model (UEB). Computer model technical description and users guide, Utah Water Research Laboratory and USDA Forest Service Intermountain Research Station (<http://www.engineering.usu.edu/dtarb/>). (Accessed Jul. 31, 2004).
- U.S. Army Corps of Engineers. 1956. Snow Hydrology, Summary Report of the Snow Investigations. U.S. Army Corps of Engineers, North Pacific Division, Portland, Oregon. 142 pp.
- Wigmosta MS, Vail LW, Lettenmaier DP. 1994. A distributed hydrology-vegetation model for complex terrain. *Water Resources Research* **30**(6): 1665-1679.
- Williams MW, J.S. B, N. C, R. S, Sanford. R J. 1996. Nitrogen saturation in the Rocky Mountains,. *Environmental Science and Technology*, **30**: 640-646.
- Winstral A, Elder K, Davis R. 2002. Modelling the effects of wind induce snow redistribution with terrain-based parameters to enhance spatial snow modelling. *Journal of Hydrometeorology* **3**(5): 524-528.

CHAPTER 4  
TERRAIN BASED PARAMETERIZATION OF THE  
SUBGRID VARIABILITY OF SNOW

Abstract:

The parameterization of the subgrid variability of snow is a theme in current snow hydrology research. A depletion curve that relates the basin average snow water equivalent to the fractional snow covered area used in the calculation of energy fluxes driving melt is one approach to the parameterization of subgrid variability. A depletion curve may be derived from the measured spatial distribution of snow water equivalent. However, this approach is limited by the size of the area that can be practically surveyed so other methods to obtain depletion curves are needed. Topography is a primary physical control variable on the snow accumulation and melt processes. Blowing wind and the accumulation of snow in drifts, as well as sliding and the accumulation of snow at the base of slopes are all governed by topography. This motivated the search for surrogate variables derived from topography from which a depletion curve can be directly estimated. This chapter evaluated depletion curves derived from: Elevation; accumulation factor estimated from snow covered area images; and peak accumulation estimated based on regression with accumulation factor and elevation as predictor variables. A spatially explicit model was used as reference. This chapter also evaluated the depletion curves derived from spatial distributions of accumulation and melt

combined using the convolution integral either assuming independence or explicitly recognizing the spatial dependence between accumulation and melt. It was found that the depletion curve derived using the distribution of elevation only, or assuming that accumulation and melt are independent are markedly different from the reference. The best overall result was obtained from the approach that combined accumulation and melt explicitly accounting for the spatial dependence. This is important because accumulation and melt are fundamentally different processes, related to different topographic attributes and this approach provides a formal way for these different effects to be correctly combined in the estimation of depletion curves for the parameterization of the subgrid variability of snow. The results indicate that it is possible to get depletion curves that approach the reference depletion curve based on surrogate variables, but that the better estimates still require some reliance on spatially explicit modeling.

## INTRODUCTION

Snowmelt is a surface water input of importance to many aspects of hydrology and water resources management. Snowmelt is primarily driven by energy exchanges at the snow surface that have variability down to horizontal scales of 1 to 10 m (hereafter referred to as the point scale). This variability leads to a non-uniform spatial distribution of snow water equivalent and patchiness in the snowcover during melt. The physical processes responsible for snowmelt at the point scale are relatively well understood and modeled by a variety of “point” models (Anderson, 1976; Morris, 1990; Jordan, 1991; Tarboton *et al.*, 1995; Tarboton and Luce, 1996). However when larger scales are

considered it is frequently computationally prohibitive, or there are insufficient data, to apply such models in a distributed way at each grid point with 1 to 10 m spacing as would be required for explicit physical representation of the process. Therefore, it is necessary to develop modeling approaches that can parameterize subgrid variability.

The surface energy fluxes driving snowmelt only melt snow when there is snow present, so an important process to consider in the parameterization of the subgrid variability of snow is the evolution of the snow covered area over time. Depletion curves have been developed to characterize the reduction in snow covered areas during the melt process.

Depletion curves have historically been used to predict runoff based on temperature index based melt estimates (e.g. Anderson, 1973; Martinec, 1980; Hall and Martinec, 1985; Brubaker *et al.*, 1996). In such models, the amount of melt is multiplied by the snow covered area to estimate the total input of water to a basin. Snow covered area has also been used in the modeling of basinwide snow water equivalent (Dunne and Leopold, 1978; Ferguson, 1986; Buttle and McDonnell, 1987; Luce *et al.*, 1999). In this sort of modeling, information about the total mass of snow in the area (from direct measurement of the snowpack or estimated from accumulated precipitation) is used, and conservation of mass is considered.

Luce *et al.* (1999) suggested the use of the depletion curve as a parameterization of subgrid variability in a physically based mass and energy balance snowmelt model. Rather than relating snow covered area to accumulated melt or degree days, as in earlier depletion curve methods, Luce *et al.* (1999) related snow covered area to the total mass of

snow remaining on the ground, or the area-averaged snow water equivalent. The area-averaged snow water equivalent was normalized by the maximum snow water equivalent accumulated to date during the current season. These modifications addressed two goals: first, they avoided the problem of assigning dates and peak or average depth at the onset of melt; second, they avoided the need for a new depletion curve each season. The depletion curve was naturally scaled by maximum snow accumulation in any given year, requiring only a non-dimensional functional form of the depletion curve to be specified. Luce *et al.* (1999) derived equations that estimated a dimensionless depletion curve from the distribution function of snow water equivalent at peak snow accumulation. Luce and colleagues' derivation focuses on differential accumulation as a cause for spatial variability. In their derivation the melt process is approximated as being spatially uniform. Luce *et al.* (1999) showed that basin average snow water equivalent and surface water input modeled using a depletion curve estimated from the peak snow accumulation distribution were practically as good as results from a fully distributed, physically-based mass and energy balance model for the Upper Sheep Creek Watershed.

Luce (2000) and Luce and Tarboton (2001) analyzed the parameterization of subgrid variability in snow accumulation and melt processes recognizing that spatial variability in energy inputs due to topography, as well as spatial variability in accumulation, contribute to the spatial variability of snowmelt. The spatial variability of energy inputs was accommodated in the derivation of depletion curves by scaling the peak snow accumulation by a normalized radiation exposure measure. This moved the

derived depletion curve closer to observations and results obtained from a detailed distributed model.

The approaches developed in the earlier work (Luce *et al.*, 1999; Luce, 2000; Luce and Tarboton, 2001) depend upon spatially distributed snow water equivalent measurements. Obtaining these measurements is impractical for large watersheds. The purpose of this paper is to explore approaches for deriving depletion curves from more fundamental and readily available topographic attributes.

Topography is a primary control on the spatial variability of snow accumulation and melt. Elevation is related to air temperature expressed through the lapse rate, and air temperature is related to snowmelt through sensible heat fluxes (Gray and Male, 1981) and incident longwave radiation (Marks and Dozier, 1979) from the atmosphere. Topography also influences shortwave radiation inputs through the exposure to sunlight which is controlled by slope, aspect (slope direction) and terrain shading (Dozier, 1980). Diffuse radiation is dependent upon sky view factors (Dozier and Frew, 1990).

There is also variability in the distribution of snowcover due to other processes like wind drifting, sloughing or avalanching ( Gray and Male, 1981; Elder *et al.*, 1991; Blöschl and Kirnbauer, 1992). Luce *et al.* (1998) and Prasad *et al.* (2000) demonstrated that wind plays an important role in the distribution of snow in the Upper Sheep Creek watershed. Elder *et al.* (1991) examined factors affecting alpine snow distribution in regions above the treeline, and attributed much of the observed spatial heterogeneity to redistribution by wind. Research on the redistribution of snow due to wind (Schmidt, 1982; Tabler *et al.*, 1990) has led to the development of the Prairie Blowing Snow

(Pomeroy *et al.*, 1993) and SnowTran-3D (Liston and Sturm, 1998) models, which model physical wind redistribution processes. Winstral *et al.* (2002) and Winstral and Marks (2002) adopted a statistical approach to relating topographic attributes with snow accumulation and found that statistical model predictions of snow accumulation based on topographic variables were significantly improved when wind related parameters were used as inputs.

The accumulation factor approach (Tarboton *et al.*, 1995; Tarboton and Luce, 1996; Luce *et al.*, 1998; Prasad *et al.*, 2000) has been developed to empirically relate the spatial pattern of snow accumulation over an area to point precipitation measurements. Each point is assumed to have a propensity to accumulate snow represented by a factor that is multiplied by the measured precipitation to obtain spatially distributed precipitation inputs. Past work has obtained the distribution of accumulation factor over a watershed using measurements of snow water equivalent (Luce *et al.*, 1998) or by running a blowing snow model (Prasad *et al.*, 2000). Marks and Winstral (2001) derive the accumulation factor by classifying the watershed using slope, aspect, and terrain variables specifically designed to represent the propensity for snow accumulation or scour due to wind, such as the slope angle and distance to source location in the direction from which the prevailing wind blows.

Chapter 3 gave an approach for calibration of the accumulation factor from snow covered area images which are more readily available than the snow water equivalent for a large watershed. Bounds on the accumulation factor were calibrated in accordance with the date the snow cover disappeared. The lower bound on the accumulation factor was

obtained from the last day snow cover was observed, while the upper bound was obtained on the first day snow was not observed at each point. Grid cells at the edges of the snow covered area were assumed to be about to melt completely so their accumulation factor was estimated at the lower bound while cells in the snow free area adjacent to a snow covered area were assumed to have just become snow free so their accumulation factor was estimated at the upper bound. The accumulation factor values from these edge grid cells where a single value rather than a range for the accumulation factor was estimated were used to develop regression models based on terrain variables that interpolate the accumulation factors over the entire domain. This approach provides a way to estimate the accumulation factor using a combination of meteorological data and the snow covered area images.

Depletion curves, which serve as a subgrid parameterization are directly related to the spatial distribution of snow as characterized by a spatial probability density function (pdf) (Luce *et al.*, 1999). The spatial distribution of snow is related to topography. The goal of this chapter is to explore ways to obtain a depletion curve directly from topographic attributes. We evaluate a number of approaches. First we assume that the distribution of snow is linearly related to the distribution of elevation and use the pdf of elevation to derive a depletion curve. Second, we assume that the distribution of snow is linearly related to the accumulation factor, derived from snow covered area images using the procedure presented in chapter 3. This approach incorporates elevation to some extent because elevation was one of the attributes used in developing the model in chapter 3. Third, we explicitly combine accumulation factor and elevation using linear



weighting. The fourth approach evaluated combines the spatial distribution of melt estimated from topography, based on the ABC model approach (Williams and Tarboton, 1999), with the spatial distribution of accumulation from the accumulation factor and elevation. In developing this last approach, new theory that relates depletion curves to the spatial distribution of snow was developed to explicitly combine the snow accumulation and snow melt distributions with mean accumulation and melt, to arrive at a depletion curve. This is important because accumulation and melt are fundamentally different processes, related to different topographic attributes and this approach provides a formal way for these different effects to be correctly combined. Depletion curves derived from each approach were used as subgrid parameterizations in a large scale snowmelt model. Results were evaluated against observations of snow covered area and distributed model simulations.

## METHODS

The UEB model (Tarboton *et al.*, 1995; Tarboton and Luce, 1996, also see chapter 2) was used in this work. Two forms of the model were used. The first is the point model described in chapters 2 and 3. The second is the large scale model where the depletion curve parameterization of subgrid variability is included following Luce *et al.* (1999). In chapter 3 the accumulation factors necessary to apply the point form of the model were calculated based upon snow covered area data. The model applied in a spatially explicit mode to each 10 m grid cell in the domain using these accumulation factors provides the best available estimate of the spatially distributed snow processes

over the domain. These results are taken as reference and referred to as the "distributed modeled" results.

To facilitate application of snowmelt models over large areas it is necessary to have larger model elements than the 10 m grid cells. What we refer to as the large scale lumped model consists of one model element over the entire study area, with subgrid variability within this domain parameterized using a depletion curve. Different depletion curves, estimated in different ways are evaluated.

*Large scale lumped model with depletion curve parameterization*

The UEB model (Tarboton *et al.*, 1995; Tarboton and Luce, 1996, also see chapter 2) is an energy and mass balance snow melt model. The time evolution of the snowpack is driven by the energy exchange between the snowpack, the air above and the soil below according to mass and energy balance equations using spatially averaged climatic inputs (Figure 4-1), applied over the fraction of the area that is snow covered. The large scale form of the model with depletion curve parameterization has three state variables: 1)  $W_a$ , the basin average snow water equivalent; 2)  $U$ , the snowpack energy content of the snow-covered area; and 3) the fraction of area that is snow covered,  $A_f$ . In updating the energy and mass balance the snow covered area snow water equivalent,  $W_{sc}$ , is first calculated from the basin average snow water equivalent,  $W_a$ ,

$$W_{sc} = W_a / A_f . \quad (4-1)$$

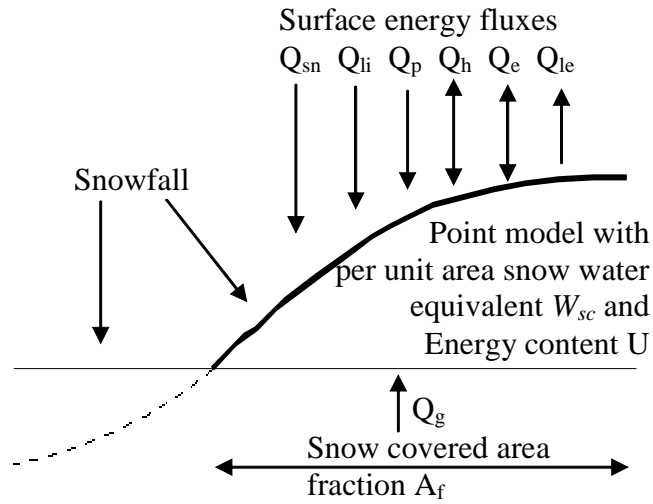


Figure 4-1 Schematic of lumped snowmelt model

Then point energy balance equations are applied

$$\frac{\partial U}{\partial t} = Q_{sn} + Q_{li} - Q_{le} + Q_e + Q_h + Q_g + Q_p - Q_m \quad (4-2)$$

$$\frac{\partial W_{sc}}{\partial t} = P_r + P_s - M_r - E \quad (4-3)$$

where  $Q_{sn}$  is net solar radiation;  $Q_{li}$  is incoming longwave radiation;  $Q_{le}$  is outgoing longwave radiation;  $Q_p$  is advected heat from precipitation;  $Q_g$  is ground heat flux;  $Q_h$  is the sensible heat flux;  $Q_e$  is the latent heat flux;  $Q_m$  is heat advected with melt water;  $P_r$  is the rate of precipitation as rain;  $P_s$  is the rate of precipitation as snow;  $M_r$  is the melt rate; and  $E$  is the sublimation rate. The same parameterizations as used in the point model are used for each energy and mass exchange term.

Runge-Kutta finite difference approximations are used to propagate  $W_{sc}$  and  $U$  forward in time resulting in a change in the snow covered area snow water equivalent,  $\Delta W_{sc}$ , for the time step being calculated. Area average snow water equivalent is then updated according to

$$W_a = W_a + A_f \cdot \text{Min}(\Delta W_{sc}, 0) + \text{Max}(\Delta W_{sc}, 0). \quad (4-4)$$

In this equation when  $\Delta W_{sc} < 0$  melt is occurring over the snow covered area only and  $W_a$  is reduced by  $A_f \cdot \Delta W_{sc}$  as calculated by the *Min* term. When  $\Delta W_{sc} > 0$ , snow is accumulating due to snowfall; this occurs over the entire area so  $W_a$  is increased by  $\Delta W_{sc}$  as calculated by the *Max* term.

Once  $W_a$  has been updated at each time step the fraction of area that is snow covered is updated using a depletion curve

$$A_f = A_{dc}(W_a). \quad (4-5)$$

Here  $A_{dc}(W_a)$  is the depletion curve representing the functional relationship between the basin averaged snow water equivalent and fractional snow covered area, illustrated schematically in Figure 4-2. On the left axis, is the fractional snow covered area (ranging from 0 to 1) and the lower axis is the basin average snow water equivalent. Note that the depletion curve is expressed in dimensionless form  $A_{dc}^*(W_a)$  with the lower axis

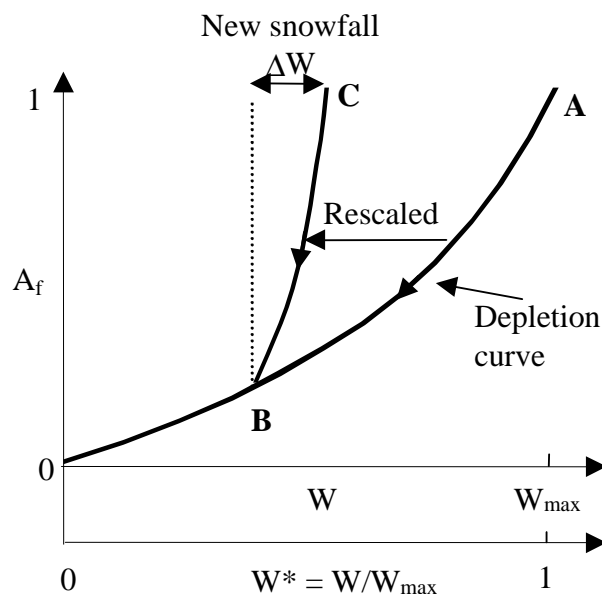


Figure 4-2 Depletion curve parameterization of subgrid variability in a lumped snowmelt model (after Luce *et al.*, 1999). As basin average snow water equivalent is reduced snow covered area reduces along this curve which is made dimensionless scaled by the maximum snow accumulation

dimensionless snow water equivalent  $W^* = W_a / W_{amax}$ , scaled relative to the maximum basin average snow water equivalent  $W_{amax}$  experienced to date within the season (since  $W_a$  was last 0)

$$A_{dc}(W_a) = A_{dc}^* (W_a / W_{amax}). \quad (4-6)$$

This lets the onset of melt be determined naturally from the modeling of physical processes, rather than using parameters determining the “beginning” of the melt season (Luce *et al.*, 1999). This also provides for a natural year to year adjustment of the depletion curve as  $W_{amax}$  varies from year to year, avoiding the need to have a depletion

curve specific to the snow accumulation amount for each year. A procedure for accommodating new snowfall part of the way through the season given by Luce *et al.* (1999) is used. When there is new snowfall at point B say,  $W_a$  is incremented by the new snowfall water equivalent,  $\Delta W_{sc} > 0$ , (taken over the whole area) and  $A_f$  goes to one. This is point C in Figure 4-2. The new snowfall (covering the whole element) will be subjected to the same processes that lead to spatial variability as the old snow. Also, it will melt first. Therefore it is assumed that the system returns along a rescaled depletion curve to the point of original departure, B. In this fashion multiple accumulation and melt periods can be accommodated. In principle there could be multiple rescalings and multiple points B, reminiscent of hysteresis loops in soil wetting and drying characteristic curves. However we only keep track of one departure point B.

*Relationship between depletion curve and spatial distribution of snow*

The dimensionless depletion curve function,  $A_{dc}^*(W_a)$ , may be estimated from the probability density function (pdf) of snow water equivalent sampled spatially following Luce *et al.* (1999). Implicit in this derivation is the assumption that spatial variability is created primarily by differential accumulation, and that melt is uniform. Imagine a cross section through this snowpack and that this snowpack experiences a spatially uniform cumulative potential melt depth,  $m$ . (This is potential because if the quantity of snow at a point is less than  $m$  it is not realized.) We can convert the spatially explicit representation of the snowpack water equivalent to a generic probability density function (pdf) of snow water equivalent,  $f_g(w)$ , that retains a consistent shape through the melt season (spatially

uniform melt), so that the parameter,  $m$ , represents a shift of the  $w = 0$  axis over the pdf to the right as the snow ablates (Figure 4-3). Then for any particular melt depth,  $m$ , the tail to the left of the y-axis represents snow-free area. The remaining shaded portion of the distribution represents the snow water equivalent distribution over the fraction of area that is snow covered. The first moment of this truncated distribution represents the mean snow water equivalent,  $W_a$ , which divided by  $A_f$  gives the snow covered area snow water equivalent,  $W_{sc}$ , equation 4-1.

Two different depletion curve functions representing the reduction of snow covered area as a function of cumulative potential melt depth,  $A_m(m)$  and the reduction of snow covered area as a function of basin average mean snow water equivalent,  $A_{dc}^*(W_a)$  exist. These can both be derived from integrating the generic pdf over the shaded area represented in Figure 4-3.

First the fraction of area that is snow covered is evaluated as a function of  $m$  to obtain  $A_m(m)$  as:

$$A_m(m) = \int_0^{\infty} f_g(w+m) dw = \int_m^{\infty} f_g(w) dw = 1 - F_g(m) \quad (4-7)$$

where  $F_g(m)$  is the cumulative distribution function of  $f_g(w)$  evaluated at  $m$ . For any arbitrary  $m$ ,  $A_m(m)$  is the fraction of the basin that had snow water equivalent  $W$  at peak accumulation greater than  $m$ . Practically, the function  $A_m(m)$  may be numerically evaluated directly from a sample of snow water equivalent values across the area of interest.  $A_m(m)$  is the number of samples with snow water equivalent greater than  $m$

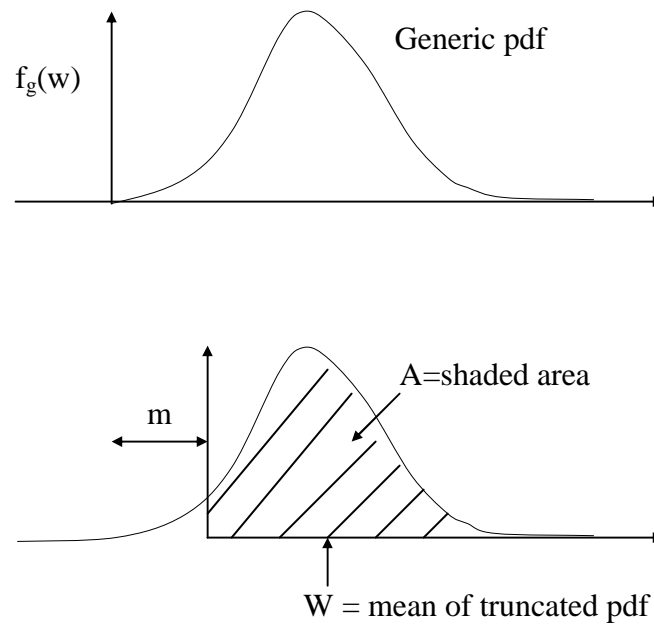


Figure 4-3 Schematic of generic snow water equivalent probability distribution (after Luce *et al.*, 1999)

divided by the total number of samples. The function  $A_m(m)$  is the classic depletion curve expressed as the fraction of area that is snow covered as a function of potential melt depth.

To obtain the second depletion curve function  $A_{dc}^*(W_a)$  the basin average snow water equivalent is calculated as the mean of the generic pdf for any specific  $m$ . The probability distribution of snow water equivalent for any particular  $m$  has a nugget at zero because a negative  $W$  has no physical interpretation. The finite probability of the areally sampled snow water equivalent being zero is  $1-A_m(m)$ . The part of the pdf to the right of the axis represents the snow water equivalent pdf for non-zero snow water equivalent (all of the snow-covered points in the areal sampling). Consequently, a function giving the



basin-average snow water equivalent in terms of  $m$ ,  $W_m(m)$  is calculated (from the usual definition of a mean) as:

$$W_m(m) = \int_m^{\infty} (w - m) f_g(w) dw \quad (4-8)$$

which can be integrated by parts (see Luce *et al.*, 1999 for derivation ) to obtain

$$W_m(m) = \int_m^{\infty} A_m(w) dw . \quad (4-9)$$

Numerical integration of  $A_m(m)$  can be used to obtain  $W_m(m)$ . For any potential  $m$  this function gives the basin average snow water equivalent,  $W_a = W_m(m)$ . The function inverse of this is  $m = W_m^{-1}(W_a)$ . Now the functions  $A_m(m)$  and the function inverse,  $W_m^{-1}(W_a)$ , are combined to obtain

$$A_{dc}(W_a) = A_m(W_m^{-1}(W_a)) . \quad (4-10)$$

This expresses the depletion curve with basin average snow water equivalent as the input argument. This snow water equivalent depletion curve may be calculated by evaluating  $A_m(m)$  and  $W_m(m)$  for many values of  $m$ . The maximum basin average snow water equivalent  $W_{amax}$  under the generic pdf  $f_g(w)$  occurs when  $m=0$ , i.e.

$$W_{amax} = W_m(0). \quad (4-11)$$

The dimensionless snow water equivalent depletion curve is then written as

$$A_{dc}^*(w^*) = A_{dc}^*(w_a / W_{amax}) = A_{dc}(w_a), \quad (4-12)$$

A generic probability density function  $f_g(w)$  has mean position (first moment) and scale (second moment) parameters given as follows

$$\mu = \int_0^{\infty} w f_g(w) dw, \quad (4-13)$$

$$\sigma^2 = \int_0^{\infty} (w - \mu)^2 f_g(w) dw. \quad (4-14)$$

Consider a rescaling of  $w$ , say  $x=cw$ . The rescaled generic pdf is

$$f_x(x) = \frac{1}{c} f_g\left(\frac{x}{c}\right) \quad (4-15)$$

using  $f_x(x)$  in equations 4-7 to 4-12 one obtains a dimensionless depletion curve

$A'_{dc}^*(W_a)$  that is equivalent to  $A_{dc}^*(W_a)$  derived from  $f_g(x)$ . This is shown in the appendix. This equivalence is due to the rescaling involved in equation 4-12. As a consequence of this, the dimensionless depletion curve is insensitive to specific values for the mean and variance of  $f_g(w)$ , it is sensitive only to the ratio of them, the coefficient of variation,  $CV = \sigma / \mu$ .

#### *Derivation of depletion curve from terrain attributes*

The approach described above provides a way to obtain a depletion curve from any probability distribution representative of the spatial distribution of snow. Here we hypothesize that the distribution of snow is related to the distribution of specific terrain attributes and use the procedure above to derive the depletion curve from the distribution of terrain attributes. Simulations based on the depletion curve so obtained are compared to simulations with the detailed distributed model to evaluate the effectiveness of the depletion curve parameterization.

*Elevation based depletion curve derivation.* Elevation influences the distribution of snow through the air temperature which lapses with elevation as well as due to the orographic effects of topography upon precipitation or other processes such as melt and evaporation/condensation which affect snow accumulation. Here we assume a linear relationship between the snow accumulation and elevation:

$$a = \alpha z + \beta, \tag{4-16}$$

where  $a$  is accumulation of snow,  $z$  is elevation,  $\alpha$  and  $\beta$  are parameters. Here  $a$  has been introduced as a variable denoting snow accumulation, rather than  $w$  because later  $w$  will be used to denote snow water equivalent combining the effects of accumulation and melt. In this method, the pdf of the snow accumulation,  $f_a(a)$ , can be written as a scaled and shifted version of the pdf of elevation,  $f_z(z)$ :

$$f_a(a) = \frac{1}{\alpha} f_z(z) = \frac{1}{\alpha} f_z\left(\frac{a - \beta}{\alpha}\right). \quad (4-17)$$

Given parameters  $\alpha$  and  $\beta$  the pdf from equation 4-17 could be used with the procedure described in equations 4-7 to 4-12 to derive a depletion curve. This procedure is insensitive to the specific moments of the distribution, but is sensitive to the coefficient of variation. In the case of equation 4-16 the coefficient of variation depends on parameters  $\alpha$  and  $\beta$ , specifically the datum or elevation location parameter  $\beta$  related to the range of elevation scaled by  $\alpha$ . Here  $\alpha$  and  $\beta$  were determined by taking  $a$  as the snow water equivalent at the date of peak snow accumulation (5/2/1996) from the spatially explicit model and using regression to fit equation 4-16. The depletion curve derived for this method and the results obtained using this depletion curve were labeled as “elevation only.”

Accumulation factor based depletion curve derivation. The accumulation factor derived in chapter 3 relates the propensity of a location to accumulate snow to terrain attributes. Here a depletion curve was derived based on the distribution of accumulation

factor, assuming that variability in snow accumulation is the dominant cause for the spatial variability of snow during melt. In terms of the accumulation factor the snow accumulation can be written as:

$$a = P \cdot \phi . \quad (4-18)$$

Here  $P$  is the precipitation, and  $\phi$  is the accumulation factor. The pdf of the snow accumulation,  $f_a(a)$ , is a scaled version of the pdf of accumulation factor  $f_\phi(\phi)$ :

$$f_a(a) = \frac{1}{P} f_\phi(\phi) = \frac{1}{P} f_\phi\left(\frac{a}{P}\right) . \quad (4-19)$$

Since the depletion curve only depends on the coefficient of variation of the distribution, the depletion curve is insensitive to  $P$  and can be derive from  $f_\phi(\phi)$  directly. The depletion curve derived from this method and the results obtained using this depletion curve were labeled as “accumulation factor only.”

*Elevation and accumulation factor depletion curve derivation.* The previous two approaches used elevation and accumulation factor separately to derive a depletion curve. Both elevation and accumulation factor are quantities related to the spatial variability of snow and inputs to consider for deriving a depletion curve.

There is some interdependence between  $\phi$  and  $z$ , because  $z$  was a predictor variable used to obtain  $\phi$  (Chapter 3). Nevertheless, recognizing that  $z$  may also have

direct explanatory capability towards the distribution of snow, we evaluate a depletion curve obtained by combining  $\phi$  and  $z$  directly. We write

$$a = c\phi + dz + e , \quad (4-20)$$

where  $c$ ,  $d$ , and  $e$  are parameters. The probability distribution of  $a$  is obtained from the distribution of  $\phi$  and  $z$  in the domain. The parameters  $c$ ,  $d$ , and  $e$  effectively provide a weighting between  $\phi$  and  $z$  in the distribution of  $a$ , and a location of the  $z$  distribution, recognizing the arbitrariness of a  $z$  datum. Here  $c$ ,  $d$ , and  $e$  were obtained by taking  $a$  as the snow water equivalent at the date of peak snow accumulation (5/2/1996) from the spatially explicit model and using multiple linear regression. The derived depletion curve and corresponding modeling results were labeled “elevation and accumulation factor.”

*Derivation of depletion curve from differential accumulation and differential melt.*

The above three approaches approximate the peak snow accumulation and assume uniform melt across the watershed. Topography also leads to variability in the snow melt through variability in the energy components such as incident shortwave radiation, longwave radiation, and turbulent heat fluxes. Here we combine accumulation and melt in the derivation of the depletion curve. The snow water equivalent at a point is given by

$$w = a - m , \quad (4-21)$$

where  $a$  is the accumulation and  $m$  is the melt at a specific point. Equation 4-21 can also be expressed in terms of the spatial mean of accumulation,  $\bar{a}$ , and the spatial mean of potential melt,  $\bar{m}$ , perturbed by factors  $a'$  and  $m'$ , respectively:

$$w' \bar{w} = a' \bar{a} - m' \bar{m}. \quad (4-22)$$

Here  $a'$  and  $m'$  are interpreted as quantities that vary spatially according to distributions that represent the spatial patterns of accumulation and melt, the weighting of which, through  $\bar{a}$  and  $\bar{m}$  determines the spatial pattern of  $w'$  relative to its mean  $\bar{w}$ . Taking the expectation  $E(a' \bar{a}) = \bar{a}$ ,  $E(m' \bar{m}) = \bar{m}$ , therefore  $E(a') = 1$  and  $E(m') = 1$ . The expectation or mean of  $w$  (denoted  $\bar{w}$ ) can be written as:

$$\bar{w} = \bar{a} - \bar{m}. \quad (4-23)$$

Dividing equation 4-22 by equation 4-23 gives:

$$w' = \frac{w}{\bar{w}} = \frac{a' \bar{a} - m' \bar{m}}{\bar{a} - \bar{m}} = \frac{a' - m' (\bar{m} / \bar{a})}{1 - (\bar{m} / \bar{a})}, \quad (4-24)$$

where  $w'$  is the perturbation of snow water equivalent. This shows that the general distribution of  $w'$  depends only on the ratio  $\bar{m} / \bar{a}$ , not on their separate values. This is useful in developing depletion curves because only a single parameter needs to vary.

Here we note that the distribution of  $w'$  in equation 4-24 is a mathematical solution which can be negative. Physically locations where  $w' < 0$  are interpreted as snow free. Also the melt  $\bar{m}$  is the mean of potential melt not the mean of actual melt which is constrained by the amount of snow water equivalent present.

Figures 4-4 a to c illustrate the processes involved. In (a) accumulation probability distributions of  $a$  at times 1 and 2 are shown, with  $\bar{a}_2 > \bar{a}_1$ . Figure 4-4 b shows the melt removed from a specific accumulation, say  $\bar{a}_2 a_2'$  for different melt quantities. At a specific location at time 2 the melt is  $\bar{m}_2 m_2'$ . Figure 4-4 c shows the probability distribution of snow water equivalent that results from the combination of these effects.

Given a specific  $\bar{a}$ , when  $\bar{m}$  is 0,  $\bar{w} = w_{amax}$  the maximum possible basin average accumulation for this  $\bar{a}$ . Since  $f(a)$  has support only on the domain  $a > 0$  the snow covered area fraction is 1. As  $\bar{m}/\bar{a}$  increases some fraction of area has  $w'$  in equation 4-24 less than zero representing snow free area. This is the area to the left of the axis in Figure 4-4 c.  $\bar{m}/\bar{a}$  provides an index for the calculation of  $w'$ , and from the distributions of  $a'$  and  $m'$ , the snow covered area fraction  $A_f$ .  $\bar{m}/\bar{a}$  also provides an index for the evaluation of basin average snow water equivalent  $W_a$  (different from  $\bar{w}$ ) because it is the integral of  $w' \bar{w}$  over the positive part of the distribution representing snow covered area. This gives a depletion curve. We have



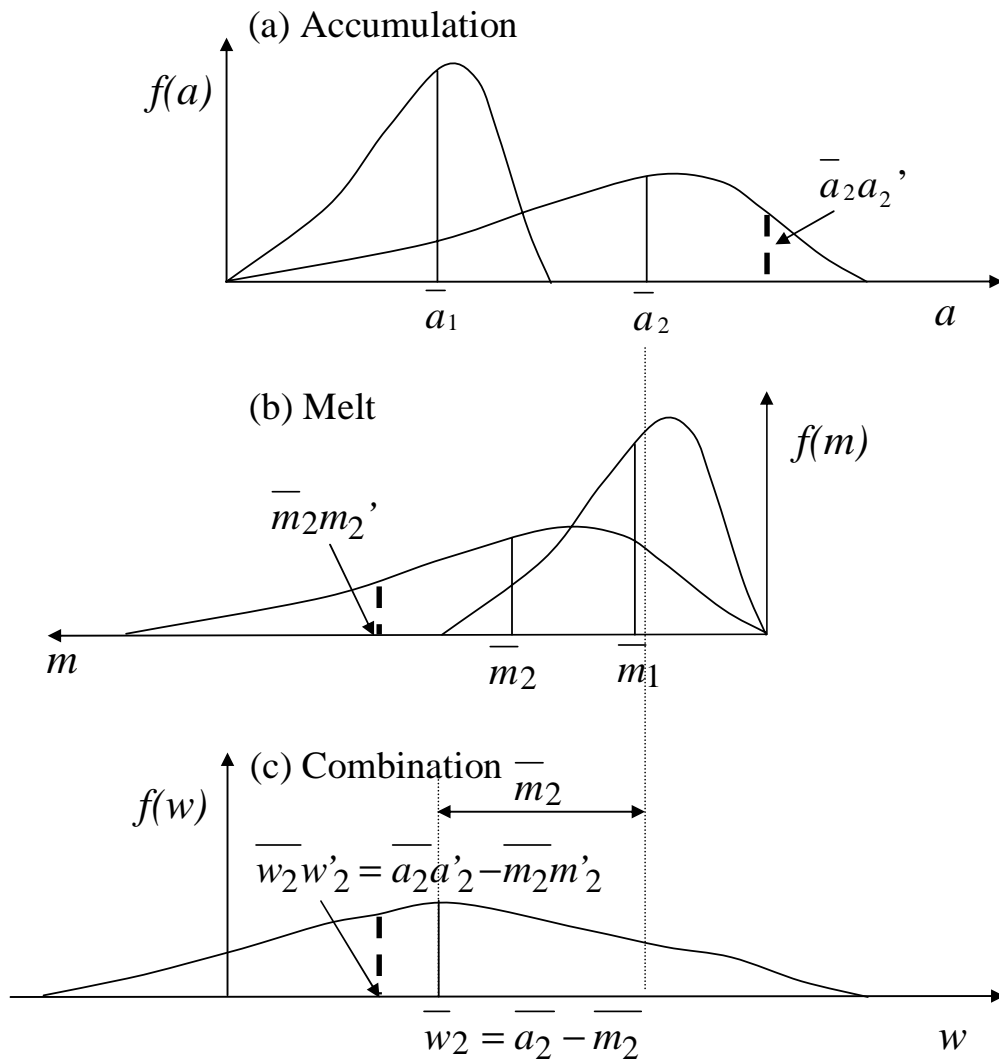


Figure 4-4 Illustration of the time evolution of snow accumulation and melt distributions and the combined snow water equivalent distribution that results

$$w'\bar{w} = w'(\bar{a} - \bar{m}) = w'(1 - \bar{m}/\bar{a})\bar{a} . \tag{4-25}$$

This shows that the distribution of  $w$  is indexed by  $\bar{m}/\bar{a}$  times  $\bar{a}$  which we are holding constant, without loss of generality in the final depletion curve, due to the insensitivity of depletion curves to rescaling shown earlier.

Two separate assumptions regarding the dependence between  $a'$  and  $m'$  are considered.

Case 1.  $a'$  and  $m'$  are dependent.

The domain provides us with an explicit spatial sampling of these and for a range of  $\bar{m}/\bar{a}$  we can develop the distribution of  $w$  and the depletion curve using the procedure described previously.

Case 2.  $a'$  and  $m'$  are assumed to be independent.

Given the distributions of accumulation and melt,  $a'$  and  $m'$ , these are taken as independent random variables combined in a weighted linear convolution given by equation 4-24. The weighting is determined by  $\bar{m}/\bar{a}$ . Convolution of the distributions of  $a'$  and  $m'$  gives the distribution of  $w'$  for each  $\bar{m}/\bar{a}$  from which the depletion curve is again derived.

Luce (2000) and Luce and Tarboton (2001) considered the way that the spatial pattern of potential melt affects a depletion curve. They used radiation exposure,  $E_r$ , as an index of melt potential and scaled the distribution of snow water equivalent,  $W$ , at the time of peak accumulation by this index to define an effective snow water equivalent.

$$W_e = W / E_r. \quad (4-26)$$

Both  $W$  and  $E_r$  were spatially distributed inputs, evaluated explicitly at each grid location, equivalent to the dependent case above. They then used  $W_e$  in the procedure of equations 4-7 to 4-12 to derive a dimensionless depletion curve, again relying on the

insensitivity of a dimensionless depletion curve to scalar multiplication. If we equate  $E_r$  to  $m'$  this approach is equivalent to case 1 above.

Equations 4-21 and 4-22 can be written:

$$\frac{w}{m'} = \frac{a'}{m'} \bar{a} - \bar{m} = \bar{a} \left( \frac{a'}{m'} - \frac{\bar{m}}{\bar{a}} \right). \quad (4-27)$$

The procedure developed by Luce (2000) and Luce and Tarboton (2001) is equivalent to case 1 with  $a'$  and  $m'$  dependent when  $E_r$  and  $m'$  are equated because then in this equation  $w/m'$  has a probability distribution the same shape as the distribution of  $a'/m'$  (scaled by  $\bar{a}$ ) and the procedure of equations 4-7 to 4-12 is equivalent to increasing the index  $\bar{m}/\bar{a}$  shifting this distribution to the left.

Williams and Tarboton (1999) suggested that snowmelt was linearly related to elevation and radiation input at each point over a watershed. This idea is expressed as:

$$m = A + Bz + CR = m' \bar{m}, \quad (4-28)$$

where  $A$ ,  $B$ , and  $C$  are parameters,  $z$  is elevation, and  $R$  is the shortwave radiation exposure. This is referred to as the ABC model. Thus the perturbation of melt,  $m'$ , can be derived from the elevation and the radiation exposure (incident short wave radiation). Williams and Tarboton (1999) suggest that  $A$ ,  $B$ , and  $C$  be calculated at each time step using measurements at several points within the domain. Here continuous melt measurement was not available so we instead used a distributed snowmelt model to

represent the pattern of potential snowmelt. The point UEB model described in chapter 3 was utilized with a very thick uniform snowpack (10 m snow water equivalent) on May 2, 1996 and run using observed climate input until August 30, 1996, the assumed end of the winter season. This model provided cumulative potential melt  $m$  at each location, together with cumulative modeled shortwave radiation,  $R$ , calculated by the model accounting for topography and seasonal sun angle effects. The elevation was an input to the model so by this procedure we have  $m$ ,  $z$  and  $R$  for equation 4-28.

Two options are available to us for  $m$ : (1) use the model derived  $m$ ; (2) fit equation 4-28 using the grid cells in the domain and obtain  $m$  from equation 4-28. These were both used and are referred to as UEB model derived  $m$  and ABC model derived  $m$ .

Since the objective of this work is to estimate the depletion curve from topography and parameters derived therefrom we used  $a$  from the elevation and accumulation factor regression (Equation 4-20) together with the ABC model derived  $m$  to obtain a depletion curve using the method given in equations 4-21 to 4-24. This is referred to as the depletion curve from differential accumulation and melt parameterized by topography (DAMPT). Discrepancies between the output from this modeling approach and observation are due to both the approximations involved in deriving the depletion curve and in parameterizing the inputs  $m$  and  $a$  from the terrain.

To decompose the errors we also used the method given in equation 4-21 to 4-24 with UEB model derived potential melt,  $m$ , from the May 2, 1996 to August 30, 1996 run initialized with 10 m snow water equivalent, and  $a$  from the UEB modeled peak accumulation on May 2, 1996. This is our best estimate of the inputs  $a$  and  $m$ , and

provides an assessment of the errors due to the depletion curve approach, while minimizing the errors involved in parameterizing  $a$  and  $m$ . This is referred to as the depletion curve from differential accumulation and melt UEB modeled (DAMUM).

## STUDY SITES AND DATA

The 8.1 km<sup>2</sup> Green Lakes Valley watershed (GLV) is a high Rocky mountain basin with steep cliffs, talus slopes, and limited soil cover located 40 km west of Boulder, CO (see Figure 4-5). Bare rock comprises about 1/3 of the basin area, talus slopes comprise about 1/3 of the basin area, and soil comprises the other 1/3 of the basin area. The 8-ha Arikaree cirque glacier lies at about 3800 m just below the Continental Divide within the basin. Elevation in Green Lakes Valley watershed ranges from 3204 to 4087 m, with most of the basin lying above treeline. Mean monthly minimum temperatures are below 0 °C from October through May with monthly maxima below freezing from November to April (Berg, 1986). The area is characterized by a mountain continental climate, annually receiving about 1000 mm of precipitation (Williams *et al.*, 1996), 80% of which is in the form of snow (Caine, 1995). Weather data has been collected at the four stations shown whose locations range from valley to ridge top. This comprises air temperature, relative humidity, wind speed and direction, and incident solar radiation. Precipitation is only measured at station D1. Digital elevation data at 10-m resolution that was produced photogrammetrically was available. High-resolution orthophotos (~10 m) produced from Metric 1:24,000 aerial photographs taken on four dates in 1996 were

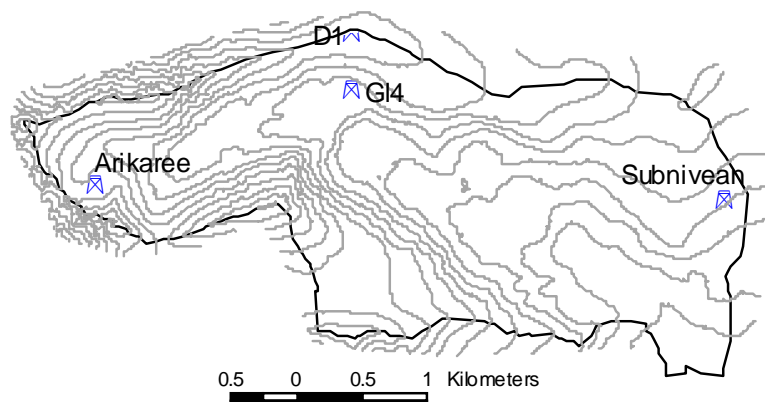


Figure 4-5 Green Lakes Valley watershed location map. The contour interval is 50 m. Four weather stations are located

also available. The snow covered area images classified from these orthophotos provide information about the snowpack depletion processes.

## RESULTS

### *Estimation of depletion curves*

The spatially explicit distributed version of the new UEB snowmelt model described in chapter 3 was used to provide reference results for comparisons to the output from the lumped model with various depletion curves. Figure 4-6 gives the regressions used to obtain some of the parameters used in the depletion curves. Figure 4-7 gives the depletion curves estimated from each approach. The distributed modeled reference depletion curve represents simulations of snow covered area versus snow water equivalent during the melt period from the spatially explicit distributed version of the new UEB snowmelt model described in chapter 3. This is used as a reference for the

assessment of other depletion curves. The spikes are when there is snowfall and whole area becomes briefly snow covered before returning to the same depletion curve. This process apparent here in explicit spatially distributed simulations is represented in the depletion curve subgrid parameterization illustrated in Figure 4-2.

Figure 4-6a plots distributed modeled peak snow water equivalent on May 2, 1996 versus elevation. Despite the fact that the relationship is weak, linear regression was used

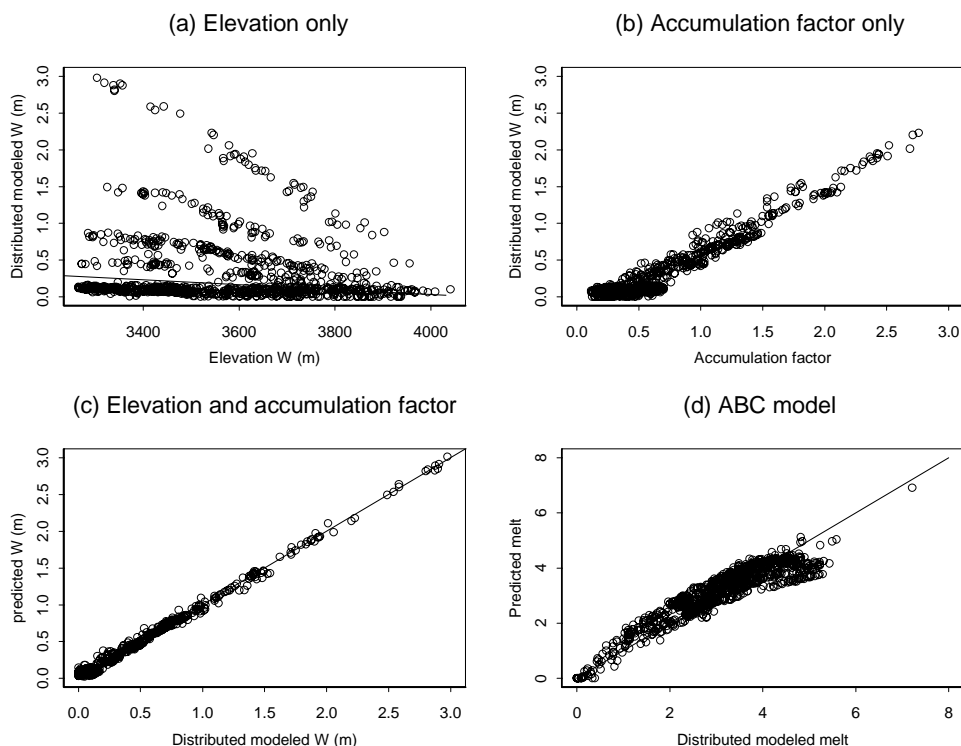


Figure 4-6 Relationships involved in the derivation of depletion curves. Each plot displays only 1000 sample points from the total of 85698 cells in the domain used in the relationships. a) Distributed modeled snow water equivalent on May 2, 1996 versus elevation. b) Distributed modeled snow water equivalent on May 2, 1996 versus accumulation factor. c) Predicted versus distributed modeled reference snow water equivalent on May 2, 1996 from the multiple linear regression of equation 4-20. d) ABC model fit to distributed modeled melt between May 2, 1996 and August 30, 1996 with 10 m snow water equivalent initial conditions

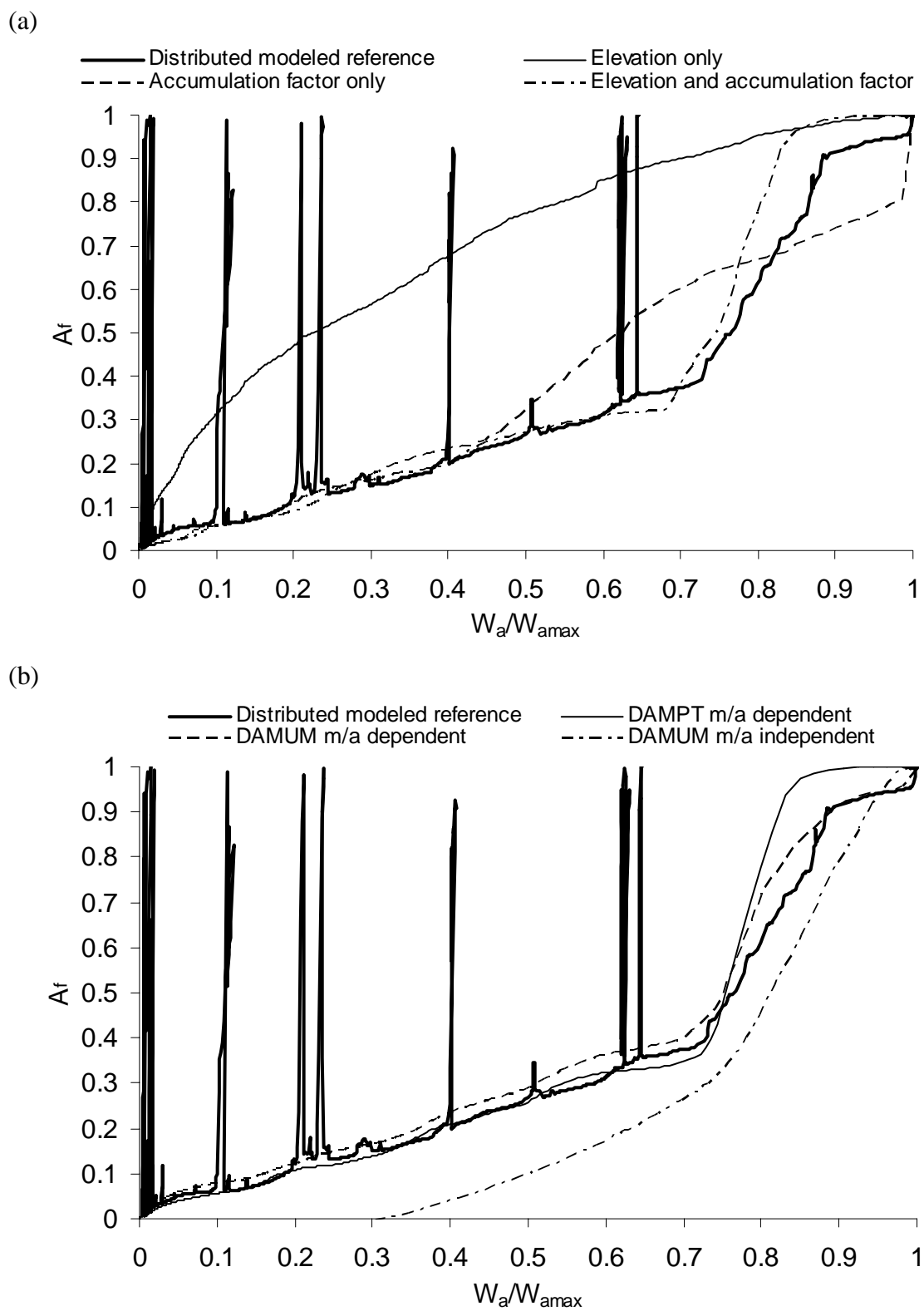


Figure 4-7 Depletion curves derived with the different approaches evaluated



to estimate  $\alpha$  and  $\beta$  in equation 4-16.  $\alpha$  has a value of -0.0034 and  $\beta$  has a value of is 1.36. The five line clusters in the plot are due to the accumulation factor originally being quantified from five interpolation models for different time intervals (see Chapter 3) between the dates of the snow covered area images. The depletion curve estimated from the distribution of  $a$  from equation 4-16 using the procedure in equations 4-7 to 4-12 given in Figure 4-7. This differs notably from the distributed modeled reference depletion curve indicating poor performance of the elevation only method.

Figure 4-6b plots distributed modeled snow water equivalence versus accumulation factor. There is a linear relationship between distributed modeled snow water equivalent and accumulation factor in large part due to the fact that the distributed modeled snow water equivalent was modeled using accumulation factor as an input. Fitting equation 4-18 to the data in Figure 4-6b we obtained  $P=0.84$  m. This is less than the observed precipitation up to May 2, 1996 of 0.91 m due to the melt and sublimation that occurs during the accumulation season. The distribution of accumulation factor is used directly in the procedure in equations 4-7 to 4-12 to estimate the accumulation factor only depletion curve shown in Figure 4-7. The accumulation factor only depletion curve is somewhat closer to the distributed modeled reference than elevation only.

The elevation and accumulation factor depletion curve derivation requires fitting of equation 4-20. The parameters obtained from the multiple linear regression are:  $c=0.91$ ,  $d=0.00065$ , and  $e=-2.6$ . The predicted snow water equivalent fits the distributed modeled snow water equivalent well as shown in Figure 4-6c. The Nash-Sutcliffe goodness of fit measure (NSC) (Nash and Sutcliffe, 1970) was used to quantify the

fraction of variance explained by the model. The NSC of the predicted and the distributed modeled snow water equivalent is 0.99, consistent with the good fit. The depletion curve derived in this approach shown in Figure 4-7a was found to have shape close to the reference distributed modeled snow water equivalent depletion curve.

Implementing the DAMPT approach, multiple linear regression was used with equation 4-28 to estimate A, B and C taking as input the elevation,  $z$ , and modeled shortwave radiation,  $R$ , for the period May 2, 1996 to August 30, 1996. The multiple linear regression resulted in parameter values:  $A=14.0$  m,  $B=-0.039$ , and  $C=2.3E-6$  m/(kJ/m<sup>2</sup>). The NSC of the predicted and the modeled potential melt is 0.87 which indicates that the regression model is relatively effective. Figure 4-6d illustrates distributed modeled reference versus predicted melt from this regression.

Figure 4-7b includes the depletion curve labeled DAMPT. This was derived from the equations 4-21 to 4-24 using ABC model estimates of melt from equation 4-28 and accumulation  $a = \bar{a}$  estimated from elevation and accumulation factor using the  $c$ ,  $d$  and  $e$  estimated above in equation 4-20. A range of  $\bar{m}/\bar{a}$  are used to derive the depletion curve from equation 4-24. Only the depletion curve from explicit spatial sampling of the joint distribution is shown.

The use of the ABC model melt estimates does introduce some uncertainty into the procedure. To separate this uncertainty from other uncertainty inherent in the depletion curve approximation Figure 4-7b also includes depletion curves labeled DAMUM derived from equations 4-21 to 4-24 with potential melt,  $m$ , from the new UEB model with 10 m initial snow water equivalent over the period May 2, 1996 to August 30,

1996 and accumulation  $a$  from the distributed modeled reference snow water equivalent on May 2, 1996. These are presumed to be our best estimates of the inputs  $a$  and  $m$ , so discrepancies that result are inherent in the depletion curve approximation. Both cases of independent and explicit spatial sampling to capture dependence are presented. The depletion curve labeled DAMUM  $m/a$  dependent in Figure 4-7 was derived based on the joint distribution of  $a$  and  $m$  pairs over the entire domain of 85698 grid cells. The depletion curve labeled DAMUM  $m/a$  independent in Figure 4-7 was derived based on the convolution of separate distributions of  $a$  and  $m$  from the 85698 grid cells. The depletion curve that recognizes the spatial dependence between  $a$  and  $m$  is much closer to the distributed modeled reference depletion curve indicating the importance of the spatial dependence between  $a$  and  $m$ .

DAMUM  $m/a$  dependent uses spatially distributed UEB modeled melt which in part defeats the purpose of the need for a depletion curve because if it is feasible to run a high resolution model over the entire domain then one does not need a subgrid parameterization and depletion curve. However this was included here to illustrate the sensitivity of the approach to topography based estimates of  $a$  and  $m$ . Because of the importance of spatial dependence between  $m$  and  $a$  as shown by the results using distributed modeled melt we did not include the depletion curve from the independent case with melt parameterized from the topography.

A depletion curve is a parameterization of subgrid variability related to the spatial distribution of snow. Depletion curves derived using a number of methods have been presented. To interpret these it is insightful to evaluate the relationship between a

depletion curve and underlying probability distribution following the procedure in equations 4-7 to 4-12. Luce and Tarboton (2001) presented depletion curves for the normal, log-normal, exponential and gamma distribution to illustrate the effect of distribution shape on the derived depletion curve. Here nine depletion curves were derived from the gamma distribution with different degrees of variability (Figure 4-8). Recognizing the insensitivity of depletion curves to specific values of the mean and variance of the distribution the coefficient of variation was used to quantify the degree of variability.

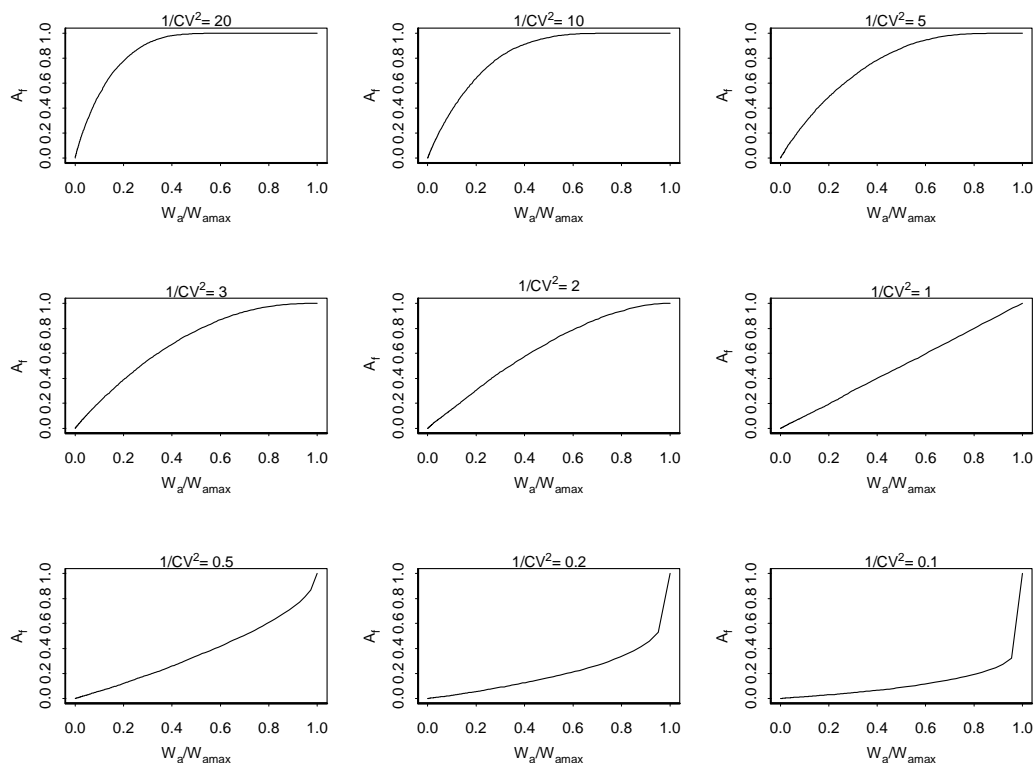


Figure 4-8 Depletion curves derived from gamma distributions with different Coefficients of Variation. The shape parameters of the gamma distribution ( $1/CV^2$  Chow *et al.*, 1988) from upper left to low right are 20,10, 5, 3, 2, 1, 0.5, 0.2, 0.1. The lower the shape parameter, the higher the coefficient of variation

Comparison of the depletion curves in Figure 4-7 with the depletion curves in Figure 4-8 suggests that the distribution of snow within the watershed has a highly skewed distribution with high CV. Depletion curves other than that derived only from elevation have patterns similar to that derived from high skewed gamma distribution with a shape parameter between 0.2~0.5. The depletion curve derived from elevation has a pattern similar to that derived from the low CV gamma distribution (Figure 4-8), which indicates that the depletion curve derived only from the elevation significantly underestimates the subgrid variability of snow.

*Evaluation of lumped model results using different depletion curves*

The lumped model was run for the period 9/1/1995 to 8/30/1996 using each of the depletion curves derived above as input. Model predictions are here compared to observations of snow covered area and the distributed model results which serve as reference. Table 4-1 gives the snow covered area fraction on each date it was observed from the aerial photographs compared to modeled snow covered area fraction. Time series of snow covered area fraction are given in Figure 4-9 while Figure 4-10 presents a bar-graph comparison of modeled and observed snow covered area fraction on each date

Table 4-1 Comparisons of measured and modeled area fraction

Date	Observed	Distributed Modeled reference	Elevation only	Accumulation factor only	Elevation and Accumulation factor	DAMPT m/a dependent	DAMUM m/a dependent	DAMUM m/a independent
5/22/96	0.33	0.34	0.75	0.59	0.32	0.35	0.39	0.32
6/9/96	0.29	0.26	0.44	0.35	0.30	0.32	0.33	0.23
6/29/96	0.14	0.13	0.00	0.16	0.16	0.13	0.16	0.11
7/21/96	0.06	0.05	0.00	0.05	0.04	0.05	0.05	0.04

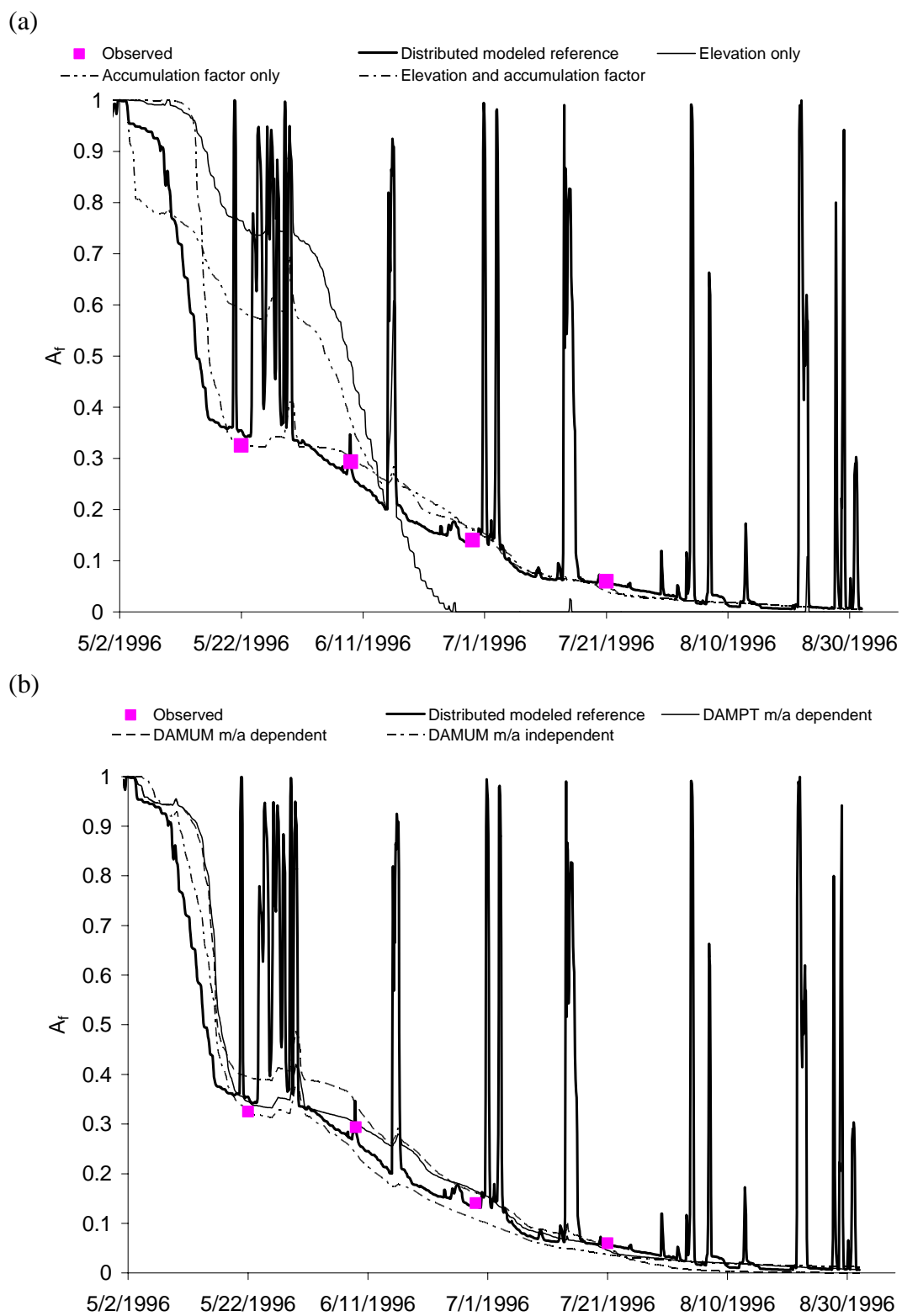


Figure 4-9 Comparisons of measured, modeled snow covered area fraction by large scale snowmelt model and distributed snowmelt model

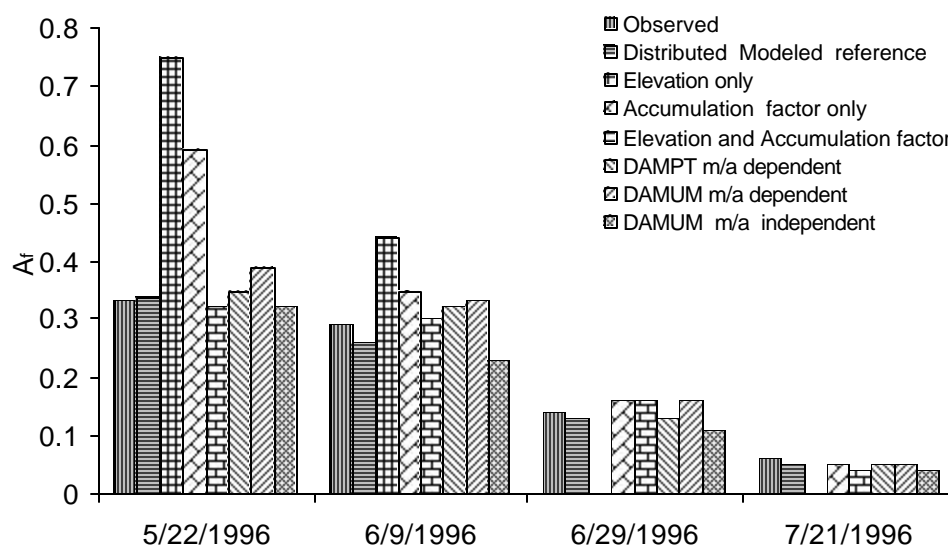


Figure 4-10 Comparisons of measured, modeled snow covered area fraction at four dates by large scale snowmelt model and distributed snowmelt model

it was observed. The modeled snow covered area fraction is close to the observed values at four dates for the depletion curves derived from the reference distributed model as well as using depletion curves from elevation and accumulation factor, DAMPT and DAMUM dependent. On the contrary, the snow covered area fraction modeled with depletion curve derived only from the elevation or only from the accumulation factor, or where independence between  $a$  and  $m$  is assumed differs more from the observed values. The modeled time series of snow covered area fraction (Figure 4-9) and basin average snow water equivalent have similar responses (Figure 4-11).

## DISCUSSION AND CONCLUSIONS

Several approaches were developed to derive the subgrid variability of snow from topography and topographically derived variables. The derived depletion curves and

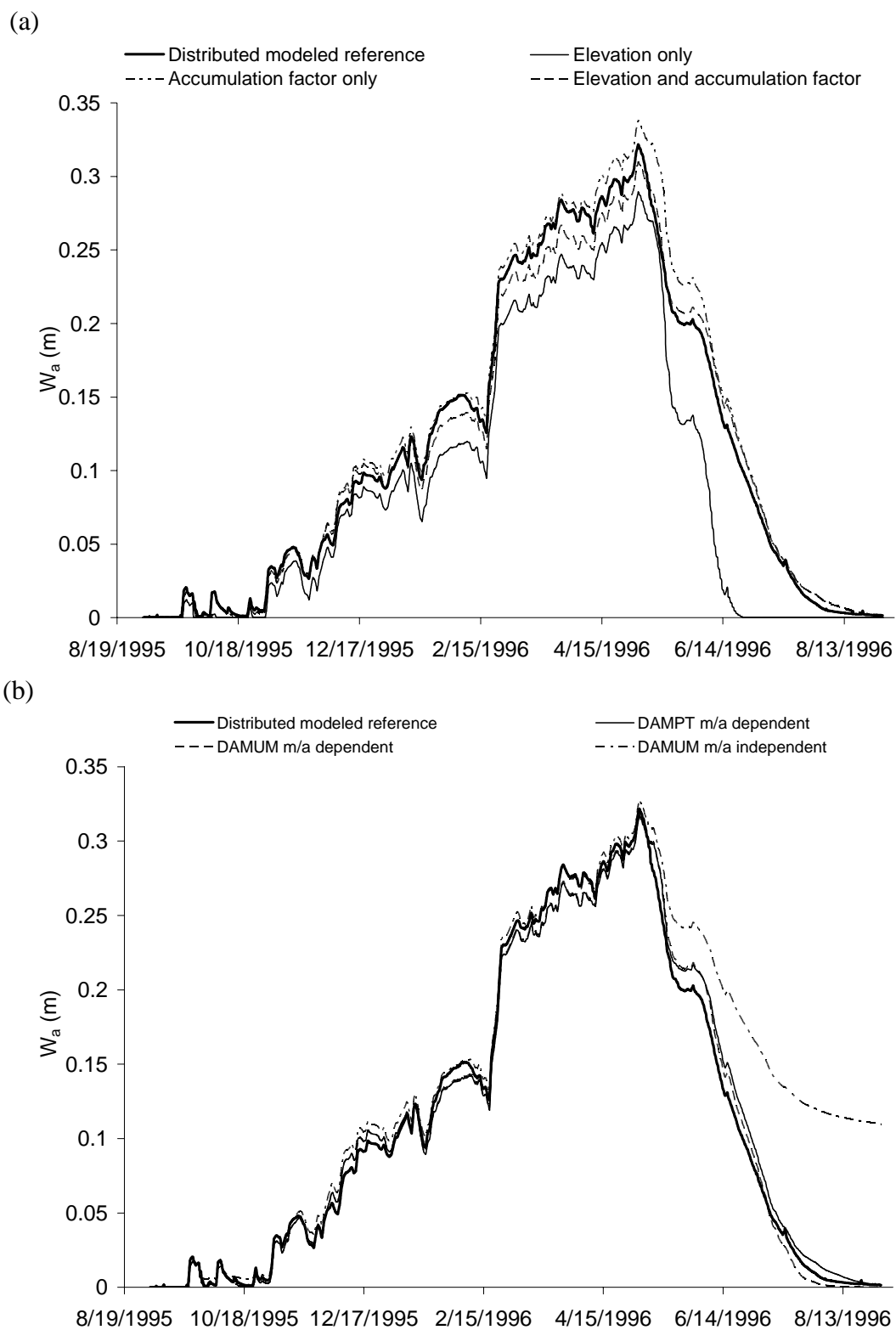


Figure 4-11 Comparisons of modeled time series of basin average snow water equivalent by large scale snowmelt model and distributed snowmelt model



model results using these depletion curves were evaluated against the observed snow covered area fraction and the reference model results from the explicitly distributed snowmelt model. A limitation of the results presented here are that the accumulation factors were derived from only four snow covered area images obtained during the melt season when less than 35% of the watershed was snow covered. This was the case even for the reference results. The lower bound on accumulation factor was unconstrained over a significant part of the domain. Therefore the upper parts of the depletion curves ranging from full snow cover to the first observation have considerable uncertainty and differences between depletion curves over this range should not be given as much weight as differences for the lower part of the depletion curve range from the first observation to disappearance of the snowcover.

The best results overall were obtained from the differential accumulation and melt approach accounting for the spatial dependence between accumulation and melt with melt estimated from a distributed model. The DAMUM dependent depletion curve in Figure 4-7 is closest on average to the reference and correctly captures the initial reduction of snow covered area with the onset of melt, although this is uncertain due to the lack of measurements at this time. The snow covered area and snow water equivalent comparisons for this case were good.

These results support the validity of the combination of distributions of accumulation and melt given in equation 4-25 for the derivation of a depletion curve. This is an important contribution because accumulation and melt are fundamentally

different processes and this theory provides a formal way for these different effects to be correctly combined.

Despite the theoretical appeal of the approach combining accumulation and melt distributions, further work is needed to make this method practical. In the DAMUM dependent results a spatially explicit distributed model was run to obtain the melt distribution. This defeats the purpose of the subgrid parameterization. The DAMPT results estimated the distribution of melt from elevation and radiation exposure using the ABC model. The discrepancy of the depletion curve so obtained is evident in Figure 4-7 b and is indicative of the error introduced by the approximate melt distribution. This depletion curve does not capture the reduction in snow covered area with initial melt observed in the reference. Again this is a difference where the uncertainty is highest due to the lack of measurements. The DAMPT dependent depletion curve is therefore still a reasonable approximation to the reference and about equally as good as the depletion curve derived empirically combining elevation and accumulation factor. These both provide adequate simulations of the snow covered area and basin average snow water equivalent.

The depletion curves derived using the distribution of elevation only, or assuming that accumulation and melt are independent are markedly different from the reference. From this we conclude that elevation alone is insufficient to parameterize the subgrid variability of snow. We also conclude that the spatial variability that is responsible for variability in accumulation and variability in melt is related and it is inadequate to neglect this dependence in deriving a depletion curve.

Although this work has made progress towards the parameterization of snow subgrid variability based on topography alone the solution is still not complete. The distributions of snow accumulation used were derived (based on chapter 3) from aerial photographs and a small scale distributed model. Other researchers have made progress on the parameterization of snow accumulation from wind blowing snow models (Liston and Sturm, 1998; Prasad *et al.*, 2000; Winstral *et al.*, 2002; Winstral and Marks, 2002), but it still remains to be tested whether the accumulation predicted by such a model, when combined with a terrain derived distribution of the melt distribution can provide a depletion curve that gives a satisfactory subgrid parameterization at large scale.

#### REFERENCES

- Anderson EA. 1973. National Weather Service River Forecast System -- Snow Accumulation and Ablation Model. NOAA Technical Memorandum NWS HYDRO-17, U.S. Dept of Commerce. Silver Spring, MD; 217 pp.
- Anderson EA. 1976. A Point Energy and Mass Balance Model of a Snow Cover. NOAA Technical Report NWS 19, U.S. Department of Commerce. 150 pp.
- Berg N. 1986. Blowing snow at a Colorado alpine site: measurements and implications. *Arctic and Alpine Research* **18** (2): 147-161.
- Blöschl G, Kirnbauer R. 1992. An analysis of snow cover patterns in a small alpine catchment. *Hydrological Processes* **6**: 99-109.
- Brubaker K, Rango A, Kustas W. 1996. Incorporating radiation inputs into the snowmelt runoff model. *Hydrological Processes* **10**: 1329-1343.
- Buttle JM, McDonnell JJ. 1987. Modelling the areal depletion of snowcover in a forested catchment. *Journal of Hydrology* **90**: 43-60.
- Caine N. 1995. Snowpack influences on geomorphic processes in Green Lakes Valley, Colorado Front Range. *Geographical Journal* **161**(1): 55-68.

- Chow VT, Maidment DR, Mays LW. 1988. *Applied Hydrology*. McGraw Hill: New York.
- Dozier J. 1980. A clear-sky spectral solar radiation model for snow-covered mountainous terrain. *Water Resources Research* **16**: 709-718.
- Dozier J, Frew J. 1990. Rapid Calculation of Terrain Parameters for Radiation Modeling From Digital Elevation Data. *IEEE Transactions on Geoscience and Remote Sensing* **28**(5): 963-969.
- Dunne T, Leopold LB. 1978. *Water in Environmental Planning*. W H Freeman and Co: San Francisco.
- Elder K, Dozier J, Michaelsen J. 1991. Snow accumulation and distribution in an alpine watershed. *Water Resources Research* **27**(7): 1541-1552.
- Ferguson RIMS-IP. 1986. Parametric modelling of daily and seasonal snowmelt using snowpack water equivalent as well as snow covered area. In Morris EM (eds.), *Modelling Snowmelt-Induced Processes*. Proc. Budapest Symp., July 1986, IAHS Publ. no. 155: 151-161.
- Gray DM, Male DH. 1981. *Handbook of Snow, Principles, Processes, Management & Use*. Pergamon Press: New York.
- Hall DK, Martinec J. 1985. *Remote Sensing of Ice and Snow*. Chapman and Hall: London.
- Jordan R. 1991. A One-dimensional Temperature Model for a Snow Cover. Technical documentation for SNTHERM.89, special technical report 91-16, US Army CRREL. 49 pp.
- Liston GE, Sturm M. 1998. A snow-transport model for complex terrain. *Journal of Glaciology* **44**(148): 498-516.
- Luce CH. 2000. Scale influences on the representation of snowpack processes. Ph. D Dissertation, Civil and Environmental Engineering: Utah State University, Logan, Utah.
- Luce CH, Tarboton DG. 2001. Modeling snowmelt over an area: modeling subgrid scale heterogeneity in distributed model elements. In *Proceedings of MODSIM 2001, International Congress on Modelling and Simulation*, Canberra, Australia, December 10-13; 341-346.

- Luce CH, Tarboton DG, Cooley KR. 1998. The influence of the spatial distribution of snow on basin-averaged snowmelt. *Hydrological Processes* **12**(10-11): 1671-1683.
- Luce CH, Tarboton DG, Cooley KR. 1999. Subgrid parameterization of snow distribution for an energy and mass balance snow cover model. *Hydrological Processes* **13**: 1921-1933.
- Marks D, Dozier J. 1979. A clear-sky longwave radiation model for remote alpine areas. *Archev fur Meteorologie Geophysik und Bioklimatologie, Ser B*, **27**: 159-187.
- Marks D, Winstral A. 2001. Comparison of snow deposition, the snow cover energy balance, and snowmelt at two sites in a semiarid mountain basin. *Journal of Hydrometeorology* **2**(3): 213-227.
- Martinec J. 1980. Snowmelt-runoff forecasts based on automatic temperature measurements. Hydrological Forecasting. Proc. Oxford Symp. 129, IAHS-AISH. Wallingford; 239-246 pp.
- Morris EM. 1990. Physics-based models of snow. In *Recent Advances in the Modeling of Hydrologic Systems*, Bowles DS, O'Connell PE (eds). Kluwer Academic Publishers: Dordrecht, The Netherlands; 85-112.
- Nash JE, Sutcliffe JV. 1970. River flow forecasting through conceptual models, 1. A discussion of principles. *Journal of Hydrology* **10**(3): 282-290.
- Pomeroy JW, Gray DM, Landine PG. 1993. The Prairie Blowing Snow Model: characteristics, validation, operation. *Journal of Hydrology* **144**: 165-192.
- Prasad R, Tarboton DG, Liston GE, Luce CH, Seyfried MS. 2000. Testing a blowing snow model against distributed snow measurements at Upper Sheep Creek. *Water Resources Research* **37**(5): 1341-1350.
- Schmidt RA. 1982. Vertical profiles of wind speed, snow concentration, and humidity in blowing snow. *Boundary Layer Meteorology* **34**: 213-241.
- Tabler RD, Pomeroy JW, Santana BW. 1990. Drifting snow. In *Technical Council on Cold Regions Monograph*, Ryan WL, Crissman RD (eds). American Society of Civil Engineering: New York; 95-145.
- Tarboton DG, Chowdhury TG, Jackson TH. 1995. A spatially distributed energy balance snowmelt model. In *Proceedings of a Boulder Symposium*, Tonnessen KA, Williams MW, Tranter M (eds). Boulder, CO., July 3-14, IAHS Publ. no. 228.

- Tarboton DG, Luce CH. 1996. Utah Energy Balance Snow Accumulation and Melt Model (UEB). Computer model technical description and users guide, Utah Water Research Laboratory and USDA Forest Service Intermountain Research Station (<http://www.engineering.usu.edu/dtarb/>). (Accessed Jul. 31, 2004).
- Williams KS, Tarboton DG. 1999. The ABC's of snowmelt: a topographically factorized energy component snowmelt model. *Hydrological Processes* **13**: 1905-1920.
- Williams MW, Baron JS, Caine N, Sommerfeld R, Sanford RJ. 1996. Nitrogen saturation in the Rocky Mountains. *Environmental Science and Technology* **30**: 640-646.
- Winstral A, Elder K, Davis R. 2002. Modelling the effects of wind induce snow redistribution with terrain-based parameters to enhance spatial snow modelling. *Journal of Hydrometeorology* **3**(5): 524-528.
- Winstral A, Marks D. 2002. Simulating wind fields and snow redistribution using terrain-based parameters to model snow accumulation and melt over a semi-arid mountain catchment. *Hydrological Processes* **16**(18): 3585-3603.

CHAPTER 5  
TESTING THE SCALING PROPERTIES OF A LUMPED MASS  
AND ENERGY BALANCE SNOWMELT MODEL

Abstract:

This paper examines the applicability of and limitations to using the depletion curve approach for parameterizing the subgrid variability of snow in a steep mountainous watershed. The coefficient of variation of snow water equivalent has been shown to be an important parameter related to the shape of the depletion curve. We present theory that relates the coefficient of variation to the variability of processes that drive the spatial variability of snow. We then use numerical modeling of snow processes over the Green Lakes Valley Watershed to examine the contribution of different causative processes to the overall variability of snow water equivalent. We find that both the accumulation factor that characterizes the spatial snow drifting and accumulation processes as well as spatially variable sublimation and condensation are needed to represent the full variability observed. We then examine the effectiveness of the depletion curve approach for different size model elements. We were interested in scale limitations of the depletion curve approach. We found that the depletion curve is able to suitably parameterize the subgrid variability up to the scale of the entire watershed (8.1 km<sup>2</sup>) but when subwatersheds are examined some discrepancies due to nonlinearity in the snow accumulation and melt processes arise. The limitations of the depletion curve methodology due to these nonlinearities are discussed.

## INTRODUCTION

Snowmelt is a surface water input of importance to many aspects of hydrology and water resources management. Snowmelt is primarily driven by energy exchanges at the snow surface that have variability down to the horizontal scale of 1 to 10 m (hereafter referred to as the point scale). This variability leads to a non-uniform spatial distribution of snow water equivalent and patchiness in the snowcover during melt. The physical processes responsible for snowmelt at point scales are relatively well understood and modeled by a variety of “point” models (Anderson, 1976; Morris, 1990; Jordan, 1991; Tarboton *et al.*, 1995; Tarboton and Luce, 1996). However, when applied to a large watershed, point snowmelt models cannot represent the snow accumulation and melt processes well without parameterizing the variability within modeling elements.

Surface energy fluxes only melt snow over the area where snow is present, so an important process to consider in the parameterization of subgrid variability of snow is the evolution of snow covered area. A depletion curve is one method to characterize the reduction in snow covered area during the progress of melt. Depletion curves have historically been used with temperature index models to predict snowmelt runoff (e.g. Anderson, 1973; Martinec, 1980; Hall and Martinec, 1985; Brubaker *et al.*, 1996). In such models, the amount of melt is multiplied by the snow covered area to estimate the total input of water to a basin. Snow covered area has also been used in the modeling of basinwide snow water equivalent (Dunne and Leopold, 1978; Ferguson, 1986; Buttle and McDonnell, 1987; Luce *et al.*, 1999). In this sort of modeling, information about the total



mass of snow in the area (from direct measurement of the snowpack or estimated from accumulated precipitation) is used, and conservation of mass is considered.

Luce *et al.* (1999) suggested the use of the depletion curve as a parameterization of subgrid variability in a physically based mass and energy balance snowmelt model. Rather than relating snow covered area to accumulated melt or degree days as in earlier depletion curve methods, Luce *et al.* (1999) related snow covered area to the total mass of snow remaining on the ground, or the area-averaged snow water equivalent and derived equations that estimated a dimensionless depletion curve from the distribution function of snow water equivalent at peak snow accumulation. This derivation focuses on differential accumulation as a cause for spatial variability and, in the derivation of the depletion curve from the peak snow accumulation distribution, approximates the melt process as being spatially uniform. The depletion curve obtained this way may be naturally scaled by maximum snow accumulation in any given year, requiring only a dimensionless functional form of the depletion curve to be specified. These contributions to depletion curve methodology addressed two problems: first the problem of assigning dates and peak or average depth at onset of melt is avoided; second the need for a new depletion curve each season is avoided. Further research demonstrated that the spatial distribution of solar radiation input can be included into this procedure to improve the representation of subgrid variability of snow (Luce, 2000; Luce and Tarboton, 2001). In chapter 4 the connection between depletion curves and other spatially distributed variables causative of spatial variability in snow was explored and relationships with the distribution of elevation, snow accumulation factor and solar radiation exposure were combined for the purposes of estimating depletion curves. Luce and Tarboton (2004)

explored the relationship between the depletion curve and the coefficient of variation (CV) of the snow water equivalent distribution. They found that the CV of the distribution of snow water equivalent at peak accumulation used to derive the depletion curve exhibits a strong relationship with the shape of the depletion curve.

The depletion curve approach has proven effective in parameterizing the subgrid variability of snow in the small Upper Sheep Creek watershed with rolling terrain (Luce *et al.*, 1999; Luce and Tarboton, 2001). However, questions still remain when applying this approach in larger steeper watersheds; these are: 1) Is the depletion curve approach effective in steep mountainous watersheds? 2) Is there a scale limitation on the size of model elements where the depletion curve approach can be used? 3) What is the relationship between the within element snow variability and the size of the modeling element? 4) Can a method be developed to estimate the CV of snow from the CV of causative processes given that shape of the depletion curve has strong relationship with the CV of snow (Luce and Tarboton, 2004)? These questions are important to understand the practical limitations associated with the depletion curve approach and to explore ways to obtain depletion curves where detailed snow surveys are impractical.

In this paper the Green Lakes Valley study area was subdivided into a number of watersheds with differing scale to explore scale limitations on the applicability of the depletion curve approach, and to examine the relationship between the variability of snow and the size of modeling element. The relationship between the CV of snow and the size of modeling element was examined systematically using nested model elements. A theory was developed to link the CV of snow to the CVs of accumulation factor, melt, and sublimation.

## THEORY

In estimating a depletion curve for the parameterization of the subgrid variability of snow, following the work of Luce and Tarboton (2004) the CV of the snow water equivalent distribution is an important parameter to quantify. However, for most situations, the intense spatial measurements of snow necessary to directly measure the CV are not available. Here we develop theory to derive the variability of snow from the CV of accumulation factor, point measurements of precipitation, and the variability of modeled melt and sublimation.

The snow water equivalent mass balance at a point is

$$\frac{dW}{dt} = p * \phi - m, \quad (5-1)$$

where  $W$  is snow water equivalent,  $t$  is time,  $\phi$  is the accumulation factor,  $p$  is the spatially average snowfall rate, and  $m$  the combined mass change rate consisting of snowmelt and sublimation. Quantities  $W$ ,  $\phi$  and  $m$  are spatially variable while  $p$  is treated as spatially constant. The time invariant accumulation factor  $\phi$  represents the propensity of a location to accumulate snow relative to the spatial average and  $p\phi$  together describe the spatially variable snowfall at a point. The field  $\phi$  is designed to parameterize the effect of all processes that result in spatial variability in snow accumulation such as wind blown drifting, sliding or avalanching and orographic precipitation. The multiplicative form of the input  $p\phi$  that separated temporal and

spatial variability is an assumption that has proved to be practically effective (Luce *et al.*, 1999; Luce and Tarboton, 2001; Luce and Tarboton, 2004). Integrating equation 5-1 the snow water equivalent at any location can then be expressed as:

$$W = P\phi - M_c, \quad (5-2)$$

where  $P$  is the cumulative average snowfall and  $M_c$  the cumulative net mass loss. The spatial mean and the variance of snow water equivalent ( $\bar{W}$  and  $\sigma_w^2$ ) can be related to the spatial mean and the spatial variance of accumulation factor and mass change through:

$$\bar{W} = P\bar{\phi} - \bar{M}_c, \quad (5-3)$$

and

$$\sigma_w^2 = P^2\sigma_\phi^2 + \sigma_{M_c}^2 - \rho_{(\phi, M_c)}\sigma_\phi\sigma_{M_c}. \quad (5-4)$$

Here  $\bar{\phi}$  is the spatial mean of accumulation factor,  $\bar{M}$  the spatial mean mass change, and  $\rho_{(\phi, M_c)}$  is the correlation between accumulation and mass change.  $\sigma_\phi^2$ ,  $\sigma_{M_c}^2$  are spatial variance of accumulation factor and mass change respectively. Thus, the coefficient of variation of snow water equivalent,  $CV_w$ , can be related to the coefficient of variation,  $CV_\phi$ , and coefficient of variation of mass change,  $CV_{M_c}$ .

$$CV_w^2 = \frac{1}{(\bar{P}\bar{\phi} - \bar{M}_c)^2} (P^2\bar{\phi}^2 CV_\phi^2 + \bar{M}_c^2 CV_{M_c}^2 - \rho_{(\phi, M_c)} P\bar{\phi} CV_\phi \bar{M}_c CV_{M_c}). \quad (5-5)$$

Equation 5-5 could also be obtained by evaluating the variance of  $w$  in equation 4-24 in chapter 4. Equation 5-5 relates the CV of snow water equivalent to the CV of input quantities and their cross correlation. Positive correlation between snow accumulation and snow melt (represented by the mass loss term) decreases the coefficient of variation of snow water equivalent, while negative correlation increases this. The implications of this equation relating the coefficient of variation of snow water equivalent to the coefficient of variation of accumulation factor, melt and their correlation is explored for the Green Lakes Valley study area through a physical energy balance snowmelt model used to simulate spatially distributed snow accumulation and melt.

### PHYSICAL ENERGY BALANCE MODEL

The new UEB snowmelt model (see chapter 2) was used in this work. Three forms of the model were used. The first is the point model described in chapters 2 and 3 run at each grid cell to form a spatially explicit distributed model. In chapter 3 the accumulation factors necessary to apply the explicitly distributed form of the model were calculated based upon snow covered area data. The model was applied in a spatially explicit mode to each 10 m grid cell in the domain using these accumulation factors to provide the best available estimate of the spatially distributed snow processes over the domain. The spatially explicit distributed snowmelt model results are referred to as "distributed modeled" and provide the reference results against which to evaluate the

performance of the depletion curve approach in different model elements and investigate the variability of snow.

The second model is the large scale model where the depletion curve parameterization of subgrid variability is included following Luce *et al.* (1999). To facilitate application of snowmelt models over large areas it is necessary to have larger model elements than the 10 m grid cells. What we refer to as the large scale lumped model (the second form of UEB) consists of one model element over an entire watershed or subwatershed, with subgrid variability within this domain parameterized using a depletion curve. A depletion curve for each model element was derived from the distributed modeled peak snow accumulation at May 2, 1996 following the derivation procedures (Luce *et al.*, 1999; also see chapter 4). The results obtained using this approach were labeled as “lumped.”

The third form of the model treats the whole modeling element as a single point using the mean accumulation factor of the modeling element to modify the total precipitation falling in the watershed. The results obtained using this approach were labeled "point." The results from this point snowmelt model help to assess the efficiency of the depletion curve for the lumped parameterization of subgrid variability.

A 2-hour time step was used for all modeling options. Both the large scale snowmelt model and the point snowmelt model require an effective slope, aspect and elevation for the calculation of energy balance inputs. Slope and aspect are used in the calculation of solar radiation inputs and elevation is used to adjust air temperature from the measurement elevation based upon lapse rate. The large scale and point models both used the average slope, aspect and elevation to drive the model. Average slope and

aspect were calculated using vector averages comprising separate averages of the slope in the east-west direction (with downward slope to the east as positive) and the north-south direction (with downward slope to the north as positive). These directional averages were then converted to magnitude and direction that were used as effective slope and aspect inputs to the model. This vector averaging approach avoided the discrepancy associated with averaging aspect angles where aspects of  $359^\circ$  and  $1^\circ$  are practically equivalent, but average to the opposite direction of  $180^\circ$ .

## STUDY SITES

The  $8.1 \text{ km}^2$  Green Lakes Valley watershed (GLV) is a high Rocky mountain basin with steep cliffs, talus slopes, and limited soil cover located 40 km west of Boulder, CO. Bare rock comprises about 1/3 of the basin area, talus slopes comprise about 1/3 of the basin area, and soil comprises the remaining 1/3 of the basin area. The 8-ha Arikaree cirque glacier lies at about 3800 m just below the Continental Divide within the basin. Elevation ranges from 3204 to 4087 m, with most of the basin lying above tree line. Mean monthly minimum temperatures are below  $0^\circ\text{C}$  from October through May with monthly maxima below freezing from November to April (Berg, 1986). The area is characterized by a mountain continental climate, annually receiving about 1000 mm of precipitation (Williams *et al.*, 1996), 80% of which is in the form of snow (Caine, 1995). Weather data has been collected at the four stations shown in Figure 5-1 whose locations range from valley to ridge top. This comprises air temperature, relative humidity, wind speed and direction. This data, measured at 10-minute intervals, was averaged to obtain two hour time step inputs to drive the models in order to be consistent with the

measurements of shortwave radiation that had a two hour time step. Weather data was adjusted for elevation, slope and aspect using the procedures described in chapter 3. Daily precipitation was measured at station D1 and spread evenly over 2-hour steps. Digital elevation data at 10-m resolution that was produced photogrammetrically was available. High-resolution orthophotos (~10 m) produced from Metric 1:24,000 aerial photographs taken on four dates in 1996 were also available. The snow covered area images classified from these orthophotos provide information about the snowpack depletion processes.

Figure 5-1 shows the spatial extent of subwatersheds delineated in the Green Lakes Valley watershed using the Tardem software (Tarboton and Ames, 2001; Tarboton, 2002). The entire study area is designated as Element 0. Element 1 is the watershed delineated by Tardem as draining to the GLV outlet. The study area (Element 0) is larger than Element 1 because it contains some area that according to the DEM does not drain to the outlet such as the area around the Subnivean snow laboratory. Elements 2, 3 and 4 are nested model elements that ranged in scale and were used to explore whether scale limitations exist for the depletion curve approach. The other model elements were selected to span a range of size, orientation, elevation and relief so as to test performance of the lumped snowmelt model for a range of conditions. Model element size ranges from 1165 to 85698 10-m grid cells. The model elements selected include steep south-facing subwatersheds, steep north-facing subwatersheds, high subwatersheds, and small flat subwatersheds.

A variability analysis was performed using all the model elements shown in Figure 5-1. The spatially explicit distributed snowmelt model results were used to



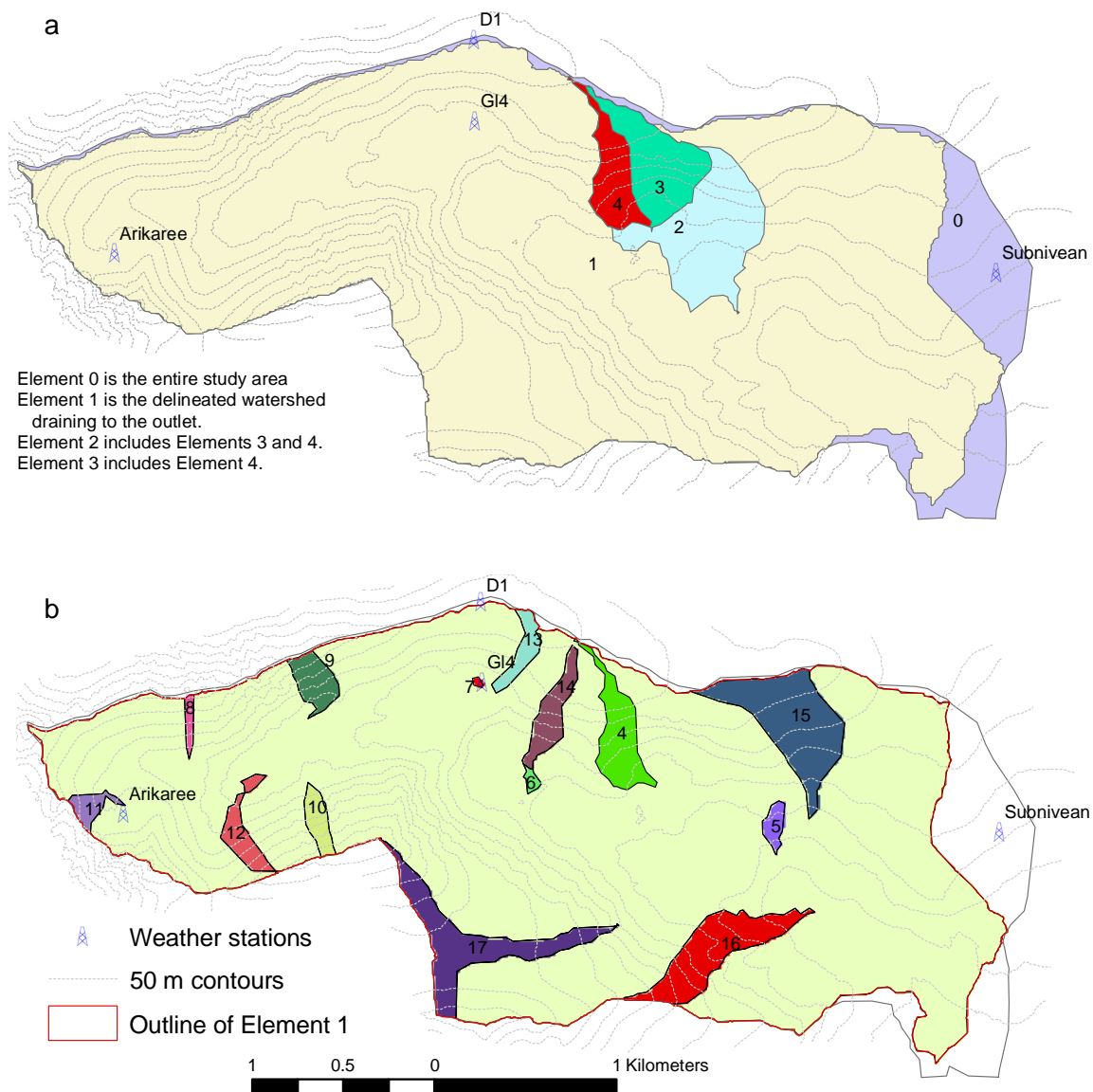


Figure 5-1 Model elements (subwatersheds) within Green Lakes Valley watershed. Four weather stations are located. Element 0 is the whole watershed, (a) shows larger scale model elements numbered 1-4, (b) shows smaller scale elements numbered 5-17

analyze the dependence of the variability of snow on the size of model elements. In addition, the relationship between the CVs of elevation, accumulation factor, melt,

sublimation and incident shortwave radiation and the size of modeling element was investigated.

Cumulative precipitation, cumulative mean melt, and cumulative mean sublimation for the accumulation period from September 1, 1995 to May 2, 1996 were calculated for all 18 subwatersheds. The CV of the cumulative melt and CV of cumulative of sublimation were also calculated from the distributed modeled results. These variables were applied in estimating the CV of snow at the peak accumulation using equation 5-5 and compared with the CV of distributed modeled snow on May 2, 1996, calculated for all 18 subwatersheds.

## RESULTS AND ANALYSIS

### *Distributed model variability*

The spatially explicit distributed snowmelt model described in chapter 3 was used to provide reference results for comparisons to the output from the lumped model with depletion curves derived for different modeling elements. Figure 5-2 plots the Coefficient of Variation (CV) of the reference model outputs for the study subwatersheds. The snow water equivalent shown in Figure 5-2 and 5-3 is the modeled snow water equivalent on May 2, 1996, the date of peak accumulation. The plotted melt and sublimation are the cumulative values from September 1, 1995 to May 2, 1996.

The CV of each variable has an increasing trend with the size of the modeling element, with wide variations for the small and medium modeling elements. The CV reaches relatively stable values when the modeling element reaches some threshold size. For example, the variability of accumulation factor was found to stabilize at a size of

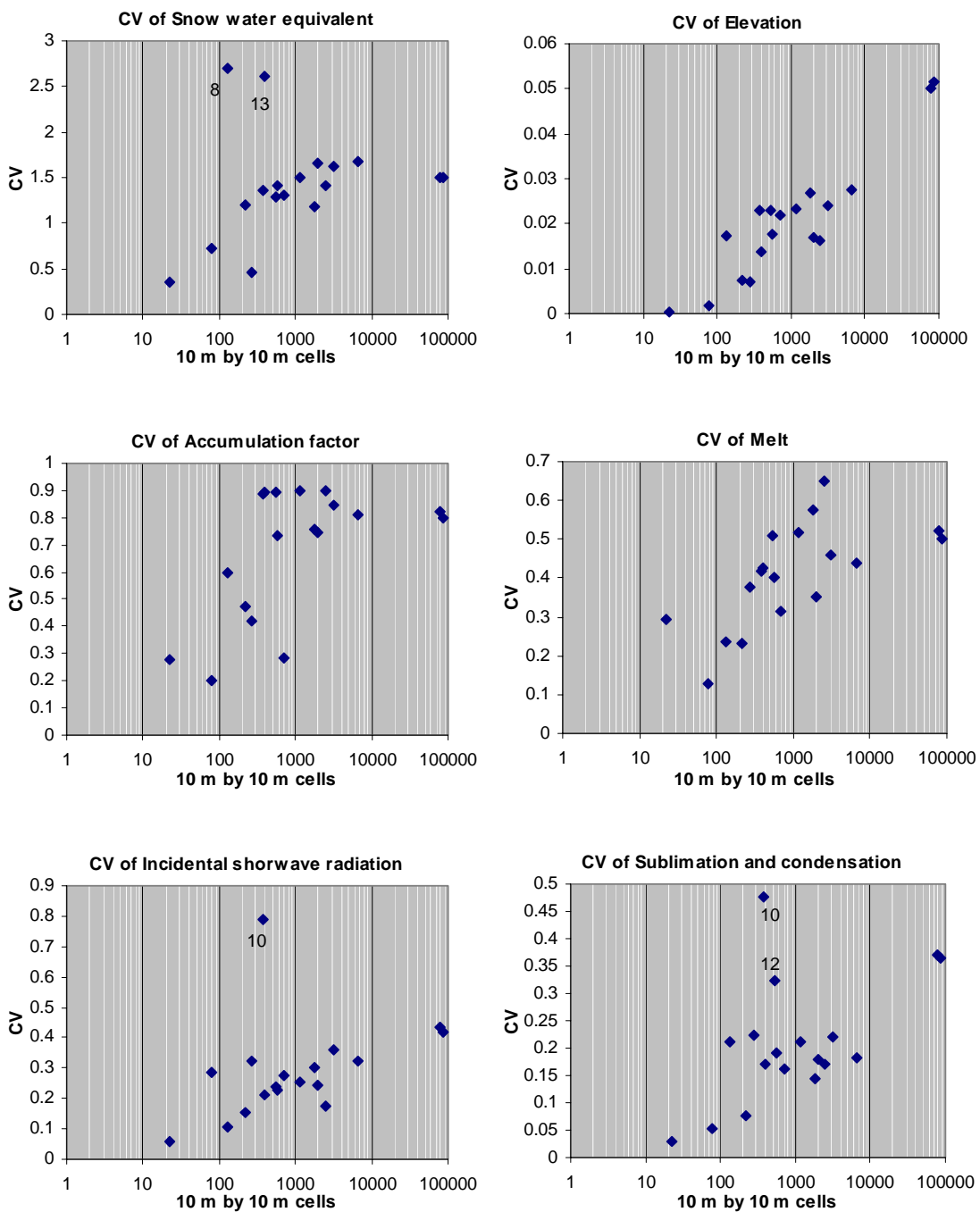


Figure 5-2 Coefficient of variation of variables for model elements with different sizes

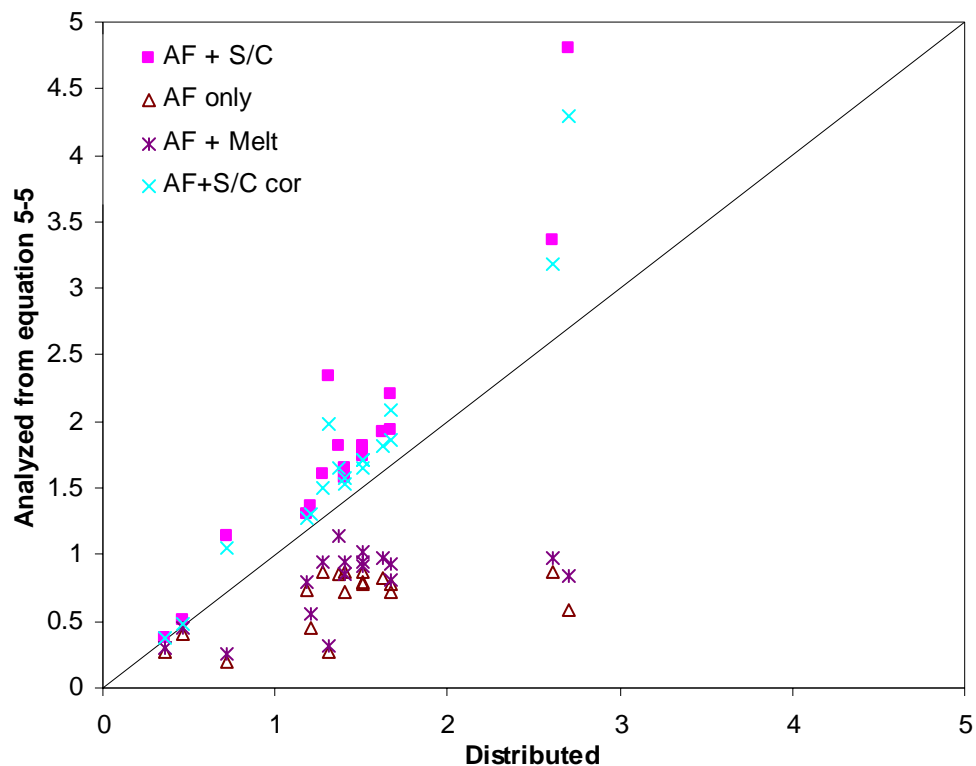


Figure 5-3 CV of peak Snow Water Equivalent calculated from equation 5-5 under various assumptions versus the CV obtained from the spatially explicit distributed model

400 grid cells. This represents an area of  $4 \times 10^4 \text{ m}^2$ . The length scale (square root of area) associated with this area is 200 m. Accumulation factor describes the variability due to wind blowing and drifting. The scale of 200 m is close to Bathurst and Cooley's (1996) finding that the influence zone of wind blowing snow is around 250 m.

Four outliers were found in the CV plots. In the CV plot of snow water equivalent the outliers, element 8 and 13, are two south facing subwatersheds. South facing areas tend to have smaller mean snow water equivalent while the variance is relatively large leading to large CV. Element 10 is an outlier on the incident shortwave

radiation CV plot. This is a north-facing low-sunlit subwatershed with small mean incident shortwave radiation leading to the large CV. In the CV plot of sublimation and condensation, elements 10 and 12 are outliers. These are both on north facing slopes where mean energy inputs and consequently sublimation is small relative to the variance leading to large CV. Except for these few outliers, the variation of the CV of snow with scale shows that the potential exists to establish some relationship between the CV of snow and the size of model element. However, the wide range of the CV of snow for the small and medium size model elements indicates that estimation of the CV from the size of model element alone is inadequate for these small elements.

*Relationship between CV of snow and CV of causative processes*

Equation 5-5 predicts the CV of snow water equivalent given the CV of accumulation and depletion processes and their cross correlation. We are interested in this because of the connection between the CV of the distribution used to derive a depletion curve and the shape of the depletion curve described by Luce and Tarboton (2004) mentioned above. For deriving a depletion curve the cumulative mass loss  $M_c$  should really be potential mass loss because actual mass loss is limited by the snow water equivalent actually present, truncating the resulting distribution and leading to a bias (reduction) of  $\sigma_{M_c}^2$  and  $CV_{M_c}$ . To limit the effect of this we examine, in Figure 5-3, the CV of distributed modeled  $W$  at peak accumulation on May 2, 1996 versus calculations using various input choices for the  $CV_\phi$ ,  $CV_{M_c}$  and cross correlation terms in equation 5-5. The  $x$  axis in Figure 5-3 gives the CV of snow water equivalent across each of the study subwatersheds from the spatially explicit model simulations. On the  $y$  axis,

the points give the CV calculated from equation 5-5 using the following approaches:

1) Accumulation factor only ignoring the variability due to mass change by setting  $CV_{M_c}=0$  (labeled AF only); 2) Accumulation factor and melt variability assumed independent. The  $CV_{M_c}$  input is taken as the coefficient of variation of modeled melt during the accumulation season neglecting the effects of sublimation and condensation. The correlation between  $\phi$  and  $M_c$  was taken as 0 (labeled AF + melt); 3) Accumulation factor and sublimation and condensation variability. The  $CV_{M_c}$  input is taken as the CV of net sublimation and condensation during the accumulation season. Again the correlation between  $\phi$  and  $M_c$  was taken as 0 (labeled AF +S/C); 4) Accumulation factor and sublimation and condensation accounting for correlation. The  $CV_{M_c}$  input is taken as the CV of net sublimation and condensation during the accumulation season. The correlation between accumulation factor and net sublimation and condensation calculated from the spatially explicit distributed model was used as an input (labeled AF +S/C cor). It may also seem logical to include  $CV_w$  calculated from using total mass change comprising melt, sublimation and condensation for the  $CV_{M_c}$  terms in equation 5-5.  $CV_w$  was calculated using this as input, but for reasons that are not clear the results were erratic, comparing poorly with the distributed modeled  $CV_w$  so are not shown.

Examining Figure 5-3 we find that using drift factor alone (i.e. neglecting the variability due to mass change) results in an underestimation of the variability in the peak snow accumulation. Accounting for variability due to melt in the accumulation period (assumed uncorrelated with accumulation factor) only slightly improves the CV estimates. The combination of accumulation factor and net sublimation and condensation in the accumulation period results in an overestimate of the CV. This overestimate is

reduced when correlation between accumulation factor and net sublimation and condensation is incorporated into the calculations. With this accounting for the correlation between accumulation factor and net sublimation and condensation there remains a small bias in the CV inferred from equation 5-5, due, we surmise, to the sublimation and melt being constrained by the snow accumulation.

The results presented above show that the theory developed in equation 5-5, although not perfect, presents a viable approach for estimating the CV of snow at peak accumulation given the CVs from the spatial distribution of accumulation factor and the spatial distribution of net sublimation and condensation. Therefore given information on the CV of accumulation factor and net sublimation and condensation, a depletion curve could be derived from an assumed distribution type with the calculated CV. Our results that indicate the importance of net sublimation and condensation are consistent with Hood and colleagues' (1999) findings that sublimation is important in the Green Lakes Watershed during a snow accumulation period.

*Performance of depletion curve approach  
and size of modeling element*

The four model elements numbered 0, 2, 3 and 4 have sizes, in terms of the number of 10m x 10 m grid cells, of 85698, 6524, 3120, and 1165, respectively. These represent a range of scales with a factor of 75 difference in size between the smallest and largest. The CVs of the snow water equivalent at the peak accumulation on May 2, 1996 are 1.51, 1.68, 1.63, and 1.51, respectively. From this single comparison CV does not appear to have a strong size dependence. Depletion curves derived from the reference distributed modeled snow water equivalent at peak accumulation for each of these model

elements are shown in Figure 5-4. They have similar shapes. Because the CV of snow is similar for these four elements of different sizes we infer that shape of the depletion curve is more related to the CV of the peak snow accumulation than the size of watershed. These depletion curves show that elements 4, 3, and 2 have a relatively higher fraction of cells with relatively small snow water equivalent at the peak accumulation than the watershed as a whole. The small steps in the depletion curve are artifacts due to the accumulation factor having been estimated based on four snow covered area images (chapter 3).

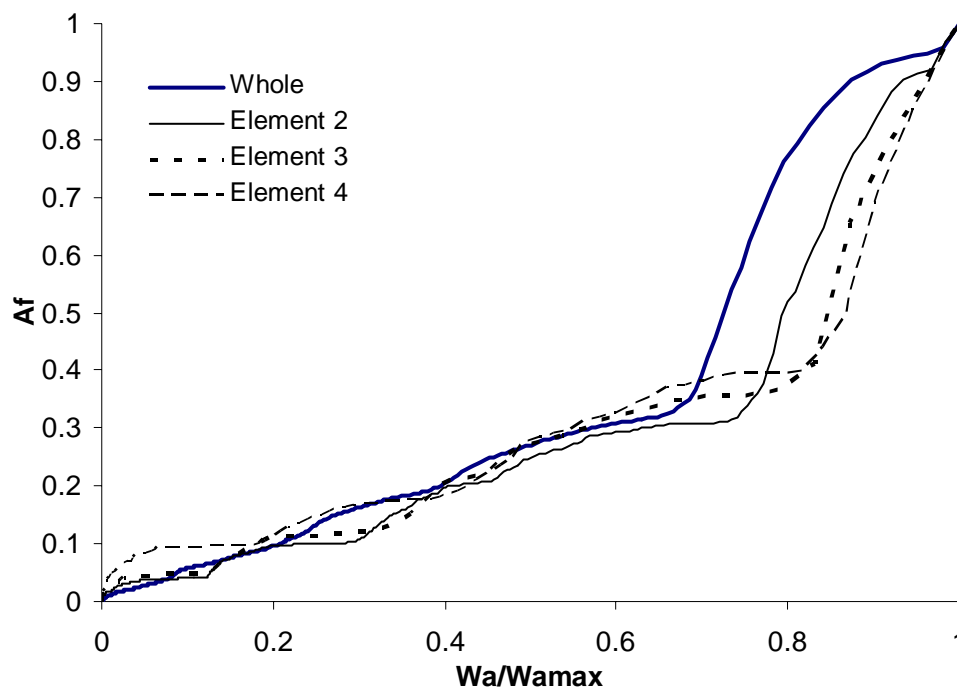


Figure 5-4 Derived depletion curves for 4 modeling elements from the distributed modeled snow water equivalent at peak accumulation on May 2, 1996



The modeled time series of fractional snow covered area and basin average snow water equivalent for the three models are shown in Figure 5-5 and 5-6 for the four nested model elements. The lumped model used depletion curve derived from the reference distributed modeled snow water equivalent on May 2, 1996 (peak accumulation). In Figure 5-6 the point model which does not parameterize subgrid variability results in early disappearance of snow. In comparison to this, the results from the spatially explicit distributed model reference and lumped model are relatively close. Both distributed and lumped simulations compare well with the observed snow covered area shown in Figure 5-5. These comparisons indicate that the variability of snow in modeling elements of different sizes can be parameterized well using depletion curves.

The depletion curve approach is however not successful in all topographic settings. Figure 5-7 gives results for model elements 7, 11, 14, and 17 (see Figure 5-1 for the location of these). Element 7 is a small flat foothill subwatershed with 22 cells; 11 is a high east-facing small subwatershed with mean elevation of 3824 m; 14 is south-facing subwatersheds with elevation range of 240 m; and 17 is a northeast-facing subwatershed with larger elevation range of 400 m. These examples span the range of aspects present in the Green Lakes Valley study area.

Figure 5-7 shows comparisons between the point, lumped, and distributed reference snowmelt model in these elements. In element 7 the three models are very similar in the modeling of snow water equivalent because this subwatershed is a small flat subwatershed, and the snowcover is almost uniform.

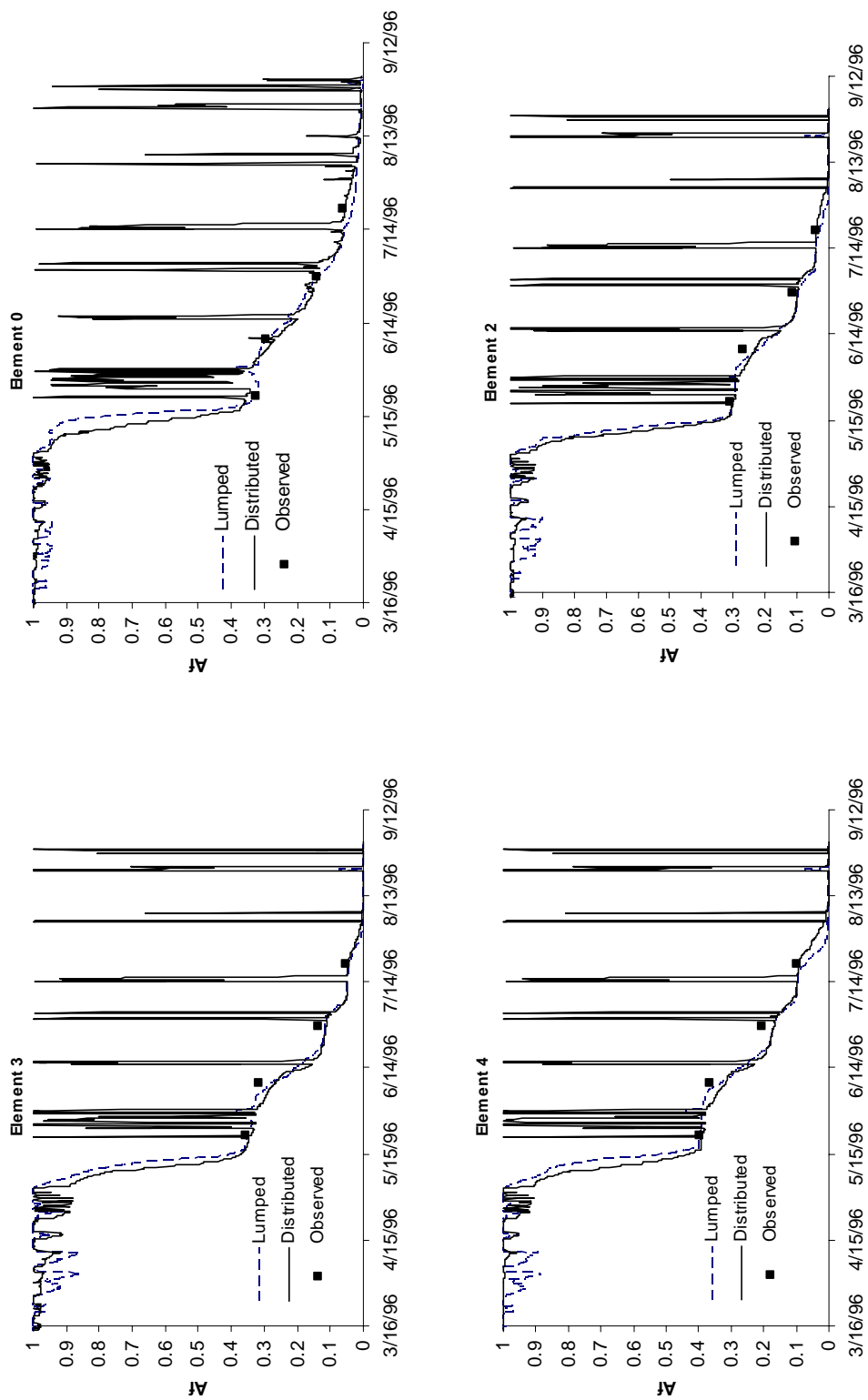


Figure 5-5 Modeled time series of snow covered area fraction using three snowmelt models for four modeling elements

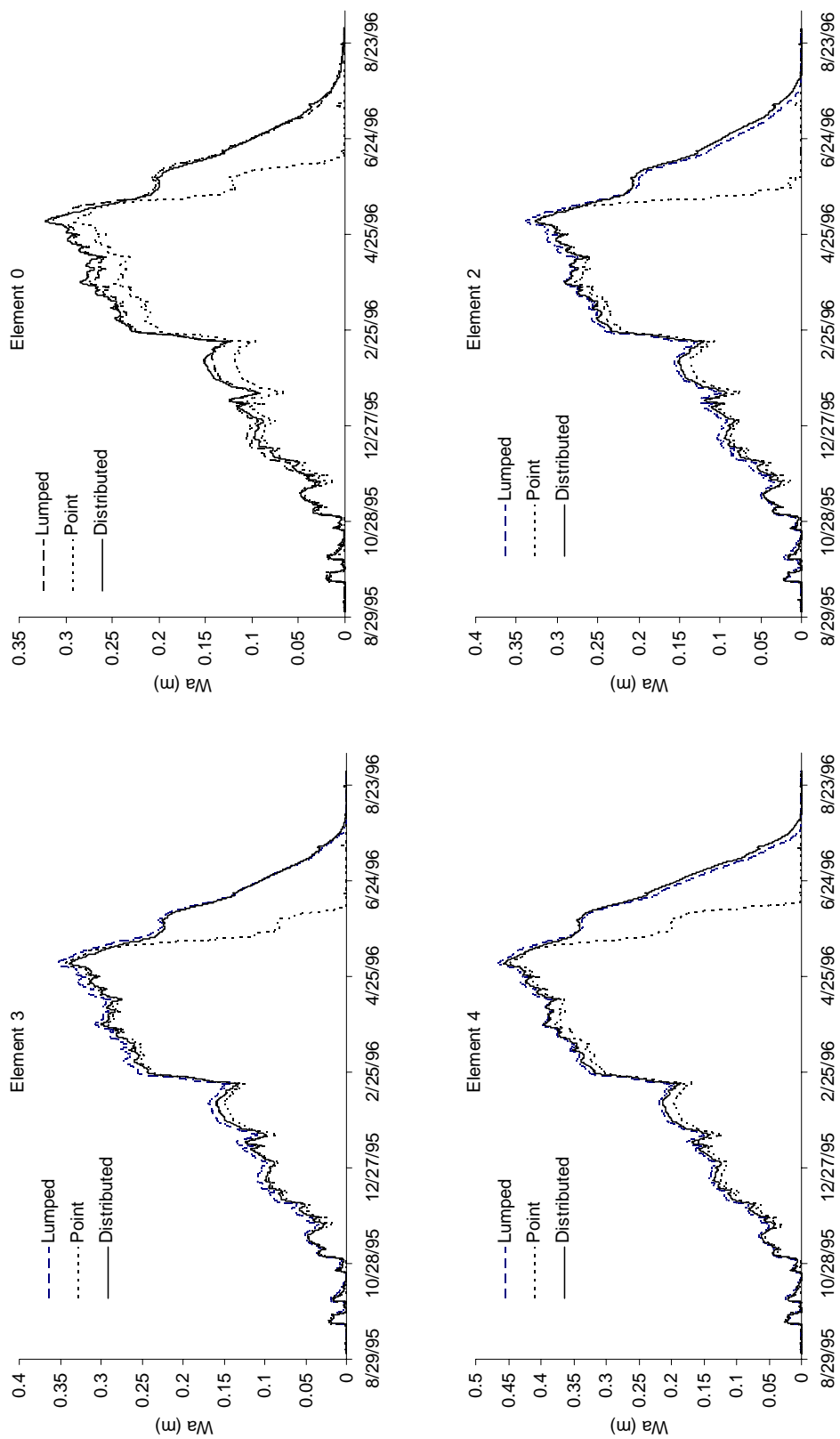


Figure 5-6 Modeled time series of snow water equivalent using three snowmelt models for four modeling elements

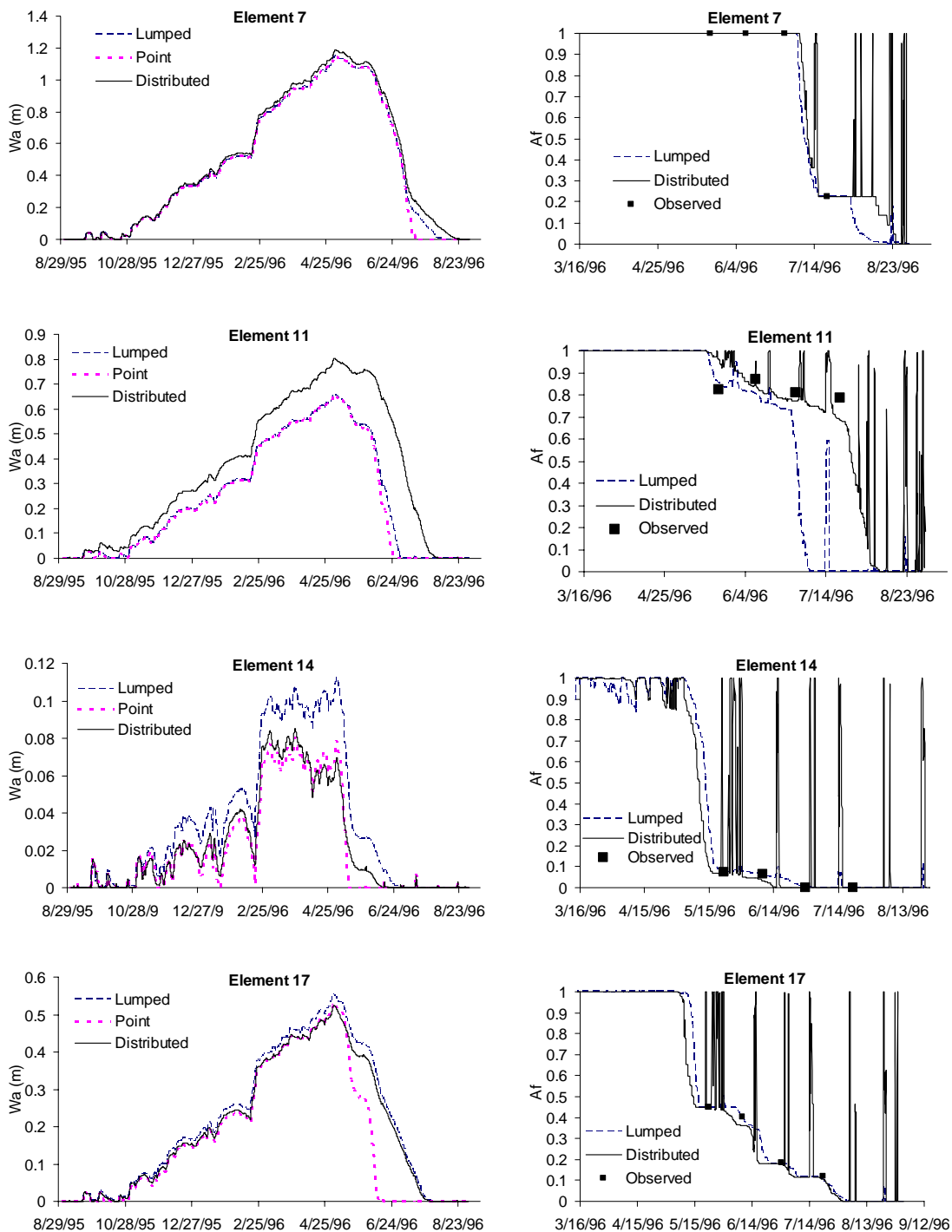


Figure 5-7 Modeled snow water equivalent and snow covered area fraction for some example subwatersheds with specific topographical settings

In northeast-facing element 11, the estimated snow water equivalent from the lumped snowmelt model and the point snowmelt model are almost identical since this subwatershed is fully snow covered during most of the winter season. However both of these model elements differ from the explicitly distributed model taken as reference. The distributed model reference snow covered area compares better to observations lending credibility to it being used as a reference.

The bias between distributed and lumped model snow water equivalent in element 11 is examined more closely in Figure 5-8 which shows the mass change rate modeled in the lumped snowmelt model versus the reference distributed snowmelt model. Element 11 is a high elevation model element. Relative to the distributed model the lumped model underestimates the net mass accumulation and overestimates the net mass loss during the accumulation season. Since the same accumulation factor was used in both models the reason for this difference is primarily differences in condensation during accumulation and sublimation and melt during melt that although small in each time step end up having a net effect of an underestimation of the peak snow water equivalent by 20%.

In South facing element 14 the lumped and point models differ, with the lumped model overestimating snow water equivalent relative to the distributed reference. This effect also occurred in other south-facing subwatersheds with large elevation range where melt and sublimation have considerable variability. In north-facing element 17 there is again good agreement between distributed reference and lumped snow water equivalent model estimates.

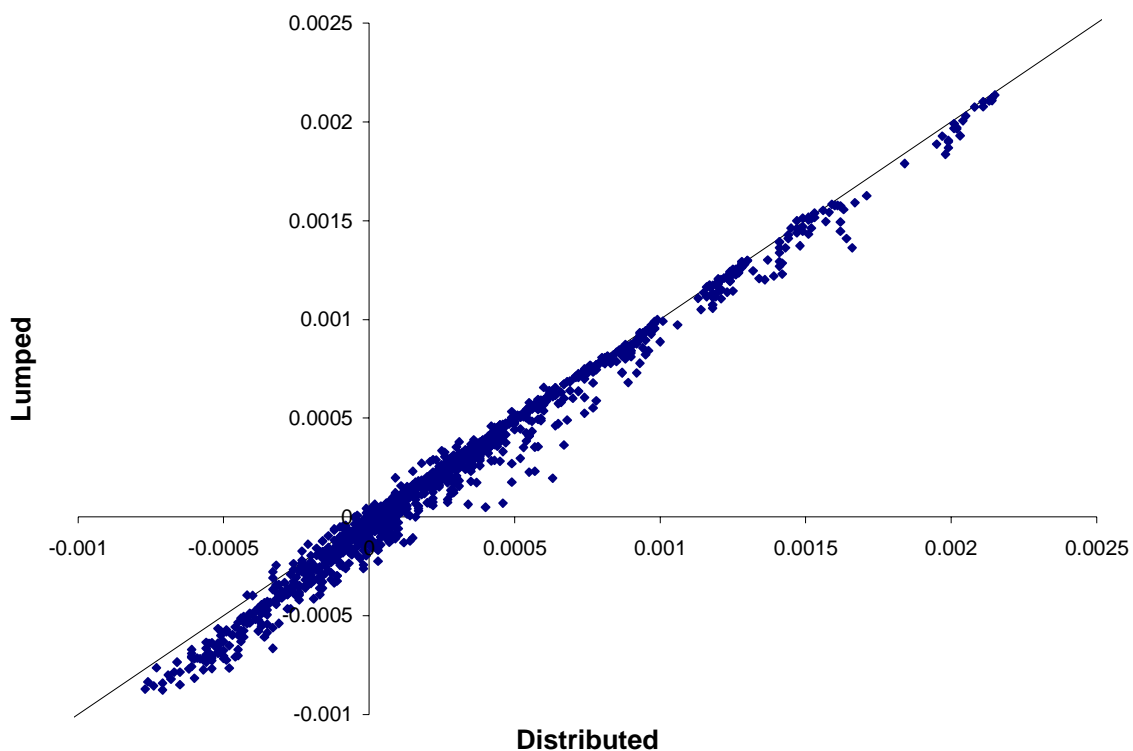


Figure 5-8 Comparison of mass changes in model element 11 for each time step during the accumulation season (Sept. 1, 1995 ~ May 2, 1996) between the lumped snowmelt model and reference distributed snowmelt model. Positive values represent mass increase (condensation/new snow) while negative value represent mass reductions (melt/evaporation)

To better understand the reasons for the discrepancies exemplified by elements 11 and 14 we examined the snow water equivalent change for these two model elements for a single 2-hour time step from 18:00-20:00 on January 11, 1996, chosen for illustration because this time step is one in which the difference in Figure 5-8 is largest. The distribution (over the 10 m grid cells) of mass loss (S+M) for this time step for both elements 11 and 14 is shown in Figure 5-9 (a). Figures 5-9 (b-d) examine the relationship between mass loss and the topographic variables: elevation, slope and aspect

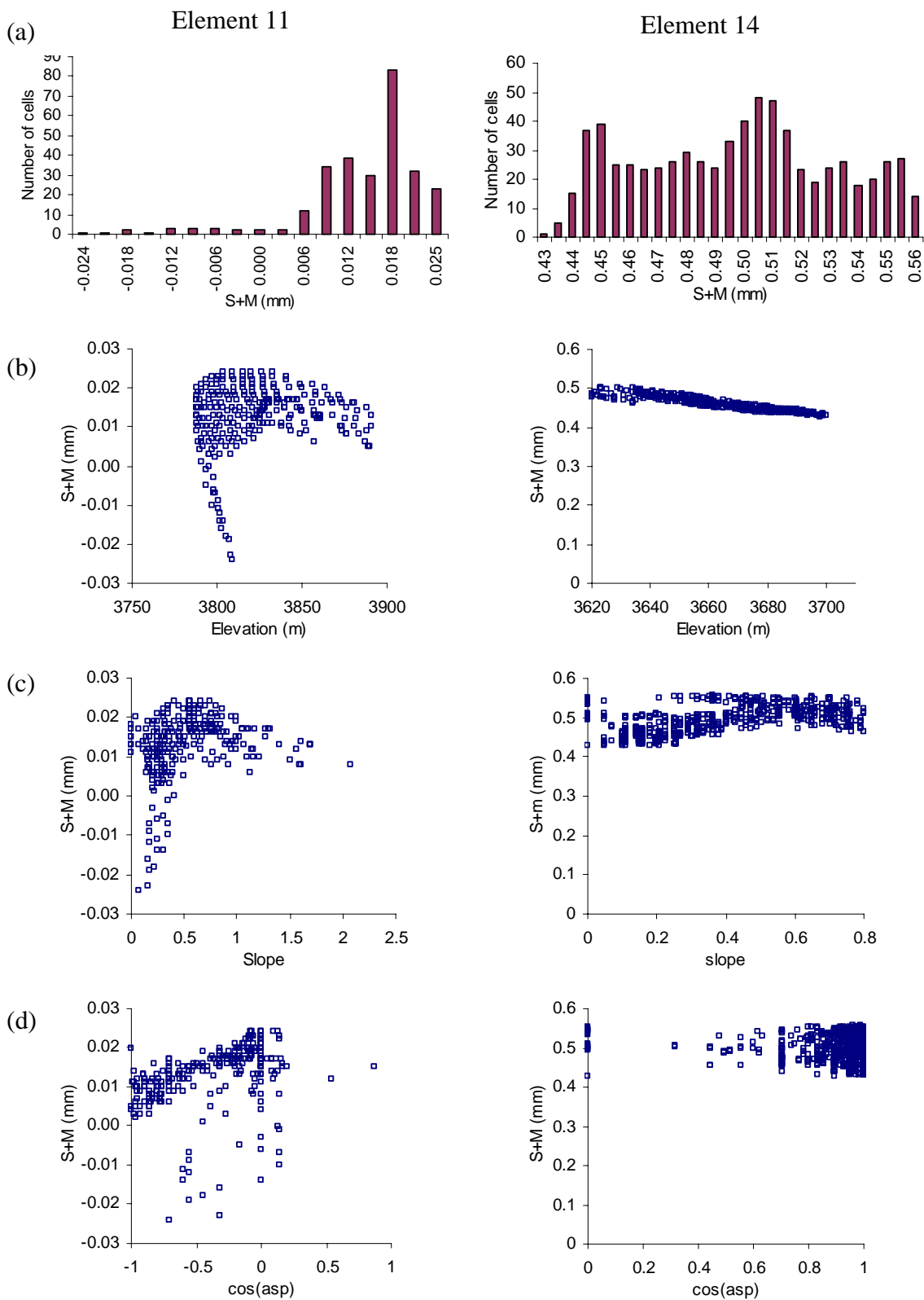


Figure 5-9 Distribution of mass loss (E+M) from 18:00 to 20:00 January 11, 1996 and its relationship with topography and topographical variables

(cosine of aspect is used to avoid the abrupt discontinuity associated with the  $0^\circ$  to  $360^\circ$  break). The nonlinearity present in these figures suggests that using the average elevation, slope, and aspect in the lumped snowmelt model may lead to the mass loss discrepancies found when comparing to with the distributed snowmelt model. Specifically for this time step in element 11 the large scale snowmelt model produced a sublimation of 0.33 mm using the average aspect, elevation, and slope to drive the model, while the distributed snowmelt model only produced an average of 0.01-mm sublimation. We believe that this difference is due to the difference between lumped and distributed model energy inputs. This is discussed further below.

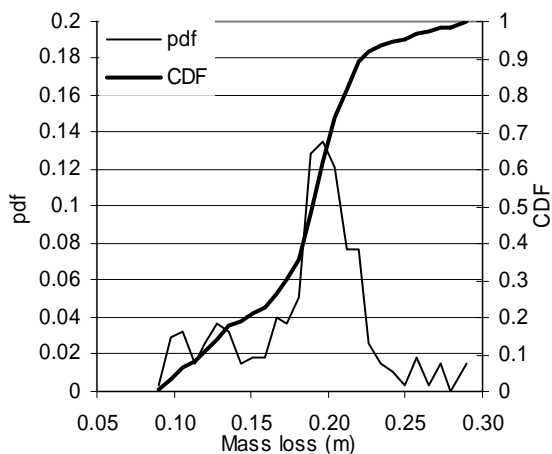
The snow water equivalent change in a single time step involves variability in the history of the snowpack and driving forcing. Here we compare the distribution of the cumulative snow water equivalent change from the start of modeling on September 1, 1995 to May 2, 1996, the accumulation period. Figure 5-10 gives the distribution of mass loss (S+M) for elements 11 and 14. The snow water equivalent and mass loss due to sublimation and melt up until May 2, 1996 are shown in Table 5-1. The distribution of the mass loss has large variability and is skewed for both the elements 11 and 14. This variability coupled with the nonlinearity illustrated earlier is what we believe leads to the modeled total mass loss in the lumped snowmelt model differing from the mean mass loss modeled from the distributed snowmelt model. Even worse, the modeled mass loss in the lumped snowmelt model may fall outside the range of the value modeled in the distributed snowmelt modeling, e.g. 0.32 m mass loss modeled in element 11 (see Table 5-1 and Figure 5-10). This we again believe is due to the difference between lumped model and distributed model energy inputs.



Table 5-1: Modeled snow water equivalent and mass loss in different models (m) for the period September 1, 1995 to May 2, 1996

	Distributed snowmelt model		Lumped snowmelt model		Point snowmelt model	
	Element 11	Element 14	Element 11	Element 14	Element 11	Element 14
W at May 2, 1996	0.8	0.07	0.66	0.11	0.65	0.08
Mass loss due to sublimation and melt	0.18	0.42	0.32	0.38	0.33	0.41

Element 11



Element 14

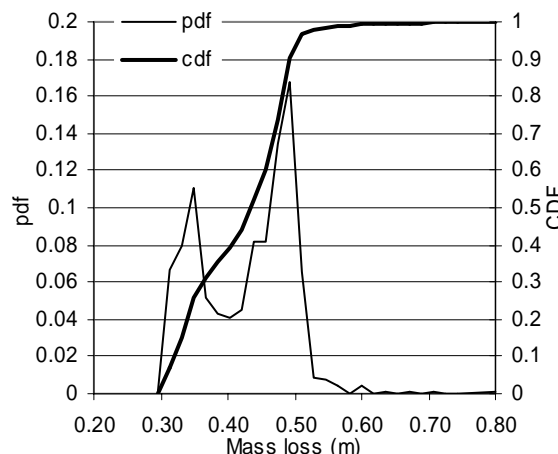


Figure 5-10 Distribution function of snow water equivalent change in distributed snowmelt model during the period Sept 1, 1995 to May 2, 1996

The point and lumped snowmelt models use subwatershed average elevation, slope and aspect. For element 11 these are: Mean slope = 24.1°, Mean aspect = 71.2°, averaged using vector averaging. These average topographic variables result in differences between lumped and distributed radiation energy components. The cumulative radiation components in the lumped and point model for the accumulation period from September 1, 1995 to May 2, 1996 are 1.95 M kJ/m<sup>2</sup> (M kJ/m<sup>2</sup> denotes million kJ/m<sup>2</sup>) for incident shortwave radiation, 5.29 M kJ/m<sup>2</sup> for longwave radiation, for

a combined radiation input of  $7.24 \text{ M kJ/m}^2$ . The ranges from the distributed snowmelt model are  $0.47 - 3.6 \text{ M kJ/m}^2$  for shortwave radiation,  $4.9 - 5.0 \text{ M kJ/m}^2$  for longwave radiation, and  $5.4 - 8.0 \text{ M kJ/m}^2$  for the combination. Only 24 out of 274 cells have the combined radiation higher than the lumped model average of  $7.2 \text{ M kJ/m}^2$  (Figure 5-11). This mean bias in radiation is one of the reasons for discrepancies between the lumped and reference distributed model results. If we consider the variability of albedo under different sunlit conditions, this radiation discrepancy may be even more significant.

We note here that the absolute discrepancy ( $0.04 \text{ m}$ ) between modeled snow water equivalent at peak accumulation using the lumped snowmelt model and the distributed snowmelt model is relatively small for element 14. This  $0.04 \text{ m}$  discrepancy may be within the typical error in a hydrologic model. However the relative discrepancy

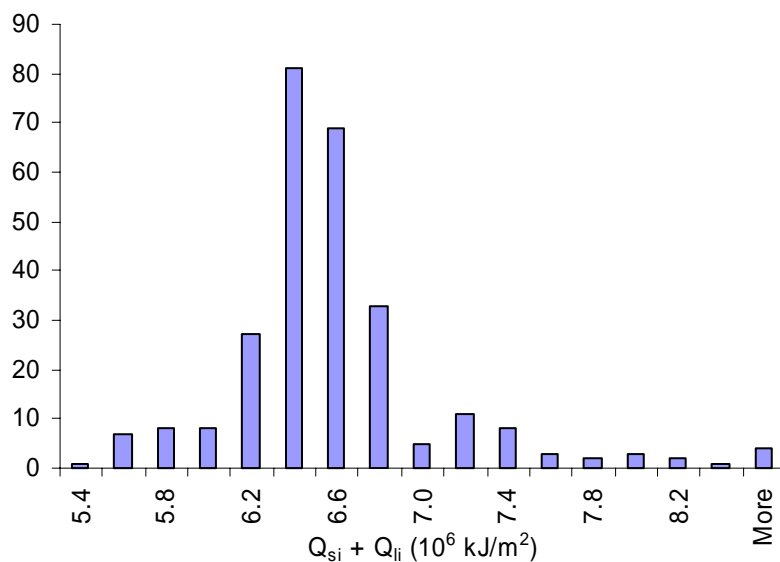


Figure 5-11 Distribution of cumulative radiation during the period Sept 1, 1995 to May 2, 1996.

is significantly larger than the relative discrepancy for element 11. This suggests that these potential discrepancies need to be taken into account in the application of the large scale lumped snowmelt model to large modeling elements with topographical settings similar to those found in elements 11 and 14.

## DISCUSSION AND CONCLUSIONS

A spatially distributed snowmelt model run on 10 m grid cells over the Green Lakes Valley Watershed provided the reference against which to examine the spatial variability of snow water equivalent and the depletion curve approach used to parameterize subgrid variability. This model was previously (chapter 3) verified against snow covered area data. Theoretically the coefficient of variation of snow water equivalent is related to both the coefficient of variation of snow accumulation processes, the coefficient of variation of snow depletion processes and the cross correlation between these processes. By examining the coefficient of variation of each of these effects on snow variability over a range of scales we showed that, in this setting, to quantify the full variability of snow water equivalent, the variability of both the accumulation processes and sublimation and condensation processes needs to be represented. The coefficient of variation of accumulation processes reached a plateau at a scale compatible with a linear scale of 200 m consistent with an earlier finding that the length scale associated with snow drifting processes is 250 m.

The depletion curve parameterization in the lumped model was shown to produce acceptable results in comparison to both the reference explicitly distributed model and observed snow covered area fraction when applied to the entire study area as a single

model element. This would suggest that there is not a scale limitation on this theory up to the scale of  $8.1 \text{ km}^2$  in this setting. However when the depletion curve parameterization was applied to selected subwatersheds within this domain, discrepancies were noted in certain topographic settings. The first discrepancy found was that in high elevation model elements nonlinearities in the processes associated with sublimation and condensation, and perhaps the interpolation of driving weather variables result in a consistent bias between the explicitly distributed reference and lumped model. A second discrepancy involved south facing model elements with large elevation range. South facing model elements tend to lose snow more rapidly due to radiation exposure and the large elevation range results in some parts of the model element losing snow at the same time as other parts of the element are gaining snow. The depletion curve subgrid parameterization does not represent this effect.

In some of the sub-watersheds examined discrepancies between modeled snow water equivalent using the large scale snowmelt model and distributed snowmelt model were attributed to the difference between incident radiation calculated using the average slope, aspect, and elevation and the incident radiation calculated from the spatially explicit distributed model. This exposes a limitation of the lumped approach that is quantifiable and in principal rectifiable. In fact, Ranzi and Rosso (1995) have suggested improved methods for the calculation of direct radiation over a drainage basin that may serve as the basis for correcting this limitation in future work.

The fact that the discrepancies in certain sub-watersheds do not impact the overall results when applied to a large watershed suggests perhaps that there are offsetting errors, or that these discrepancies occur in a relatively small fraction of the area. Nevertheless

the physical cause and limitations implied by these issues need to be considered when delineating model elements for use with a depletion curve parameterization of the subgrid variability of snow in steep mountainous areas.

## REFERENCES

- Anderson EA. 1973. National Weather Service River Forecast System -- Snow Accumulation and Ablation Model. NOAA Technical Memorandum NWS HYDRO-17, U.S. Dept of Commerce. Silver Spring; 217 pp.
- Anderson EA. 1976. A Point Energy and Mass Balance Model of a Snow Cover. NOAA Technical Report NWS 19, U.S. Department of Commerce. 150 pp.
- Bathurst JC, Cooley KR. 1996. Use of the SHE hydrological modelling system to investigate basin response to snowmelt at Reynolds Creek, Idaho. *Journal of Hydrology* **175**(1996): 181-211.
- Berg N. 1986. Blowing snow at a Colorado alpine site: measurements and implications. *Arctic and Alpine Research* **18** (2): 147-161.
- Brubaker K, Rango A, Kustas W. 1996. Incorporating radiation inputs into the snowmelt runoff model. *Hydrological Processes* **10**: 1329-1343.
- Buttle JM, McDonnell JJ. 1987. Modelling the areal depletion of snowcover in a forested catchment. *Journal of Hydrology* **90**: 43-60.
- Caine N. 1995. Snowpack influences on geomorphic processes in Green Lakes Valley, Colorado Front Range. *Geographical Journal* **161**(1): 55-68.
- Dunne T, Leopold LB. 1978. *Water in Environmental Planning*. W H Freeman and Co: San Francisco.
- Ferguson R. 1986. Parametric modelling of daily and seasonal snowmelt using snowpack water equivalent as well as snow covered area. In *Modelling Snowmelt-Induced Processes*. Morris EM (eds). Proc. Budapest Symp., July 1986, IAHS Publ. no. 155: 151-161.
- Hall DK, Martinec J. 1985. *Remote Sensing of Ice and Snow*. Chapman and Hall: London.

- Hood E, Williams M, Cline D. 1999. Sublimation from a seasonal snowpack at a continental, mid-latitude alpine site. *Hydrological Processes* **13**: 1781-1797.
- Jordan R. 1991. A One-dimensional Temperature Model for a Snow Cover. Technical documentation for SNTHERM.89, special technical report 91-16, US Army CRREL. 49 pp.
- Luce CH. 2000. Scale influences on the representation of snowpack processes. Ph. D Dissertation, Civil and Environmental Engineering: Utah State University, Logan, Utah.
- Luce CH, Tarboton DG. 2001. Modeling snowmelt over an area: Modeling subgrid scale heterogeneity in distributed model elements. In *Proceedings of MODSIM 2001, International Congress on Modelling and Simulation*, Canberra, Australia, December 10-13; 341-346.
- Luce CH, Tarboton DG. 2004. The application of depletion curves for parameterization of subgrid variability of snow. *Hydrological Processes* **18**: 1409-1422.
- Luce CH, Tarboton DG, Cooley KR. 1999. Subgrid parameterization of snow distribution for an energy and mass balance snow cover model. *Hydrological Processes* **13**: 1921-1933.
- Martinez J. 1980. Snowmelt-runoff forecasts based on automatic temperature measurements. Hydrological Forecasting. Proc. Oxford Symp. 129, IAHS-AISH. Wallingford; 239-246
- Morris EM. 1990. Physics-based models of snow. In *Recent Advances in the Modeling of Hydrologic Systems*, Bowles DS, O'Connell PE (eds). Kluwer Academic Publishers: Dordrecht, The Netherlands; 85-112.
- Ranzi R, Rosso R. 1995. Distributed estimation of incoming direct solar radiation over a drainage basin. *Journal of Hydrology* **166**: 461-478.
- Tarboton DG, Ames DP. 2001. Advances in the mapping of flow networks from digital elevation data. in *World Water and Environmental Resources Congress*, Orlando, Florida, May 20-24, ASCE.
- Tarboton, D. G. (2000). TARDEM, a suite of programs for the analysis of Digital Elevation Data. <<http://www.engineering.usu.edu/dtarb/tardem.html>>, (Accessed Jul. 31, 2004). Utah State University, Logan, UT.
- Tarboton DG, Chowdhury TG, Jackson TH. 1995. A spatially distributed energy balance snowmelt model. In *Proceedings of A Boulder Symposium*, Tonnessen KA, Williams MW, Tranter M (eds). Boulder, CO., July 3-14, IAHS Publ. no. 228.

Tarboton DG, Luce CH. 1996. Utah Energy Balance Snow Accumulation and Melt Model (UEB). Computer model technical description and users guide, Utah Water Research Laboratory and USDA Forest Service Intermountain Research Station (<http://www.engineering.usu.edu/dtarb/>). (Accessed Jul. 31, 2004).

Williams MW, Baron JS, Caine N, Sommerfeld R, Sanford RJ. 1996. Nitrogen saturation in the Rocky Mountains. *Environmental Science and Technology* **30**: 640-646.

## CHAPTER 6

### SUMMARY, CONCLUSIONS, AND RECOMMENDATIONS

Chapters 2 to 5 report the main scientific results of this dissertation. Here I summarize and emphasize the important contributions and recommend avenues for future research.

#### SUMMARY AND CONCLUSIONS

Chapter 2 described enhancements to the Utah Energy Balance snowmelt model. A modified force restore approach was applied to parameterize the surface temperature of snow, and a new refreezing scheme was developed to approximate the heat loss after partial melt. These modifications corrected a deficiency in the model's representation of the internal energy content that had been noted previously. Performance tests of the new model demonstrated that with the enhancements presented, the single layer snowmelt model can provide a good representation of snowmelt processes for situations in which it was applied.

Chapter 3 presented a new approach that combines physically based snowmelt modeling with the use of a limited number of snow covered area images to estimate the snow accumulation factor necessary to explicitly represent spatially distributed snow processes. This work provides a way to use snow covered area images in combination with meteorological inputs to calibrate the accumulation factor needed to represent snow distribution and redistribution effects in an alpine watershed. In this chapter, although



general relationships between physical terrain attributes and accumulation factor were explored I was unable to find a single general relationship that could be extended to similar settings, without snow cover observations. Therefore application of these ideas requires snow covered area as well as meteorological and topographical information.

Chapter 4 explored the idea that topography is the governing cause of most spatial variability in snow. This chapter evaluated whether surrogate variables derived from topography could be used to derive the depletion curve used to parameterize the subgrid variability of snow. It was found that the depletion curve derived using the distribution of elevation only, or assuming that accumulation and melt are independent are markedly different from the reference depletion curve and hence are not good approaches for the parameterization of subgrid variability. The best overall result was obtained from the approach that combined accumulation and melt explicitly accounting for the spatial dependence. This is important because accumulation and melt are fundamentally different processes, related to different topographic attributes and this approach provides a formal way for these different effects to be correctly combined in the estimation of depletion curves for the parameterization of the subgrid variability of snow. The results indicate that it is possible to get depletion curves that approach the reference depletion curve based on surrogate variables, but that the better estimates still require some reliance on spatially explicit modeling.

Chapter 5 explored the scaling limitations associated with depletion curve parameterizations of the subgrid variability of snow. The depletion curve approach was able to successfully represent snow accumulation and ablation processes up to the largest scale watershed examined ( $8.1 \text{ km}^2$ ) suggesting that it is applicable in this setting up to

these scales. However we did find biases when using the depletion curve subgrid parameterization for certain subwatersheds within the study area. These were subwatersheds where there was a bias in the energy inputs or where there was a large elevation range. Analysis of the bias in energy inputs was traced to nonlinearity in the energy inputs and the use of average elevation, slope, and aspect in the large scale snowmelt model. Approaches to correct this in the future were suggested.

## RECOMMENDATIONS

This dissertation has presented some new approaches that advance the representation of the spatial variability of snow in snowmelt models. Although considerable progress was made, evaluation of these approaches was limited by the data available and further evaluation with more detailed data is needed. For example, the representation of the spatial distribution of snow from snow covered area images in this study was based on only four snow covered area images. No snow covered area images were available during the high accumulation period from January to April. In our modeling results, the watershed is modeled as fully snow covered during most of the accumulation period. This result may not be correct because it has been suggested that the snow covered area fraction rarely exceeds 85% for this watershed due to the steep topography. Snow covered area images collected during the winter season would confirm this and help better represent the spatial variability of snow. Earlier snow covered area images would also provide data critical to constrain the early part of the depletion curve which is, in the current work, somewhat speculative due to the lack of early season data.

Chapter 2 introduced new parameterizations for snow surface temperature and the refreezing of meltwater present in the snowpack. The new refreezing scheme has only been tested against the calculated internal energy content of the snowpack. Direct comparisons to the penetration of the refreezing front were not possible and are recommended in the future. This could be achieved through measurements of liquid content and its vertical distribution or through comparisons against a more detailed model that keeps track of the multiple phases present within a snowpack (e.g. SNTHRM, Jordan, 1991).

There are also a number of ideas to pursue given more frequent observations of snow covered area. The bounds on accumulation factor calculated in Chapter 3 could be reduced. These tighter bounds would allow for better examination of relationships between accumulation factors and topography. Frequent measurements of snow covered area could be combined with energy balance modeling to directly construct depletion curves.

Chapter 4 brought out the importance of the spatial correlation between accumulation and melt on depletion curves and the parameterization of snow subgrid variability. To date this correlation has only been quantified using results from spatially explicit distributed models. This is a limitation because spatially explicit models are computationally intensive and demanding of data. Research is recommended to further explore the relationship between topography and the correlation between accumulation and melt so that these approaches can be generalized.

Chapter 5 exposed biases in the energy inputs when the large-scale modeling approach using depletion curves was applied to certain sub-watersheds. This was due to

average slope, aspect and elevation not being representative, an example of a scale problem with nonlinear processes. Research is recommended in the future to exploit alternative ways to quantify the direct energy inputs over a watershed to avoid this problem, following, for example, procedures suggested by Ranzi and Rosso, (1995).

Finally, the interaction between wind and topography is the root cause of variability in both precipitation and snow drifting. In a mountainous watershed the wind field are complex and difficult to measure. This poses problems for the physical modeling of drifting and turbulent energy exchanges. Examination of spatial wind patterns, perhaps derived from hydraulic models coupled with measurements needs to be a topic of future research if we are to make progress in this area.

#### REFERENCES

Jordan R. 1991. A One-dimensional Temperature Model for a Snow Cover. Technical documentation for SN THERM.89, special technical report 91-16, US Army CRREL. 49 pp.

Ranzi R, Rosso R. 1995. Distributed estimation of incoming direct solar radiation over a drainage basin. *Journal of Hydrology* **166**: 461-478.

APPENDIX

DEPLETION CURVE DERIVATION FROM  
RESCALED DISTRIBUTION FUNCTION

This appendix shows that the rescaling of a probability distribution function used to derive a depletion curve does not change the shape of the dimensionless depletion curve that results. The procedure for deriving a depletion curve  $A_{dc}^*(W_a)$  from a general probability density function  $f_g(w)$  is given by Equations 4-7 to 4-12. Our approach is to consider a rescaling of  $f_g(w)$  and use the rescaled  $f_g(w)$  in the derivation going from Equations 4-7 to 4-12. Consider the rescaling represented by  $x=cw$ . The density function of  $x$  can be written as:

$$f_x(x) = \frac{1}{c} f_g\left(\frac{x}{c}\right). \quad (\text{A-1})$$

Now using  $f_x(x)$  in Equation 4-7 results in

$$A'_m(m) = \int_m^{\infty} \frac{1}{c} f_g\left(\frac{x}{c}\right) dx = 1 - F_g\left(\frac{m}{c}\right) = A_m\left(\frac{m}{c}\right) \quad (\text{A-2})$$

Putting this in Equation 4-8

$$W'_m(m) = \int_m^{\infty} \left(1 - F_g\left(\frac{x}{c}\right)\right) dx = c \int_{m/c}^{\infty} (1 - F_g(w)) dw = c W_m\left(\frac{m}{c}\right) \quad (\text{A-3})$$

Here  $A'_m(m)$ ,  $W'_m(m)$  are the snow covered area fraction and basin average snow water equivalent for the rescaled distribution respectively. To apply Equation 4-10 we also need the inverse function  $W_m'^{-1}(W_a)$ . For a given  $W_a$  applying Equation A-3 we get

$$W_a = W'_m(m) = cW_m\left(\frac{m}{c}\right) \quad (\text{A-4})$$

Therefore

$$\frac{W_a}{c} = W_m\left(\frac{m}{c}\right) \quad (\text{A-5})$$

and

$$\frac{m}{c} = W_m^{-1}\left(\frac{W_a}{c}\right) \quad (\text{A-6})$$

and

$$m = cW_m^{-1}\left(\frac{W_a}{c}\right) \quad (\text{A-7})$$

Hence

$$W_m'^{-1}(W_a) = cW_m^{-1}\left(\frac{W_a}{c}\right) \quad (\text{A-8})$$

Now the maximum basin average snow water equivalent under the rescaled pdf  $f_x(x)$  is following Equation 4-11

$$W_{a\max}' = W_m'(0) = cW_m(0) = cW_{a\max} \quad (\text{A-9})$$

The last two statements result from applying Equation A-3. Now applying Equation 4-10 with the rescaled results

$$A_{dc}'(W_a) = A_m'\left(W_m'^{-1}(W_a)\right) \quad (\text{A-10})$$

Substituting A-8 results in

$$A_{dc}'(W_a) = A_m'\left(cW_m^{-1}\left(\frac{W_a}{c}\right)\right) \quad (\text{A-11})$$



Now using A-2 results in

$$A'_{dc}(W_a) = A_m \left( W_m^{-1} \left( \frac{W_a}{c} \right) \right) = A_{dc} \left( \frac{W_a}{c} \right) \quad (\text{A-12})$$

Thus the depletion curve of the rescaled distribution is equivalent to the depletion curve of the original distribution with the axis rescaled. The dimensionless depletion curve is obtained from A-12 through a rescaling by  $W'_{amax}$

$$A'^*_{dc} \left( \frac{W_a}{W'_{amax}} \right) = A'_{dc}(W_a) = A_{dc} \left( \frac{W_a}{c} \right) \quad (\text{A-13})$$

Due to A-9 this is equivalent to the original dimensionless depletion curve

$$A^*_{dc} \left( \frac{W_a/c}{W'_{amax}} \right) = A^*_{dc} \left( \frac{W_a/c}{W'_{amax}/c} \right) = A^*_{dc} \left( \frac{W_a}{W'_{amax}} \right) \quad (\text{A-14})$$

## CURRICULUM VITAE

Jinsheng You

**Research Associate**

14 L. W. Chase Hall  
 High Plains Regional Climate Center  
 University of Nebraska – Lincoln  
 Lincoln, NE 68583-0728

Phone: 402-472-8765  
 Fax: 402-472-3610  
 Email: jyou2@unl.edu

**Research Interests**

Hydrological modeling  
 Scaling hydrological processes  
 Quality assurance of weather data  
 Climatology, hydrometeorology and Climate change  
 Snow hydrology and Cold region hydrology  
 Remote sensing

**Educations****Academic Degrees**

- |       |  |                          |      |
|-------|--|--------------------------|------|
| Ph.D. | Civil Engineering  | Utah State University    | 2004 |
|       | Dissertation: Snow Hydrology: Subgrid parameterization of variability of snowmelt in a mountainous watershed |                          |      |
| M.S.  | Hydrology and Water Resources  | Hohai University, China. | 1996 |
|       | Thesis: Application of GIS in flood retention areas in Huaihe River Basin of China                           |                          |      |
| B.S.  | Hydrology and Water Resources  | Hohai University, China. | 1993 |
|       | Thesis: Application of Xin'anjiang Model in a mountainous watershed  |                          |      |

**Special courses**

GIS in Water Resources, Utah State University, 1999

**Professional Experiences**

- |             |  |
|-------------|--|
| 1999 ~      | Research Assistant, Department of Civil and Environmental Engineering, Utah State university |
| 1996 ~ 1999 | Water Resources Engineer, Nanjing Institute of Hydrology and Water Resources, China          |

- 1993 ~ 1996    Research Assistant, Department of Hydrology and Water Resources, Hohai University, China.
- 1992 ~ 1993    Research Assistant, Department of Hydrology and Water Resources, Hohai University, China.

### **Professional distinctions**

Poster Competition Award, Sixth Annual Intermountain Paper & Poster Symposium, Utah State University, Logan, UT.

### **Professional Membership**

- American Geophysical Union
- Chinese Water Resources Society

### **Publications**

#### *Referred papers and reports*

National long and mid term plan of water use and supply of China, 1998

Burke, J, et al., Study of watershed management in Huaihe River Basin, 1998

Long and mid-term plan of water resources of Southwestern Rivers in China, 1997

Jinsheng You, M.S. thesis: Application of GIS in flood retention areas in Huaihe River Basin, China, 1993

Jiren Li, Xingnan Zhang, Jinsheng You, et al., Flood management system in upper reaches of Huaihe River Basin, 1992

#### *Presentations/Posters*

Jinsheng You, David. G. Tarboton, and Charles H. Luce (2003). "Spatially Distributed Snowmelt Modeling with the Utah Energy Balance Snowmelt Model."

Jinsheng You, Kenneth G. Hubbard, William S. Sorensen, Steve Goddard, and Thomas Osugi (2003). Quality Assurance of Surface Temperature and Precipitation: Performance of Spatial Test in Extreme Events. 2003 SNR Research Colloquium, University of Nebraska - Lincoln, Lincoln, NE.

Jinsheng You, David. G. Tarboton, and Charles H. Luce (2003). Spatially Distributed Snowmelt Modeling with the Utah Energy Balance Snowmelt Model. 2003 SNR Research Colloquium, University of Nebraska - Lincoln, Lincoln, NE.

- Jinsheng You, David. G. Tarboton, and Charles H. Luce (2003). Representation of spatial distribution pattern of snow in a mountainous watershed based on snow covered area images. Sixth Annual Intermountain Paper & Poster Symposium, Utah State University, Logan, UT.
- Jinsheng You, David. G. Tarboton, and Charles H. Luce (2003). Snow covered area images based representation of spatial distribution pattern of snow in a mountainous watershed. 23th Hydrology Days, Fort Collins, CO.
- Jinsheng You, David G. Tarboton, and Charles H. Luce, Spatially Distributed Snowmelt Modeling with the Utah Energy Balance Snowmelt Model, AGU Fall Meeting 2001, San Francisco, California, 2001
- Jinsheng You, David G. Tarboton, and Charles H. Luce, Modeling the Snow Surface Temperature in an Energy Balance Snowmelt Model, Hydrology Days 2001, Fort Collins, Colorado, 2001
- Jinsheng You, David. G. Tarboton, and Charles H. Luce (2001). Modeling the snow surface temperature in an energy balance snowmelt model. 21th Hydrology Days, Fort Collins, CO.
- Jinsheng You, David. G. Tarboton, and Charles H. Luce (2001). "Spatially Distributed Snowmelt Modeling with the Utah Energy Balance Snowmelt Model." Eos Trans. AGU 82(47) Fall Meet. Suppl., Abstract IP51A-0725.

*Papers written and in review*

- You, J., D. G. Tarboton, and C. H. Luce, (submitted 2004), "Modeling the Snow Surface Temperature in an Energy Balance Snowmelt Model," Submitted to Hydrological Processes.
- You, J, K. G. Hubbard, and S. Goddard, (submitted 2004), "Comparison of Estimates from Spatial Regression and Inverse Distance Method," submitted to Journal of Atmospheric and Oceanic Technology.